DYNAMIC BEHAVIOUR AND HYDRAULIC PERFORMANCE OF REACTION TURBINES IN EMBANKMENT DAMS

AMEEN MOHAMMED SALIH AMEEN

FACULTY OF ENGINEERING
UNIVERSITY OF MALAYA
KUALA LUMPUR

2018

DYNAMIC BEHAVIOUR AND HYDRAULIC PERFORMANCE OF REACTION TURBINES IN EMBANKMENT DAMS

AMEEN MOHAMMED SALIH AMEEN

THESIS SUBMITTED IN FULFILMENT OF THE REQUIREMENTS FOR THE DEGREE DOCTOR OF PHILOSOPHY

FACULTY OF ENGINEERING
UNIVERSITY OF MALAYA
KUALA LUMPUR

2018

UNIVERSITY OF MALAYA

ORIGINAL LITERARY WORK DECLARATION

Name of Candidate: Ameen Mohammed Salih Ameen

Registration/Matric No: KHA130063

Name of Degree: Ph.D.

DYNAMIC BEHAVIOUR AND HYDRAULIC PERFORMANCE OF REACTION TURBINES IN EMBANKMENT DAMS

Field of Study: WATER RESOURCES ENGINEERING

I do solemnly and sincerely declare that:

(1) I am the sole author/writer of this Work;
(2) This Work is original;
(3) Any use of any work in which copyright exists was done by way of fair dealing and for permitted purposes and any excerpt or extract from, or reference to or reproduction of any copyright work has been disclosed expressly and sufficiently and the title of the Work and its authorship have been acknowledged in this Work;
(4) I do not have any actual knowledge nor do I ought reasonably to know that the making of this work constitutes an infringement of any copyright work;
(5) I hereby assign all and every rights in the copyright to this Work to the University of Malaya ("UM"), who henceforth shall be owner of the copyright in this Work and that any reproduction or use in any form or by any means whatsoever is prohibited without the written consent of UM having been first had and obtained;
(6) I am fully aware that if in the course of making this Work I have infringed any copyright whether intentionally or otherwise, I may be subject to legal action or any other action as may be determined by UM.

Candidate's Signature Date:

Subscribed and solemnly declared before,

Witness's Signature Date:

Name:

Designation:

DYNAMIC BEHAVIOUR AND HYDRAULIC PERFORMANCE OF REACTION TURBINES IN EMBANKMENT DAMS

ABSTRACT

Dam and powerhouse operation sustainability is the main concern from the hydraulic engineering perspective. Powerhouse operation represents one of the main sources of vibration on the dam's structure and thus evaluating the turbine performance with different water level pressures is highly significant. Draft tube downstream turbines run under high pressure and suffer from connection problems such as vibrations and pressure fluctuation. Reducing the pressure fluctuation and minimizing the principal stress which is related to undesired rational components of water in the draft tube turbine is still ongoing and requires to be resolved. In this research, a 3-D numerical turbine model with the construction of a submerged weir at the outlet of the draft tubes is developed. Secondly, an investigation for the dynamic behavior of an embanked dam due to earthquake effects is conducted. (Finally, an optimization operating turbine system is generated to reduce the principal stress). To achieve this, two different cases of fully opened gates of reaction turbines are inspected including Haditha Dam in Iraq and Temenggor Dam in Malaysia. The finding of the first agreed aim in which initiating a 1.333 m and a 1 m submerged weir for Kaplan (Haditha Dam) and Francis turbines (Temenggor Dam) was a very excellent proposition to solve the problem of negative pressure pulsation in the draft tube. In addition, the results showed that the natural frequencies decrease with the increase of the upstream water level and foundation depth. Finally, with the combination of the dam models with turbine models, a control program is generated to run the turbines inside the powerhouse based on minimizing the principal stress values in the selected nodes of the dam body, which depends on the principal stress classification.

Keywords: Dam, reaction turbine, submerged weir, seismic load, principal stress.

KELAKUAN DINAMIK DAN PRESTASI HYDRAULIK TURBIN REAKSI DI EMPANGAN-EMPANGAN TAMBAKAN

ABSTRAK

Kelestarian operasi empangan dan rumah kuasa merupakan kebimbangan utama dari perspektif kejuruteraan hidraulik. Operasi rumah kuasa merupakan salah satu sumber utama getaran pada struktur empangan dan dengan itu menilai prestasi turbin dengan tekanan paras air yang berbeza adalah sangat signifikan. Tiub draf hiliran berjalan di bawah tekanan tinggi dan mengalami masalah sambungan seperti getaran dan turun naik tekanan. Mengurangkan turun naik tekanan dan meminimumkan tekanan utama yang berkaitan dengan komponen rasional air yang tidak diingini di dalam turbin tiub draf masih berterusan dan perlu diselesaikan. Di dalam kajian ini, suatu model turbin berangka 3-D dengan pembinaan weir tenggelam di saluran luar tiub draf dibangunkan. Kedua, siasatan terhadap kelakuan yang dinamik bagi sesuatu empangan tambakan akibat beban seismos dijalankan. Akhirnya, sistem pengoptimuman pengoperasian turbin dijana untuk mengurangkan tekanan utama. Untuk mencapai matlamat ini, dua kes berbeza pintu terbuka sepenuhnya turbin reaksi diperiksa termasuk Empangan Haditha di Iraq dan Empangan Temenggor di Malaysia. Dapatan matlamat pertama yang dipersetujui di mana memulakan satu weir tenggelam 1.333 m dan 1 m untuk turbin Kaplan (Empangan Haditha) dan Francis (Empangan Temenggor) merupakan satu cadangan yang sangat terbaik untuk menyelesaikan masalah denyutan tekanan negatif dalam tiub draf. Di samping itu, keputusan menunjukkan bahawa frekuensi semula jadi berkurangan dengan peningkatan paras air hulu dan kedalaman tapak. Akhirnya, dengan kombinasi model-model empangan dengan model turbin, suatu program kawalan dijana untuk menjalankan turbin di dalam rumah kuasa berdasarkan meminimumkan nilai tegasan utama dalam nod-nod terpilih badan empangan tersebut, yang bergantung kepada klasifikasi tekanan utama.

Kata kunci: Kelestarian empangan, kelakuan turbin, weir tenggelam, beban seismos, tekanan utama.

ACKNOWLEDGEMENTS

Alhamdulillah, all praises to Allah S.W.T., The Greatest and The Most Merciful for His guidance and blessing, because without Him, I can't finish this research. I would like to express my deepest gratitude and appreciation to my supervisors Prof. Zainah Ibrahim and Prof. Faridah Othman. They have provided invaluable guidance and supervision throughout the period of my research. The research would not have been possible without their brilliant ideas and great experiences. I feel honored to have them as my supervisors. I would like to express immense appreciation to my beloved family members, especially my father, for his continuous prayers and love, my brothers and sisters for backing me up and for loving me unconditionally. Without their love and support, I would not have been able to achieve this much. My sincere and deepest gratitude goes to my beloved wife. She was very kind and supportive women over the four years of research. The proposed comments by Prof. Dr. Thamer Ahmad Mohammad from the Department of water Resources Engineering, College of Engineering, University of Baghdad are highly appreciated. I do admit that without her prayers I doubt I could finish my research. Last but not least, no words can be used to express my deep appreciation to all my friends, especially Zaher Mundher Yaseen, for the support during my study in Malaysia. Finally, my sincere thanks also go to the entire teaching and technical staff in University Malaya (UM).

TABLE OF CONTENTS

LIST OF FIGURES

LIST OF TABLES

LIST OF SYMBOLS AND ABBREVIATIONS

$\{\ddot{D}\}$	:	The global vector of nodal accelerations.
$\{\dot{D}\}$	:	The global vector of nodal velocities.
∇^2	:	Laplacian operator in two dimensions.
$[C]$	:	The global damping matrix.
$\{D\}$	:	The global vector of nodes displacement.
$[F(t)]$	:	The vector of consistent nodal forces for the applied body and surface traction forces grouped together.
H_g	:	Gross head equal to (upstream water level – downstream water level).
H_n	:	Net head.
$[K]$	:	The global stiffness matrix.
$[M]$	:	The global mass matrix.
N_{QE}	:	Specific speed.
$P_\circ$	:	Water power.
V_1	:	Velocity of water at the turbine unit entrance.
V_2	:	Velocity of water at the turbine unit exit.
a_n^s	:	Normal acceleration on dam foundation.
a_n^r	:	The normal acceleration on dam.
$c_\circ$	:	Velocity of sound in water.
f_f	:	Body force vector of the fluid medium.
p_1	:	Water pressure at the turbine unit entrance.
p_2	:	Water pressure at the turbine unit exit.
$y^{"}$	:	Accelerations.
y'	:	The velocity.

z_1	:	Elevation head at the turbine unit entrance.
z_2	:	Elevation head at the turbine unit exit.
$\alpha_\circ$	:	Wave reflection coefficient.
ρ_f	:	Fluid density.
ρ_w	:	Water density.
τ_f	:	Fluid stress tensor.
$\emptyset$	:	The applied surface traction.
∇	:	Hamilton operator.
2D	:	Two dimension.
3-D	:	Three dimension.
a	:	The first coefficients of Rayleigh Damping.
ASL	:	Above sea level.
B	:	The interaction matrix.
b	:	The second coefficients of Rayleigh Damping.
B	:	The strain matrix.
C	:	The damping Coefficient.
CFD	:	Computational fluid dynamics.
coef.	:	Coefficient.
d	:	Displacements at the points.
D/S	:	Downstream.
D/S. W.L.	:	Downstream water level
DOF	:	Degree of freedom.
E	:	The specific hydraulic energy.
e.l.s	:	End left side.
F	:	The body force per unit volume.
F(t)	:	The applied forces for the body.

FE	:	Finite element.
FFT	:	Fourier transform.
g	:	Gravity acceleration.
H	:	Head of water.
J	:	An influence matrix.
K	:	The stiffness.
l.s	:	Left side.
M	:	The mass.
max.	:	Maximum.
min.	:	Minimum.
n	:	Normal vector on the interface.
N	:	Shape functions.
n	:	The normal direction outward into the boundary surfaces.
P	:	Hydrodynamic pressure.
q	:	coefficient of absorption at reservoir bed.
Q	:	Flow rate.
S	:	Surface area.
t	:	Time
u	:	Fluid velocity vector in x direction.
U/S.W.L.	:	Upstream water level.
V	:	The volume.
v	:	Velocity components in the y direction.
w	:	Velocity components in the z direction.
α	:	Constant referred to the mass.
β	:	Constant referred to the stiffness damping.
σ_{max}	:	Maximum principal stress.

ω	:	Angular velocity.
y	:	The displacement.
ε	:	Strain vector.
η	:	Turbine efficiency.
σ	:	Stress vector.

CHAPTER 1: INTRODUCTION

1.1 General

Large dams are the most important hydraulic structure built across a river to store the excess water in a reservoir on its upstream side for impounding water for various purposes. Always, the dams are constructed in narrow valleys of rivers where the rigorous foundation is available. Dams can be classified according to different criteria. Based on materials used in construction, dams categorized into masonry, concrete and embanked dams (earth and rock-fill). In addition to the main dam structure, dam appurtenances such as spillway, conduits, and powerhouse are necessary for the dam. Globally, According to Bosshard (2009), more than 80% are embankment dams of the total constructed dams in China. While, in QuébEc, Canada, the embankment dams form about 73% of the total dams in this territory. Most of the past dam failures and incidents involved happened at sites with embankment dams.

Thus, more studies are required to increase the safety of the embankment dams. A revolution in technology came about in late 19th century when an electric generator was driven by a hydro-turbine on Fox River in Wisconsin Ravens (2007). This invention declared the born of hydropower technology.

A dam is presented to create the head difference between the headrace (the water surface elevation upstream of the dam) and the tailrace (the water surface elevation downstream of the dam). The penstock comprises of pipes or tunnels which direct flow to the turbine system. The hydro-turbine itself is a mechanical device whose rotation is driven by the extraction of energy from the flow. The electric generator converts mechanical energy into electrical energy and its rotation is driven by a shaft attached directly to the rotating hydro-turbine. Finally, the draft tube is a diffuser which collects the flow after it exits the turbine and deposits it on the lower side of the dam. The hydro-

turbine is categorized into impulse turbines (Pelton type) and reaction turbines (Francis and Kaplan types). Based on head available between upstream and downstream of the dams, most of the turbines used at the powerhouse are reaction turbines. Turbine operation is a source of vibration which affects the dam and powerhouse stability.

1.2 Motivation and problem statement

A dam is continuously in harmonic motion due to the environmental factors such as wind, water waves, floods and earthquakes. Also, the operation of a dam powerhouse produces harmonic motion that affecting dam stability.

The importance of reducing the vibrational influence on dams is required to increase their stability. With the increase in computer speed and development of programs that are specialized in modeling the influence of dynamic forces on structures, studies simulating the vibrational effects on dam bodies are intended in order to increase the factor of safety.

The seismic effect on dam bodies was studied by the civil engineering researchers in order to assess their dynamic behaviors. Khosravi & Heydari (2013), Sarkar et al. (2007) and Zeidan (2015) developed 2D numerical models for simulation of dynamic behavior of dam bodies. Ebrahimian (2012) and Mircevska et al. (2007) developed 3-D numerical models which are more capable and accurate than the 2D models. The vibrational effect produced by the hydraulic turbines was studied by mechanical engineering researchers to assess their hydraulic performance due to powerhouse operation. Bosioc et al. (2010), Casanova García & Mantilla Viveros (2010), Lai et al. (2012) were focused on modeling and analysis of pressure distribution on turbine draft tube.

Thus, it is necessary to study the impact of vibrational effect due to powerhouse operation on dam body taking into consideration dam type, powerhouse type and turbine type. Studies focusing on the modeling of dynamic behaviors and hydraulic performance

of embankment dams are essential to improve dam safety. However, the effects of both seismic and vibration due to powerhouse operation on dam bodies were not found in a single study.

In the present research, the impact of both vibrational effect due to powerhouse operation and earthquake on dam embankment will be studied by considering various reservoir and turbines conditions.

1.3 Research objectives

The main objective of this research is to provide a comprehensive assessment of selected dams including the dynamic behavior of embanked dams and hydraulic performance of reaction turbines represented by 3-D numerical models while the specific objectives are:

1. To develop 3-D numerical turbine models to improve the hydraulic performance of reaction turbines by reducing pressure fluctuation in the turbine draft tubes.

2. To investigate the dynamic behavior of embanked dam due to earthquake effects for different water levels and foundation types.

3. To optimize the turbine operating system by connecting the turbine model with the dam model in order to minimize stresses in dam body and increase dam safety.

1.4 Scope and limitation of the research

In this research, investigations due to vibrational effects on large embankment dams both rockfill and earth-fill dams with powerhouse were conducted. Haditha dam, Ambar Governorate, Iraq, which is an earth-fill, dam and Temenggor dam, Perak state, Malaysia, which is a rock fill dam, are taken as case studies. Moreover, the powerhouse was constructed within dam body at Haditha dam while the powerhouse in Temenggor dam

was constructed at a separate location from the dam body. The scope and limitations of the study include the followings:

1. To decrease the pressure fluctuations in the draft tubes of the studied dams turbines units, submerged weirs in three different heights (i.e., 1/6, 1/3, and 1/2 from the draft tube outlet height) are proposed.
2. The type of the reaction hydraulic turbine in the powerhouse of Haditha dam is vertical Kaplan turbine, while a vertical Francis turbine is used in the Temenggor powerhouse.
3. Three assumptions for dam foundation depths were adopted and these are fixed and deep foundations which equal to dam height as suggested by Fenves & Chopra (1985), and shallow foundation which is equal to 8% and 35% dam height. The later foundation condition is suggested by the present study.
4. The dams embankments and their foundations are considered homogeneous.
5. A 3-D finite element numerical model for the two embanked dams was developed using ANSYS® software while ANSYS CFX software was used to develop 3-D finite volume numerical model with one turbine unit for each powerhouse.
6. Minimum, maximum and empty water levels in the reservoirs were considered in the dam embankment modeling.
7. The discharge ranges data were obtained from site visits but flow velocity and pressure distribution under different loading cases were determined using the k-ε turbulence model.
8. The physical properties (mass density, bulk modulus of elasticity, Poisson's Ratio and damping coefficient) of the flowing water are defined and the model input includes inlet velocity, outlet pressure, and rotational turbine speed and these are changed according to the upstream and the downstream water levels and discharge ranges.

1.5 Significant of research

This study focuses on improving the safety of embankment dams by considering the effects of both seismic and vibration due to powerhouse operation on dam bodies since combining the effects of both seismic and vibrational effect from dam powerhouse in a single study was found missing in the literature. In order to minimize stresses in dam body and increase dam safety, this research optimizes the turbine operating system by integrating turbine and dam models. The types of the dam covered in the safety simulation works include both earth-fill and rockfill dams. Two types of powerhouses are considered; namely within and outside the dam bodies. The types of reaction turbines in the powerhouses are also different. A Vertical Kaplan turbine is used with powerhouse located in the dam body while a Francis turbine is used for powerhouse located outside the dam body.

The above details make the present research significant and increase its importance when compared with other studies in this field.

1.6 Thesis outlines

The foregoing objectives of this study are met in the following manner. The first chapter of this Ph.D. thesis provides a comprehensive introduction to the research which identifies the research motivations and problem statement, objectives, scope and contribution and outline of the thesis.

Chapter 2 presents an overview of the dam classifications and turbines types in addition to numerical modeling and an extensive literature review of previous studies conducted within the conducted research. Finally, the contribution that bridge the literature gap is presented in this chapter.

Chapter 3 provides a full detail of the dam and turbine formulations including, power stations, description of the inspected dams, and the dynamic analysis of the turbines. The

methodology concept of the numerical modeling is provided. Also, the analytical procedure, fluid-structure interaction, boundary conditions, and turbine vibration modeling are exhibited.

Chapter 4 discusses the stated objectives of the thesis. The modeled application is deliberated and analyzed in this chapter. Several outcomes are displayed and debated to meet the goal of the research goals.

Finally, chapter 5 presents the findings and contributions of this research and proposes several recommendations for future research.

CHAPTER 2: LITERATURE REVIEW

2.1 General

Vibration caused a problem in many mechanical and civil engineering projects. For example, wind load, earthquake, and water wave loading cause vibration in many hydraulic structures such as bridges structure, gates of lock navigations, dams and hydropower plants. The literature on dam and powerhouse reviewed in this study as a case study.

2.2 Dams classification

There are many classifications of dams in the world, but there are no clear and limited determinations and the classifications that include several criteria. Some of them are basic and each classification has branches according to the function, form, size, and construction materials. We will discuss the vibration effects on each type of dam, powerhouse, and turbines.

Almost all dams in the world were built based on several factors and with the participation of several teams, including structural, hydraulics and hydrology, geotechnical, and environmental engineers. The preliminary and common design for the dams has to provide risk-free storage of water and structurally stable against sliding, overturning, and in keeping with the reservoir basin, must be watertight and the seepage from the foundation of the dam should be minimal (Akkermann et al. (2009) and Narita (2000)). Based on the construction material, the dams are classified based on the materials used in their construction; either excavated or got from the dam site.

Dams have been an essential part of critical infrastructures in a society that contribute to social development and prosperity. They are built for a number of purposes, including flood control, irrigation, hydropower, water supply, and recreation (Doyle et al. (2003)). On the other hand, dams hold a potential risk of failure due to several technical and safety

problems. Dam failures are considered as one of the major "low-probability, but high-loss" events. The floods resulted from dam failures can lead to devastating disasters with tremendous loss of life and property. This is particularly concerned the densely-populated areas. Hence, professionals experienced in the field of dam engineering have developed and explored new aspects on design, construction, operation, and maintenance of dams to improve the safety of dams (Luo et al. (2012)). However, many existing dams still pose increasing hazards to the downstream areas due to structural deterioration, inadequate design, faulty construction, and poor operation and maintenance. These dams are referred to as distressed dams.

Based on the structure and materials used in construction, dam categorized into several types such as earth-fill, rockfill, concrete, or masonry dam that relies on gravity, arch, or buttress resistance (Foster et al. (2000)). Some dams are even constructed with a combination of different structures or materials. Dams of earth-fill or rockfill materials are called embankment dams, which is the most important type of dams. They can be built on a variety of foundations, ranging from weak deposits to strong rocks. A dam project usually encompasses several components, including water-retaining structure (e.g., dam), water-releasing structure (e.g., spillway), water-conveying structure (e.g., conduit), and hydropower generation (e.g., power plants)

2.2.1 Embankment dams

The embankment dams can be outlined as dams constructed from the usual substances excavated or obtained from another dam site (Narita (2000)). The common substances are positioned and compacted in layers without the addition of any binding agent. The two foremost types of embankment dams that are generally built include:

2.2.1.1 Earth-fill dams

In this type of dams, compacted soil is used for constructing the bulk of the dam body. An earth-fill dam is built primarily from chosen engineering soils compacted uniformly and intensively within the thin layers and at a controlled moisture content. This dam type resists the imposed forces by a combination of arch and cantilever actions. One of the crucial long-established sections designed for the earth-fill embankment dams is shown in Figure 2.1.

Figure 2.1: View of Lentini earth-fill dam (Castelli et al. (2016))

2.2.1.2 Rock-fill dams

In this type of dams, the bulk of the dam is a product of coarse-grained gravels (crushed rocks or boulders) with an impervious core of compacted earth-fill or a slender concrete. The natural sections of rock-fill dams are shown in Figure 2.2. The stability of a rock-fill dam included the frictional forces in between each and every piece ofrock gravel which ensures its safety in opposition to the sliding sort of failure during earthquakes.

Figure 2.2: View of a rock-fill dam (Xavier (2012))

2.2.2 Concrete dams

The mass construction of concrete dams began from about 1900 due to the ease of their construction and to suit complex designs like having spillway or powerhouse inside the dam body (Ali et al. (2012)). Since 1950 and onwards, mass concrete was bolstered with the aid of making use of further substances like a slag or pulverized gas-ash as a way to reduce temperature induced issues or preclude cracking and to cut back the total cost of the project. Many types of concrete dams are described and classified based on their shape, as shown below:

2.2.2.1 Gravity dams

A gravity dam relies entirely on its mass for stability. The gravity dam is triangular in shape but for useful purposes, is modified on the top, as shown in Figure 2.3.

Some gravity dams are curved, with the curvature positioned towards the upstream. It's generally due to aesthetic and other reasons other than having an arch action for providing greater stability. The gravity dam resists the imposed forces by its own weight

and is usually designed so that every dam block is stable and independent of any other blocks (Hariri-Ardebili & Seyed-Kolbadi (2015)).

Figure 2.3: View of gravity dam (Yamaguchi et al. (2004))

2.2.2.2 Buttress dams

These dams included a steady upstream face supported at normal intervals by using buttress partitions on the downstream part (Figure 2.4). These dams are lighter than the stable type of dams, however, they are likely to produce larger stresses at the foundation (Ghaemmaghami & Ghaemian (2008)). The dam wall may be flat or curved and the hydrostatic pressure is transferred to the foundation through the slab.

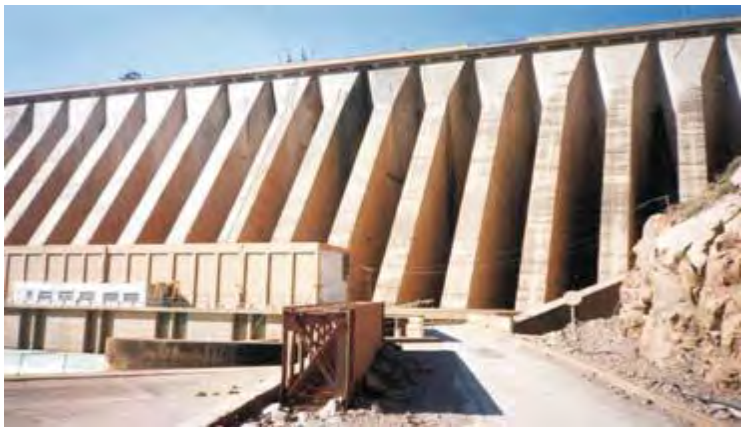

Figure 2.4: Downstream view of Sefid Rud buttress dam, Iran (Wieland (2010))

2.2.2.3 Arch dams

These dams have large upstream curvatures in their plan and depend on an arching action on the abutments by the way it passes most of the water load on the walls of the river valley (Figure 2.5). This type of dam is structurally more efficient than the gravity dams and commonly reduces the volume of concrete required. They resist the imposed forces by a combination of the arch and cantilever actions (Akbari et al. (2011)).

Figure 2.5: View of Englebright Dam and Reservoir (James (2005))

2.2.3 Classification based on dam size

Dams can be categorized by their sizes. The class of the scale can be determined by the height or storage of the dam. The height and storage of a dam shall both be situated with respect to its maximum storage potential measured from the common mattress of the natural bed to the maximum water storage elevation. For the cause of determining the size category, the highest water storage elevation shall be considered to be the height above the streambed, as outlined in Table 2.1.

Table 2.1: Dams classification based on dam size

Category	Storage (ac-ft)	Height (ft)
Small	<1000	<40
Medium	≥1000 and ≤50000	≥40 and ≤100
Large	≥50000	>100

Where ≥ is more than or equal and ≤ is less than or equal

2.2.4 Classification based on rigidity

These types are classified as the rigid dams which are constructed from stiff materials such as concrete, masonry, steel and timber. The non-rigid dams are relatively less stiff compared to a rigid dam and deform slightly when subjected to water effects and other forces. The dams constructed from earth and rock-fill are non-rigid dams and they have relatively large settlements and deformations. A rockfill dam is neither fully rigid nor fully non-rigid. They are sometimes classified as semi-rigid dams.

2.2.5 Classification based on vibration effect

Based on the vibration effects on dams, it is important to make a new classification to show the vibration effect on each type of dam and how to reduce this phenomenon by making a suitable model to analyze the danger of vibration on each type. Here, a new classification can be categorized according to the vibration effect on dams.

2.2.5.1 Embanked dams (large, medium, small)

The embanked dams are classified according to the constituent materials of dam body that can be adversely affected by the vibration phenomenon, coupled with the influence of forces acting, dam size, and its location. The vibration phenomenon is analyzed by making a 2D or 3-D model of the dam-foundation-reservoir system based on its components and the existing foundation with the upstream reservoir, considering the dam size and location. The study of the vibration influence on dams is considered as a

supplement to the study of dam stability. Also, it must know the design standards of the dam components and the limitation variables for it such as stress, strain, deflection, and deformation; must also compare the 2D or 3-D numerical model results with the measured data gotten from the dam site.

2.2.5.2 Concrete dams (large, medium, small)

These dams are classified based on their shapes (arch dam) and the connections between the parts of the dam body (gravity and buttress dams). These dams are affected by high vibration. To analyze vibration influence on these dams, it is necessary to know the constituent materials of the dam, and the foundation properties, and also make a suitable model to find out the connections between the concrete parts of dam body and the foundation and make a comparison between the results of the model with the standards limitations of stress, strain, deflection, and deformed shape. In addition to the embanked dam, it must find out the location of cracks in the concrete and test it if it acceptable or not consider the dam location (if it within the line of earthquakes and the stability of the dam).

2.2.5.3 Combined concrete-cum-earth dam

This type consists of concrete parts, mostly includes the important components of the dam (the powerhouse and the spillway).

In this kind, it must collect the first and second kinds, taking into consideration the existence of the powerhouse and the spillway, and its influence on operating the model and how to deal with the different parts in the material (concrete, soil components) to get the best results that are near to reality.

2.3 Powerhouse

A powerhouse transforms the potential energy of a mass of water flowing in a river or stream with a head. The potential annual power generation of a hydropower project depends on the available head and discharge of water. Powerhouse plants use a relatively simple concept to convert the potential energy of the flowing water to run a turbine, which, in turn, provides the mechanical energy required to drive a generator and produce electricity. The main components of a hydropower plant are shown in Figure 2.6.

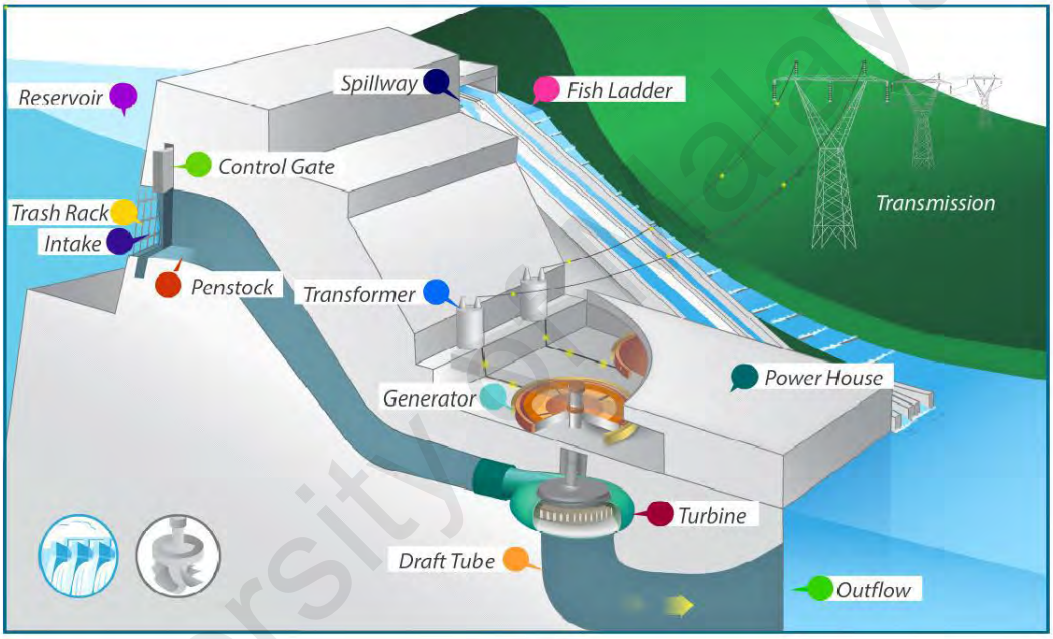

Figure 2.6: Main parts of hydropower station (Avakyan (2017))

In this research, the focus is the interaction between the hydropower plant component and the dam itself. powerhouse plant is the harnessing of energy from Earth's hydrological cycle for the generation of power. The hydrological cycle is driven by solar radiation, through the evaporation of water, primarily from Earth's oceans. This vapor then travels through the atmosphere, and about one-fifth of it is deposited on land in its liquid phase, by means of precipitation (Kumar & Saini (2010)). The remaining falls over the oceans. Water which falls on land is then driven back towards the oceans by gravitational forces. Some of the energy in the flow of river water can be extracted, and

it is this portion of the energy contained in the hydrological cycle which can be used to generate hydropower.

Hydroelectric power is a clean, renewable, and highly efficient source of electricity generation, with an enormous potential for improvement and expansion. The hydro-plant design is a site-specific because the flow resources at any location are the main factors determining how much energy can be extracted from the water. The two main flow resource parameters for a potential plant's energy-producing capacity are the river's hydrostatic head and its flow rate. The variability of sites has resulted in plants which generate less than 5 kW of power to the 22.5 GW of Three Gorges Dam in China (Stone (2011)). This specificity provides a unique challenge to engineers in each hydropower project.

2.3.1 Classification of powerhouse facilities

Conventional powerhouse plants can be classified into three types of facilities. These are run-of-river, storage and pumped storage plants (Gielen (2012)). In short, run-of-river powerhouse plants do not store river water in a reservoir but allow it to flow through the generating units as it would flow through a river. Storage plants have a reservoir to allow for more adaptation to electricity demands. Whereas, the pumped storage plants have a reservoir but can also operate in reverse through pumping water back into the reservoir to be stored for when demand is higher. The run-of-river plants required to deal with the variability of flow conditions on generation in which storage plants are not as vulnerable. The increased control of water by a storage plant results in a greater environmental impact than that caused by run-of-river plants.

2.3.1.1 Run-of-river

A run-of-river powerhouse plant transforms the water energy to electrical energy mainly from the water flows on the river (Figure 2.7).

This type of powerhouse plant could include some brief-time period of storage however, the production of electrical energy will vary depending on the local river flow conditions. As a result, the generation depends on the precipitation and runoff. The run-of-river powerhouse plant will have more viable generation profiles, especially when situated in small rivers or streams that experience a wide flow variation. In the run-of-river powerhouse, parts of the river water might be diverted to a channel or pipeline (penstock) to connect the water to a hydraulic turbine which is joined to an electricity generator.

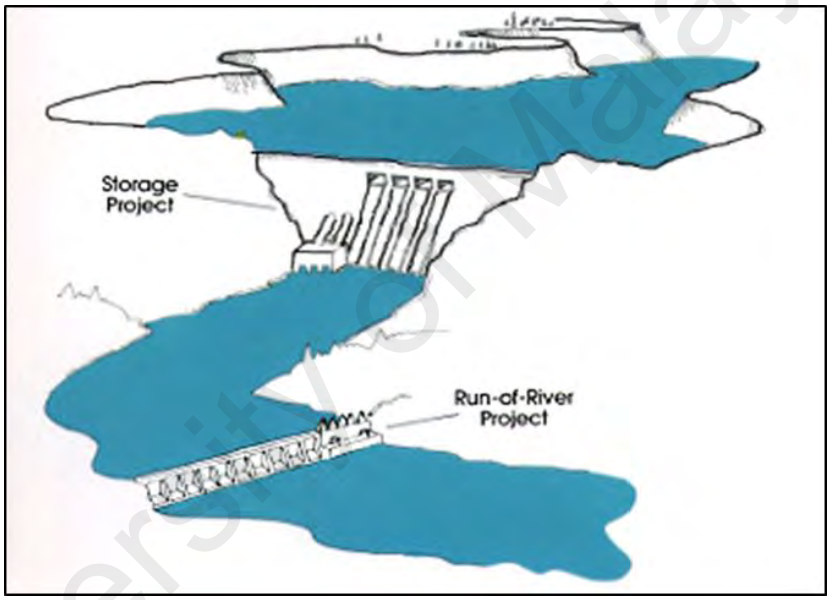

Figure 2.7: Storage and run-of-river powerhouse (Anagnostopoulos & Papantonis (2007))

2.3.1.2 Storage powerhouse

Powerhouse projects with a reservoir (as shown in Figure 2.7) are also defined as storage powerhouse in the view that they store water for later consumption. The reservoir reduces the dependence on the range of influx. The powerhouse stations are located at the dam body or downstream (separated) and connected to the reservoir via tunnels or pipelines (penstock).

2.3.1.3 Pumped storage powerhouse

A pumped storage plant is a plant that pumps water from a downstream reservoir to the upstream reservoir instead of the storage, and this form does not signify an energy source, as shown in Figure 2.8. As a rule, during the off-peak hours water discharge is reversed to generate electrical energy for the duration of the daily peak load period.

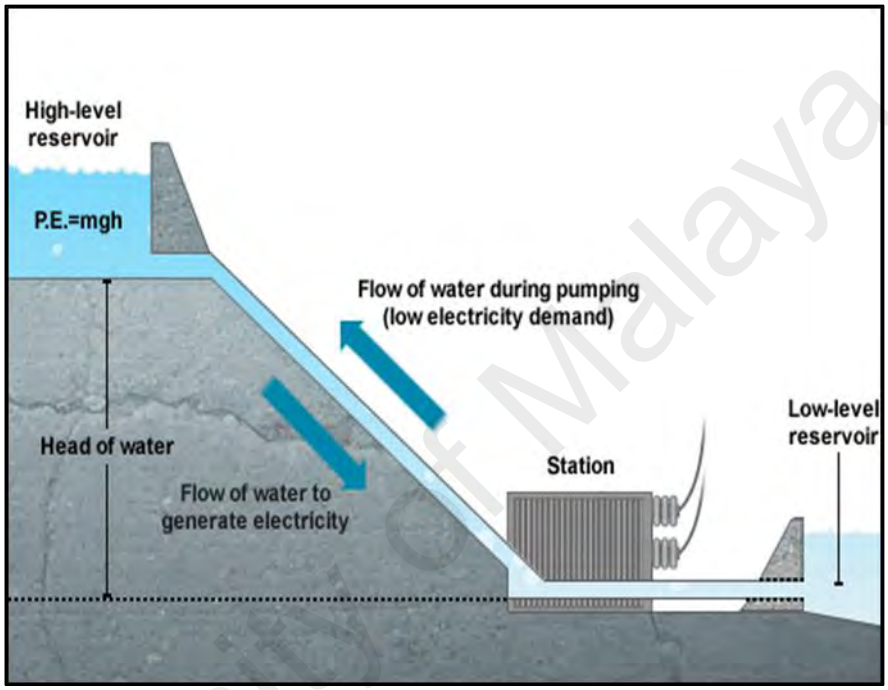

Figure 2.8: Pumped storage powerhouse (Suul et al. (2008))

2.3.2 Main components of a powerhouse plant

Most powerhouse plants rely on a dam that holds back water, making a large water reservoir that can be utilized as storage. They may also be a part of the dam body or constructed separately and located at the downstream of the dam.

The essential constituent part of the dam has to be identified as dam physique material, the form of the dam, spillway and powerhouse locations with types and sizes, quantity and type of turbines with inlet and outlet locations, length of penstock and draft tube, and purposes of dam construction.

2.3.2.1 Intake, penstock, and surge chamber

Gates on the upstream face of the dam open and deliver water through the penstock (a cavity or pipeline) to the turbine. There is often ahead race before the turbine. A surge tank is used to cut down water strain that could possibly harm or result in increased stresses on the turbine.

2.3.2.2 Turbine

The water strikes the turbine blades and run the turbine which is connected to a generator by means of a shaft. There is a range of configurations feasible with the generator above or subsequent to the turbine. Essentially, the most customary types of turbine for powerhouse plants in use in nowadays are Drtina & Sallaberger (1999):

i. Impulse turbines: This type of turbine shown in Figure 2.9 issues jets of water from a nozzle at a high speed and affect the sequence of the blades. The kinetic power of water is transferred by way of momentum to the rotating wheel (Cobb & Sharp (2013)), and the strain, on the other hand, is transferred to the inlet and the outlet.

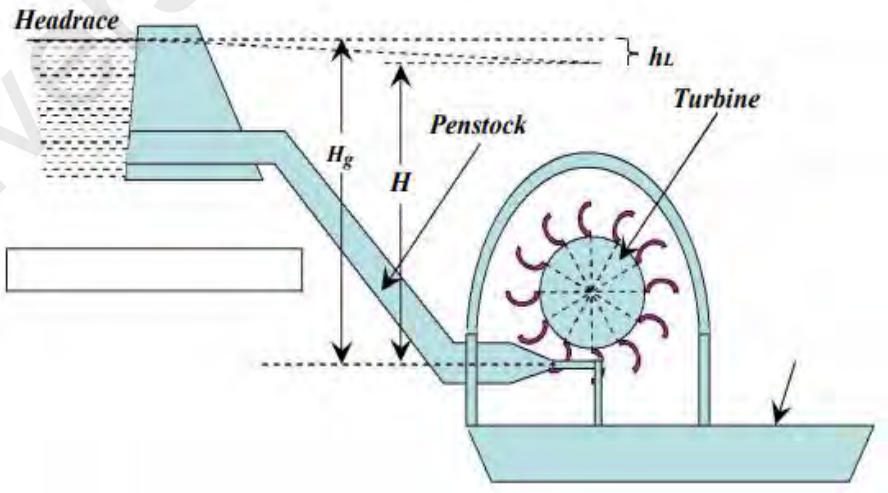

Figure 2.9: Impulse turbines (Cobb & Sharp (2013))

ii. Reaction turbines: This type issues water from the upstream of the dam and transports it through the penstock under pressure to the turbines within the powerhouse which has been installed in different directions depending on the site

topography, the head of water, and the discharge (Paish (2002)). The types of reaction turbine are Francis turbine and Kaplan turbine outlined in Figure 2.10.

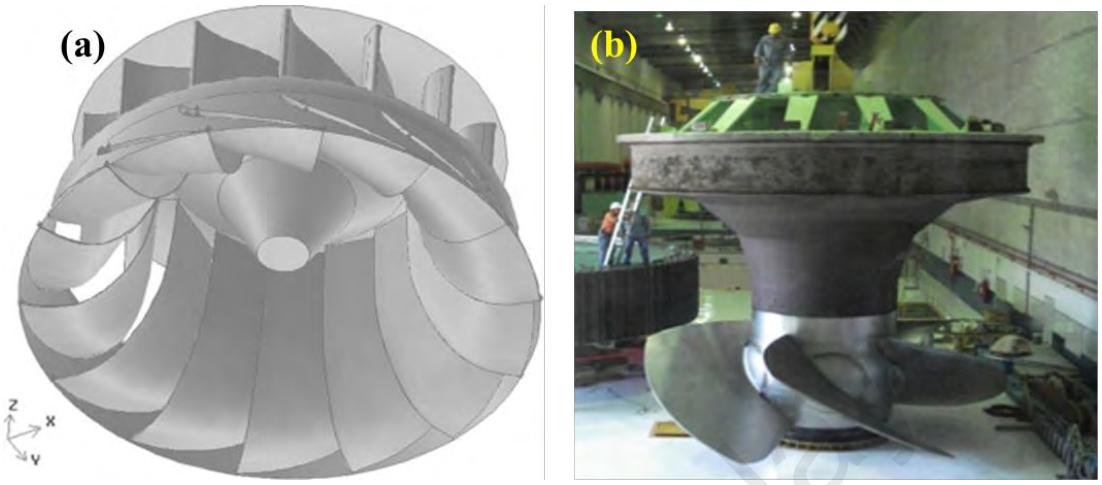

Figure 2.10: Illustration of two primary classes of reaction turbines a) Francis turbine (Negru et al. (2012)) and b) Kaplan turbine (Urquiza et al. (2014))

In a hydraulic turbine, the water is directed to the turbine from the headwater via the penstock and then discharged into the tail water. Inside the turbine, the energy of the water is converted into mechanical energy of the rotating shaft via the runner. The shaft rotates the rotor of the generator, where the mechanical energy is finally transformed into electricity and supplied to customers. This permits the runner to utilize all components of the water-energy (i.e., both pressure energy and kinetic energy). The choice of an appropriate turbine configuration (i.e. the characteristic parameters head, discharge, speed and runner diameter) depends on the local situations of the powerhouse plant and its desired operating regimes. In general, however, Kaplan and Francis turbines are designed for low, medium and high heads, respectively. These characteristics describe the turbine performance for a set of characteristic parameters (e.g., head and discharge since speed and diameter are under normal condition maintained constant).

The efficiency of a reaction turbine is significantly affected by the performance of its draft tube. Especially, at low heads and high flow rates are the draft tube losses

considerably large. Its main purpose is to recover some of the kinetic energy (velocity) leaving the runner into pressure energy which without the draft tube would be pure losses. Therefore, the main shape of the draft tube is essentially a diffuser. In addition, it enables to place the turbine above the tail water without losing head and to redirect the flow into the tail water (Moradi et al. (2013) and Ribeiro et al. (2012)). The draft tube is furthermore one of the most challenging parts to describe from a fluid flow perspective. This is due to the interaction of many complex flow features such as unsteadiness, turbulence, separation, curvature streamline, secondary flow, swirl, and vortex breakdown

2.3.2.3 Generators, transformers transmission lines and outlets

The shaft of the turbine is connected to the generator shaft and as the turbine blades turns, the rotor inside the generator also turn and produce an electrical current as magnets rotate within the constant-coil generator to provide alternating current (AC).

The transformer inside the powerhouse converts the AC voltage into a larger voltage for an efficient long-distance transport. While, the transport of the generated electricity to a grid-connection factor is performed through the transmission lines. The electrical power is transformed back to a lower voltage and fed into the distribution network.

The used water is rechanneled back into the river through pipelines referred to as tailraces. The outlet approach might also include “spillways” which allow the water to bypass the generation system and be “spilled” in times of flood or very high inflows and reservoir levels.

2.4 Finite volume method

Finite volume (FV) approach uses the integral form of the transport equations of mass, momentum, energy, turbulent quantities and species. In this method, first, the computational domain is divided into a finite number of cells for which the conservation

laws are applied. The key step of (FV) that ensures the conservation consists of the integration of transport equations over the control volumes (cells) shown in Figure 2.11. For a passive scalar quantity, the general transport equation in an unsteady flow is expressed in the conservative form as below (Versteeg & and Malaskekera (2007)):

$$\frac{\partial}{\partial t}(\rho\phi) + \nabla.\rho\phi\,\vec{U} = \nabla.\Gamma\nabla\phi + S_\phi \tag{2.1}$$

the left side of the formula indicates the unsteady (temporal) and convective terms and the right side represents the diffusive and source terms, respectively. This is similar to the Navier-Stokes equations. In the above equation (2.1), represents the diffusion coefficient. By performing volume integration on both sides of the above equation and applying the Green's divergence theorem to the volume integrals of the convective and diffusion terms, the following equation is obtained, which is the skeleton of the FV formulation:

$$\frac{\partial}{\partial t}\int_{CV}\rho\phi dV + \int_{CS}\vec{n}.(\rho\phi\,\vec{U})dS = \int_{CS}\vec{n}.(\Gamma\nabla\phi)dS + \int_{CV}S_\phi dV \tag{2.2}$$

The second term on the left-hand side and the first term on the right-hand side of the equation indicate the convective and diffusive fluxes crossing the cell control surfaces, respectively. The equation can be interpreted as the flux conservation law; therefore, the conservations are satisfied by default in the FV. This characteristic of the FV makes the method an appropriate choice for the fluid flow transport problems in general and especially in the problems involving discontinuities like shock waves; where the flow variables are not differentiable across the discontinuities but mass, momentum and energy are still conserved.

After obtaining the integral form of the transport equation, in the next step of FV, the derivatives appearing in the integral equation are replaced by some approximate expressions. In this regard, traditionally finite difference approximation based on the truncated Taylor series expansion is utilized, although other possibilities such as using

shape functions similar to the finite method can also be used for this purpose. The latter creates a class of hybrid methods named 'finite-volume-based finite-element' method.

By performing the integration over all cells present in the computational domain, finally, a set of algebraic equations is obtained which is nonlinear in the case of Navier-Stokes equations. To treat the nonlinear convective term in the momentum equations and obtain a linear set, usually some lagging or linearization techniques (e.g., Newton-Raphson linearization are typically utilized). The resulting set of equations can be solved by well-designed efficient solvers along with speed-up strategies like multi-grid algorithms and conjugate gradient methods.

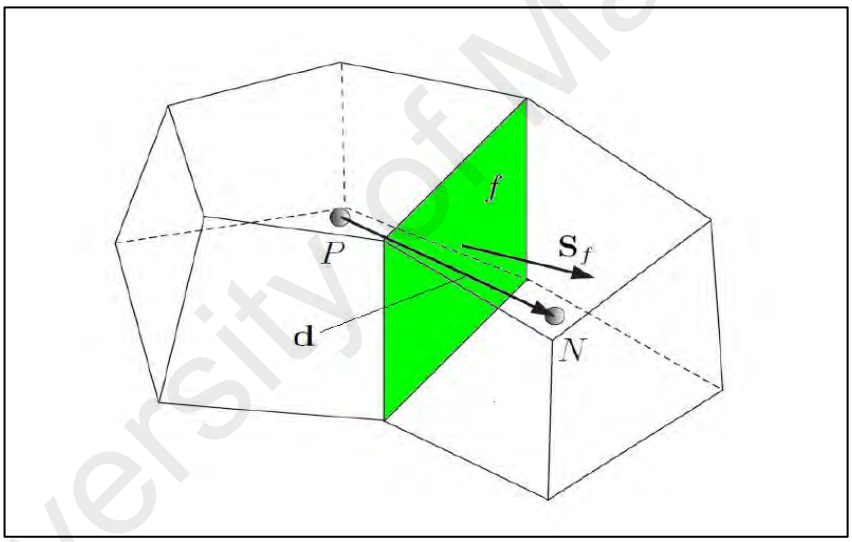

Figure 2.11: Control volumes in the finite volume method used for the discretization (Versteeg & and Malaskekera (2007))

The method can be applied to the unstructured mesh and more importantly, it can ensure the conservation in all computational cells and as a result in the whole domain. It should be mentioned that the accuracy of (FV) directly depends on the type of schemes used for the spatial and temporal discretization of the terms in the integral equations.

In general, in FVM, the information of physical quantities of the flow field like velocity, pressure and turbulent quantities can be stored on faces, grid nodes or cell centers.

2.5 Computational fluid dynamics

The computational fluid dynamics (CFD) is a comprehensive name for all sorts of numerical flow analysis, including basic scientific studies as well as industrial products and process developments. The CFD codes are today available in commercial packages and are continuously under development. In the CFD codes, the investigated flow is described by a set of partial differential equations (PDE), which generally cannot be solved analytically except in special cases; instead, they are approximated by a discretization method into a system of algebraic equations which can be solved at discrete locations in space and time. The most common method for this purpose is the finite volume method (FVM). Other available approaches are the finite difference method (FDM), the finite element method (FEM) and a hybrid control-volume-based finite element method (CV-FEM) (Ferziger & Peric (2012)). The main difference between the FVM and CV-FEM methods is that the pressure gradient and diffusion term in the Navier-Stokes equations are discretized with shape functions (linear) instead of a different scheme in the latter method. In this thesis, only the FVM method will be described briefly due to the similarities, although both the FVM and CV-FEM methods have been used in this work (CFX-4 and CFX-5 from ANSYS, respectively).

In the FVM method, the flow domain is discretized into a finite number of small cells, usually having hexahedral and/or tetrahedral shapes (structured and unstructured grids, respectively). The governing equations are integrated over each cell, such that the nodal average quantities are conserved within each cell. A difference scheme is then used to express the surface and volume integrals in terms of the nodal values. First, the integrals

are approximated, then, a difference scheme is used to express the integral approximations into nodal values. In order to preserve the accuracy, the order of the integral approximation must be at least of the same order as the difference scheme. Usually, a second order accurate scheme is used to avoid numerical diffusion. As a result, one algebraic equation is obtained for each cell in which the average cell value can be calculated from neighboring nodes. The resulting system of the algebraic equation is finally solved with an iterative method since the equations usually are non-linear. Two types of solvers exist, segregated or coupled solvers, depending on how the pressure-velocity coupling is incorporated into the Navier-Stokes equations from the Poisson equation. A segregated solver often utilizes a pressure-velocity correction approach to satisfy the continuity equation, whereby the pressure and velocities are solved separately. A coupled solver incorporates instead the pressure-velocity coupling into the continuity equation by introducing a pressure redistribution term, whereby the pressure and velocities are solved simultaneously. To avoid checkerboard oscillations, a staggered grid or a collocated grid with Rhie-Chow interpolation scheme is normally employed in both solvers (Ferziger & Peric (2012)).

2.6 Vibration effect on dam body

The dynamic behavior of embanked dams must be evaluated by analyzing the seismic influence on the dam in consideration of the interaction effect of the dam–reservoir–foundation system. These interactions are complicated by the many assumptions and factors involved in analyzing the performance of embanked dams (Yilmazturk et al. (2015)). These factors include the foundation/dam modulus of elasticity ratio, the dam-reservoir-foundation material damping, and the bottom absorption with reservoir compressibility. Such an analysis is normally conducted using either one or a combination of theoretical analysis, field testing, and finite element (FE) modeling.

Studies over the past several decades found that earthquake vibrations exert various effects on dams depending on the dam's size, shape, body material, and location from the seismic load. These studies can be divided into three groups depending on the development of the programs used to analyze the effect of earthquakes on dams. Early studies used monitoring charts for various parameters that can be used to determine the seismic effect on dams (Gazetas & Dakoulas (1992)). The peak values of these parameters and the theoretical method were used to evaluate the dynamic behavior of embanked dams.

2.6.1 Earliest dam studies

A study has been conducted for the analysis of earth-filled dam by (Gazetas et al. (1981)). In 1992, Gazetas and Dakoulas analyzed the vibration effect on rock-filled dam depending on the diagrams presented by the effect of vibration, represented by the accelerations, displacements, shear strain and seismic coefficients with time. The authors discussed changes in these parameters with the change of the depth, starting from the crest of the dam. Finally, a dimensionless graph was used in primary engineering designs to determine the peaks of the parameters.

Th variation of the accelerations, displacements, and strain to be experienced by a dam during an earthquake can be used to evaluate the maximum acceleration and predominant frequency. Figure 2.12 shows the top view of a dam with details.

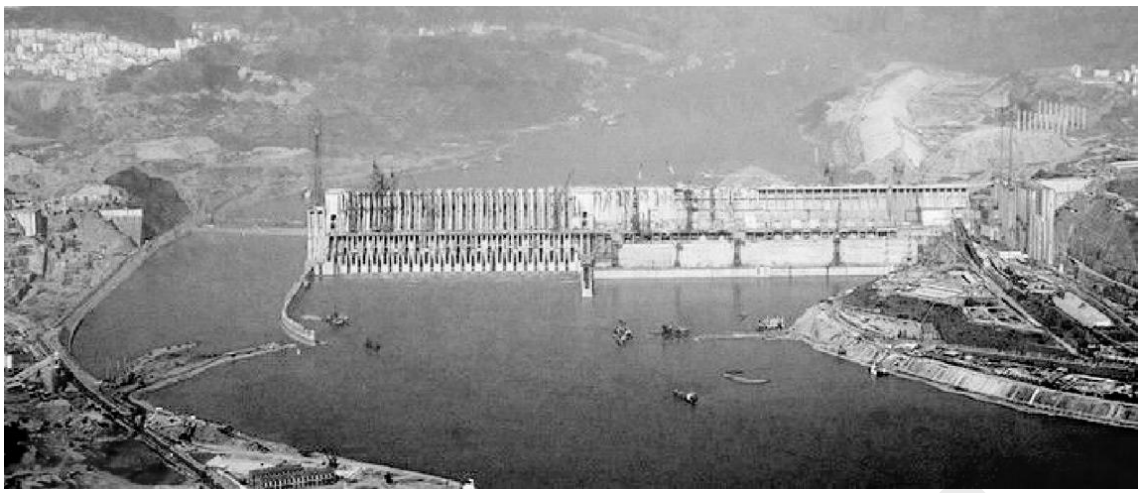

Figure 2.12: Downstream view of a dam with details (Liu et al. (2003))

(Fenves & Chopra (1985)) simplified the analysis procedure of the fundamental vibration mode response of concrete gravity dam systems for two cases: (a) dams with reservoirs of impounded water supported by a rigid foundation rock, and (b) dams with empty reservoirs supported by a flexible foundation rock. The dam model was presented as a single-degree-of-freedom system, showing the frequency-dependent hydrodynamic terms or foundation-rock flexibility terms, the maximum earth-quake-induced deformations, and the equivalent lateral forces that can be computed. In another investigation, (Bouaanani et al. (2003)) found a numerical technique based on the procedure derived by Fenves & Chopra (1985) to calculate the earthquake influence which includes the hydrodynamic pressure on the rigid gravity dams, by suggesting closed-form formulas used to solve fluid–dam interaction problem. The dam-reservoir interaction effect is represented by one of the following three assumptions:

1. The physical properties of the water that represents the mass of the reservoir added to the dam are defined.
2. The dam-reservoir interaction is described using the Eulerian approach (N. Bouaanani & Paultre (2005)). The variables used are the displacements in the dam, as well as the velocity and pressure potential in the water.

3. The dam-reservoir interaction is represented by the Lagrangian approach. The dam–reservoir behavior is expressed in terms of displacement and functions, with some constraints suggested excluding the zero-energy mode (Birk & Ruge (2007), N. Bouaanani & Lu (2009) and Lotfi & Zenz (2016)).

2.6.2 2D dam modeling

Considering the complexity of the dam–reservoir–foundation geometry, most later studies used 2D numerical models to analyze the seismic effect on the dynamic behavior of concrete dams (Khosravi & Heydari (2013), Lotfi (2003), and Shariatmadar (2009)) and embanked dams (Gui & Chiu (2009) and Khazaee & Lotfi (2014)). Most of these studies depend on the FE method.

Lotfi (2003) studied the seismic effect on gravity dams by using a MAP-76 program to make 2-D FE numerical model for a pine flat dam as verification example. The proposed technique was done by separating the model approaches in the time range to find the frequency for the dam and reservoir separately. The maximum principal tensile and compressive stresses decreased by 2.2 and 1.8 % respectively, by doubling the number of modes utilized over the initial case. Two years later Shariatmadar (2009) created 2D FE numerical to analyze the seismic effect on concrete gravity dam. The mode, shape, and hydrodynamic pressures of twenty 2D FE concrete gravity dam models were analyzed and calculated using ANSYS considering the dam-reservoir-foundation interaction mentioned below:

1. Fixed-base dams with empty reservoirs
2. Fixed-base dams with full reservoirs
3. Rock-base dams with empty reservoirs
4. Rock-base dams with full reservoirs

The conclusion of the results showed that the hydrodynamic pressures reduced by the bed rock foundation assumption. Wang et al. (2011) used the ABAQUS software to generate a 2D FE numerical model that represents a gravity dam and a part of its reservoir. The open boundary condition of higher order doubly asymptotic was developed to represent the remaining portions of the reservoir simplified as semi-infinite part with fixed depth. The hydrodynamic pressure at the heel of the dam and the horizontal displacement of the crest under two cases El Centro ground motion were calculated, and the triangular impulse acceleration represents the development for evaluating the hydrodynamic pressure in a semi-infinite reservoir of constant depth.

Khosravi & Heydari (2013) used a hybrid meta-heuristic optimization method to find the best shape of concrete gravity dams, including the dam-water-foundation-bed interaction. A 2D FE numerical model was proposed by using APDL (parametric design Language) program to represent the dam, reservoir and foundation, considering the interaction of the dam-reservoir-foundation system according to the Fenves and Chopra (1985) procedure. The numerical results suggested techniques for gravity dam shape simulation and considered the dam-reservoir-foundation interaction as an important standard for safety design requirements. Miquel & Bouaanani (2013) conducted a 2D FE model using ADINA software to represent a gravity dam. In this study, a new technique was proposed to investigate the earthquake effect on gravity dams by modifying the original input acceleration to get new accelerogram that accounts the fluid-structure interaction effect directly. The principal stress distribution, frequency, and crest displacement were evacuated by changing the dam dimension to find the dynamic behavior of gravity dam. Mehdipour (2013) analyzed a 2D FE numerical model using ANSYS software to find the foundation effect on the seismic behavior of concrete dam, taking into account the assumption of rigid and fixable foundation for dam-foundation interaction. The frequency, stress, hydrodynamic pressure, heal, crest, and toe

displacements were estimated at the beginning (0.005 s) and at the end (7.5 s) of the time to find the change percentage of these parameters. The dam-fluid interaction increases as the effective mass and vibrational frequencies of the dam are decreased.

Anastasiadis et al. (2004) made a 2D model for a high rock-filled dam. In this study, a modal analysis method was performed depending on the mode shapes evaluated for the symmetric part of dam body. The study depended on a special computer program "MAP-76". Subsequently, with the analysis of Pine flat, the dam was considered as a numerical model. This technique was applied to the dam body and the outcomes were compared with results related to direct methods of analysis. Then, the researcher commended the accuracy of the method and the convergence was controlled. A 2D FE model using FLAC2D program was used to assess the dynamic behavior of Renyitan earth-fill dam based on the acceleration record of Chi-Chi earthquake (Gui & Chiu (2009)). The displacement, pore-water pressure, and acceleration due to the seismic effect were evaluated to check the stability of the dam.

2.6.3 3-D dam modelling

With software developments and computer speed improvement, many researchers have analyzed the seismic effect and understand their dynamic behavior by using realistic 3-D FE models instead of 2D models to represent dams (Dakoulas (2012)). Hariri-Ardebili & Mirzabozorg (2011) studied the effect of four water levels coupled with a seismic effect on the dynamic behavior of arch dams. In another attempt, Hariri-Ardebili & Seyed-Kolbadi (2015) developed 3-D FE models to represent three types of concrete dams (gravity, buttress, and arch dams). These two studies clearly defined the 3-D boundary conditions for the dam-reservoir foundation interaction system.

Watanabe et al. (1996) used vibration test on a 3-D elastic model to obtain the dynamic behaviours of a fill dam. The authors developed a computer code used to simulate the

vibration test data to recognize the fundamental modes and check the validity of the code. According to topographical features effect on the dynamic behaviors of the dam, the abutment side slopes, and a bed width of the river were considered in order to test how the Eigen frequency up to fourth order fluctuates depending on each factor with a number of numerical trails using the code. A dimensionless Eigenfrequency and topographical features relation diagrams were presented as the results of the code. In 2007, a research created a 3-D FE model that represents a rockfill dam with a central clay core by using IZIIS software to calculate the nonlinear dynamic behaviors of the dam depending on the Moher-Coulomb failure criterion. The study also evaluated the tension cutoff zones, the plastic deformations, and the stress-shear strain relationship (Mircevska et al. (2007)). The results of this study showed that the 3-D analysis and the nonlinear material treatment of the dam soils represent the fundamentals in the evaluation of the stability of the rockfill dams.

Dakoulas (2012) studied the longitudinal vibration on concrete-faced rockfill dams that cause compressive stresses with a joint opening in the concrete slab panels. A 3-D hyperbolic model for the rockfill used to find the behavior of the dams subjected to longitudinal and vertical vibrations. The analysis considered the flexibility of the rocks and possible dynamic settlements of the rockfill. The dynamic settlements effect was examined and comparisons were made to the response from upstream to downstream and combined vibrations.

Some researchers estimated the dynamic behavior of concrete dams or rockfill dams and verified their results by comparing 3-D and 2D models (Jafari & Davoodi (2004) and Mirzabozorg et al. (2012)). Other researchers compared the model results within situ dynamic test data. However, comparing 2D and 3-D models is not considered a valid strategy to verify the results because both models are prepared by the researcher. In

addition, 2D models represent only one part of the dam and cannot represent irregular dams.

Jafari & Davoodi (2004) performed dynamic analysis using 2D and 3-D models of an embanked dam in ANSYS. The soil properties were calculated based on the situ dynamic tests. The effects of water depth, abutments, and foundation on modal parameters were investigated. The dam-foundation rock interaction was also considered. Yilmazturk et al. (2015) analyzed 2D and 3-D FE numerical models that represent RCC gravity dam by using an EAGD-84 program, and the vertical stress, principal stress, maximum displacement, and frequency parameters were calculated. The 2D and 3-D model results were compared to underline the calculated parameters that were used to evaluate the dynamic behaviours of the gravity dam and should be conducted for seismic safety assessment. Albano et al. (2015) created a 2D and 3-D finite difference models by using FLAC2D & FLAC3-D software to evaluate the dynamic behaviours of a bituminous concrete-faced rockfill dam built in Italy. The dam height was 90 m and the embankment built in a narrow canyon and analyzed in a highly seismic region. The validation of the residual displacement numerical model results with centrifuge test performed on a small model of the dam has proved the rockfill dam to be stable and the largest settlements can occur in the empty reservoir case. Deformation is mostly located in the upper third part of the embankment.

2.7 Vibrations of turbines and powerhouse

The powerhouses represent one of the main parts of the dams used to generate hydroelectric power at a low cost. The detection of the hydraulic characteristics in reaction turbines is a key to finding the effect of turbines operating in the dam body (Pennacchi et al. (2015)). Figure 2.13 outlines the typical system of a hydroelectric dam.

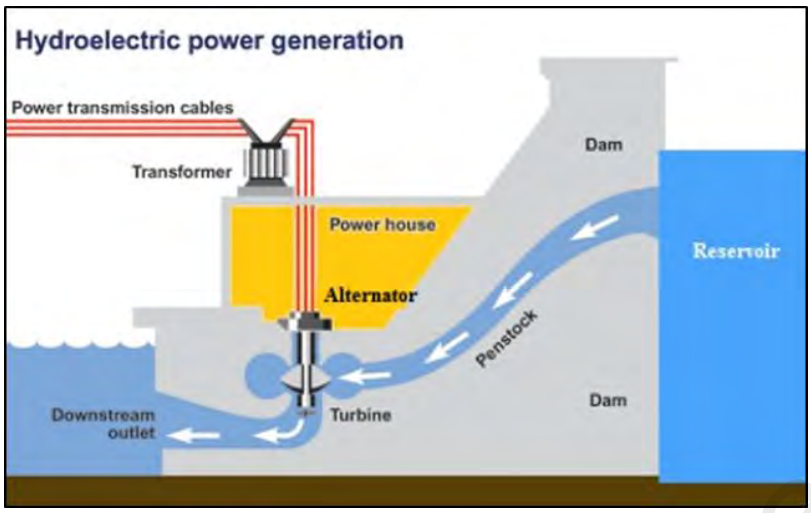

Figure 2.13: Typical system of a hydroelectric dam(Rahman (2003))

The identification of the hydraulic characteristics of Kaplan and Francis turbine units (Pennacchi et al. (2015)) serves as the main engine of a powerhouse. Kaplan and Francis turbines, which are classified as reaction turbines, are difficult to use under part-load operation because of pressure oscillation (Dixon & Hall (2013), Grassmann & Ganis (2005) and Kumar & Saini (2010)). Studies on this topic have presented the solutions for the cavitation problem in draft tubes, the vibration effect in powerhouses caused by the operating turbine, the maximization of power generation, and the generation of low-cost power (Fu et al. (2016) and Pennacchi et al. (2015)). In the last decades, there has been a very noticeable development in the computational fluid tools (Glatzel et al. (2008), Lomax et al. (1999) and Wang (2014)). It has become very efficient to perform a robust and reliable analysis of the flow pattern phenomenon inside the turbine structure.

2.7.1 Francis turbine modeling

Based on the literature, numerous studies have been conducted utilizing those tools to simulate the flow behavior in the draft tube of turbine sand inspect the critical conditions such as the vortex rope and vibration (Kumar & Saini (2010) and Thapa et al. (2012)). Researchers have studied pressure pulsation in Francis hydraulic turbine units and

discussed the cavitation phenomenon problem (Iliescu et al. (2008) and Stein et al. (2006)).

Jošt & Lipej (2011) built a 3-D numerical model for a Francis turbine unit to predict vortex rope in the draft tube based on numerical flow analyses by performing two analyses (i.e., without and with cavitation effects). Another study performed a numerical analysis of the cavitation turbulent flow in a Francis turbine under partial load operation using the k–ω shear stress transport turbulence model in the Reynolds-averaged Navier-Stokes equations (Lai et al. (2012). Qian et al. (2007)) simulated 3-D multiphase flows in a Francis turbine to calculate pressure pulsation in the spiral casing, draft tube, runner front, and guide vanes using fast Fourier transform. The investigation of the hydrodynamic effects of pressure fluctuation in the draft tube was studied by Anup et al. (2014). The cause of rotor-stator interaction simulation under partial load operation using analyzing 3-D transient state turbulence flow simulation in a Francis tube was investigated. The 3-D Navier–Stokes computational fluid dynamics (CFD) solver ANSYS CFX was used to analyze the flow through a vertical Francis turbine with different loads in situ. Most lately, Luna-Ramírez et al. (2016) calculated the pressure on the blades of a 200 MW Francis hydraulic turbine to locate the failure on the blade surface based on CFD. There are also several other studies conducted on the Francis turbine analysis through the advantages of the computational features (Gebreslassie et al. (2013), Minakov et al. (2015), Negru et al. (2012) and Trivedi et al. (2013)).

2.7.2 Kaplan turbine modeling

Other researchers have discussed pressure pulsation in Kaplan hydraulic turbine units and the methods to reduce the cavitation phenomenon problem. Ko & Kurosawa (2014) evaluated and presented the cavitation performance at a specific speed for a 400 MW Kaplan turbine using a finite volume method to solve the Reynolds-averaged Navier-

Stokes equations combined with the Reynolds stress model. The modified Rayleigh-Plesset equation was used to model the collapse and growth of cavitation bubbles. Javadi & Nilsson (2014) adopted the renormalization group k–ε turbulence model combined with the Reynolds-averaged Navier–Stokes equations to analyze the unsteady turbulent flow in a U9 Kaplan turbine model. Analyses were performed on the fluctuation of pressure in the draft tube, unsteady flow behavior, and cohesive flow structures. Another investigation was carried out on the runner outlet flow of a Francis turbine model using a two-component particle image velocimetry system by Favrel et al. (2015). The finding of the research proposed a particular shape to provide suitable optical access across the draft tube elbow. The characteristics of the flow pattern in a Francis turbine runner with a small opening valve using the Reynolds-averaged Navier-Stokes equations and the continuity equation was inspected by Mo et al. (2016). The 3-D unsteady turbulence flow throughout the entire passage of the turbine was simulated numerically based on the k-ε two-equation turbulence model using the CFD software ANSYS Fluent. The findings of the study showed that a low-pressure zone expanded around the blades of the runner when the valve was closed and the velocity increased throughout the runner area. On the other hand, the effect of hydraulic instabilities on increasing the service lifetime of Francis and Kaplan turbines was accomplished by Pennacchi et al. (2015). In particular, Caishui (2012) built a mathematical model to study the pressure distribution in the flow pattern inside the powerhouse of a powerhouse station using a fluid dynamics method (CFD) to determine the velocity distribution and pressure pattern distribution under three operating conditions: one-unit load, two-unit load, and full-load rejection (Caishui (2012)). The results of this study outlined a good flow pattern at the inlet with a steady water level fluctuation. The extensive state-of-the-art studies on the pressure pulsation in the draft tube of Kaplan and Francis turbines depends on the same methods and analysis but use

different models. Several researchers have suggested changes in the turbine design to reduce the cavitation phenomenon and increase turbine efficiency.

2.7.3 Cavitation in draft tube

Many researchers have studied different ideas on how to solve the cavitation problem in the draft tube, vibration effect in the powerhouse due to the turbine operating, and how to maximize the power generation. Some of these studies are outlined below.

Some researchers have studied the pressure pulsation in the Francis hydraulic turbine units and discussed the cavitation phenomena problem. Qian et al. (2007) simulated a 3-D multiphase flow in a Francis turbine to calculate the pressure pulsation by using Fourier Transform (FT) in the spiral case, draft tube, a front of runner and guide vanes. The results showed the pressure distribution and frequency changing with and without air admission, and the effect of air admission decreased the low-frequency pressure pulsation and increased blade frequency. Lipej et al. (2009) developed a numerical prediction of the pressure pulsation amplitude for different operating systems of Francis turbine draft tubes. The study included the numerical prediction of the vortex appearance in the design stage. The amplitude of the pressure pulsation was different for each operating system; therefore, the main goal of this research was to predict pressure pulsation amplitude versus different guide vane openings numerically and to compare the results with experimental ones. The ANSYS-CFX computer code was used to model the numerical flow analysis of a complete Francis turbine. Jošt & Lipej (2011) created a 3-D numerical model by using ANSYS-CFX that represent a Francis turbine unit to present the vortex rope prediction in the draft tube using numerical flow analysis. The size of the time step was examined in the results using LES, ω-RSM, and SAS-SST turbulent models with defined grid density and domain configurations. Two analyses were performed with and without cavitation influence. The frequency results outlined that the SAS-SST and RSM

models were less accurate with cavitation effect analysis, while no difference in the accuracy when the cavitation effect was ignored in the LES, ω-RSM, and SAS-SST turbulent models' analysis.

Zhang & Zhang (2012) performed a numerical analysis of the cavitation turbulent flow by using OpenFOAM code in a Francis turbine at partial load operation and the k-ω SST turbulence model in the Reynolds averaged Navier-Stokes equations. The turbine unit domain includes the spiral casing, the runner, the guide vanes and the draft tube with 3-D mesh system of unstructured tetrahedral shapes. A finite rate mass transfer model and mixed assumptions were introduced, while the mixed model equations were solved using a finite volume method. The results of the simulation showed that the cavitation flow in high head Francis turbine is well predicted. Anup et al. (2014) studied the hydrodynamic effects of pressure fluctuation in a draft tube at partial load operation due to rotor-stator interaction. The pressure fluctuation was simulated by analyzing a 3-D transient state turbulence flow simulation in the flow of Francis turbine having a specific speed (203.1) with an installed capacity of 70 KW. The commercial 3-D Navier-Stokes CFD solver ANSYS-CFX was used to analyze the flow through a vertical Francis turbine in its location with 72%-part load and 100% maximum load. The turbine unit includes a spiral case with 16 guide vanes, a runner of 13 blades, 8 stay vanes and a draft tube. The variation in the pressure distribution and velocity vector profile with time results presents the bases for calculating the hydraulic performance characteristics and stability of the turbine. In 2015, an investigation was conducted in the flow field through the runner outlet of a Francis turbine model using two-component particle image velocimetry system (Favrel et al. (2015)).

2.7.4 Hydraulic turbine structure design

A specific shape was designed to give a suitable optical access across of draft tube elbow. The model runs based on a discharge value of 55 to 81% of the best efficiency point. The vortex parameter evaluation with the discharge was calculated based on the initial phase-averaged velocity fields. The analysis results showed that the increase in the excitation was caused by the expansion of the vortex trajectory and a simultaneous increase in the frequency. Most recently, Mo et al. (2016) studied the characteristics of a flow- pattern around a Francis turbine runner on a small opening valve using Reynolds averaged Naiver-Stokes equations and the continuity equation. The finding of this study showed that a low-pressure increase around the blades of the runner when the valve was closed and a velocity increase over the runner area. The 3-D unsteady turbulence flow through the entire turbine passage was simulated numerically based on the k-ε two-equation turbulence model using the computational fluid dynamics (CFD) software ANSYS-FLUENT. Luna-Ramírez et al. (2016) determined the pressure on the blades of a 200 MW Francis hydraulic turbine to locate the failure on the blade surface using computational fluid dynamics (CFD). The stress distribution in the runner of the turbine was calculated in many operating conditions using finite element method. The results showed the level of stress created in the joints between the crown where cracks were noted on the blades. Pennacchi et al. (2015) studied the hydraulic instabilities on increasing the life of Francis and Kaplan turbines by developing a model that included the experimental data obtained on a full-scale Kaplan turbine unit operating in a real power plant. The model analyzed the effect of the vibration on changing the selected node locations in the shaft of the turbine in two directions and showing the change in pressure and frequency in different cases of flow.

2.7.5 Powerhouse vibration analysis

Caishui (2012) studied the pressure distribution in the flow pattern within the powerhouse using fluid dynamics method. He developed a mathematical model for a specific powerhouse station to find the velocity distribution and the pressure pattern distribution under three operating conditions (one-unit load, two-unit load, and full load rejection). The results of the study showed a good flow pattern at the inlet with steady water level fluctuation. Wel & Zhang (2010) made a 3-D numerical model for a powerhouse body using ANSYS software to determine the stress, strain in the powerhouse body and pressure, acceleration, and the frequency within the powerhouse. They concluded that the most vibration was generated because of the static and dynamic disturbance of the hydraulic turbine blades.

2.8 Current contributions

The vibration effect on dam bodies is mainly studied by the civil engineering researchers Albano et al. (2015), Dakoulas (2012), Gazetas & Dakoulas (1992), Gui & Chiu (2009), Hariri-Ardebili & Mirzabozorg (2011), Jafari & Davoodi (2004), Khazaee & Lotfi (2014), Khosravi & Heydari (2013), Lotfi (2003), Samii & Lotfi (2012), Shariatmadar (2009), Watanabe (1995) and Watanabe et al. (1996) while mechanical engineering researchers Anup et al. (2014), Caishui (2012), Favrel et al. (2015), Gebreslassie et al. (2013), Jošt & Lipej (2011), Ko & Kurosawa (2014), Lipej et al. (2009), Luna-Ramírez et al. (2016), Minakov et al. (2015), Mo et al. (2016), Negru et al. (2012), Pennacchi et al. (2015), Qian et al. (2007), Trivedi et al. (2013) and Zhang et al. (2009) study the vibration effect on turbines separately. There is no comprehensive study connecting the vibration effect on the dam body, including the powerhouse and the vibration effect generated by operating the turbines inside the powerhouse as an integral part of dam body. So, it is necessary to introduce the dam types, powerhouses, and turbines are which subjected to vibration in a single research study.

In this study, two reaction hydraulic turbines were selected as case studies, one of them is a vertical Francis that was used in the Temenggor power station, and the other is a vertical Kaplan that was used in the Haditha power station. in this study, 3-D numerical models were developed for each of the turbine units in each powerhouse and run under a real head and discharge data obtained from a site visit of finding the hydraulic characteristic performance of the turbine units.

In the current study, two powerhouse embanked dams (Haditha earth-fill and Temenggor rockfill dams) were considered as case studies. The investigations involved three main inspections. In the first case, a 3-D numerical model using ANSYS environment software for the specific embanked dam was used to analyze and evaluate the dynamic behaviors of the dam body due to seismic load for different water levels and foundations (Figure 2.14b). In the second attempt, a 3-D numerical turbine model for one unit of each powerhouse was analyzed separately from the dam to evaluate the turbine characteristics (Figure 2.14a). These two cases are similar to the previous samples cited in the literature. Finally, a third effort was made on analyzing the turbines operating effect coupled with external forces by transforming the results of the turbine model on the contact boundary between the dam body and the powerhouse (Figure 2.15). Based on the findings of this study, suitable recommendations were proposed based on the results of the 3-D numerical model analysis which were compared to the collected and measured data.

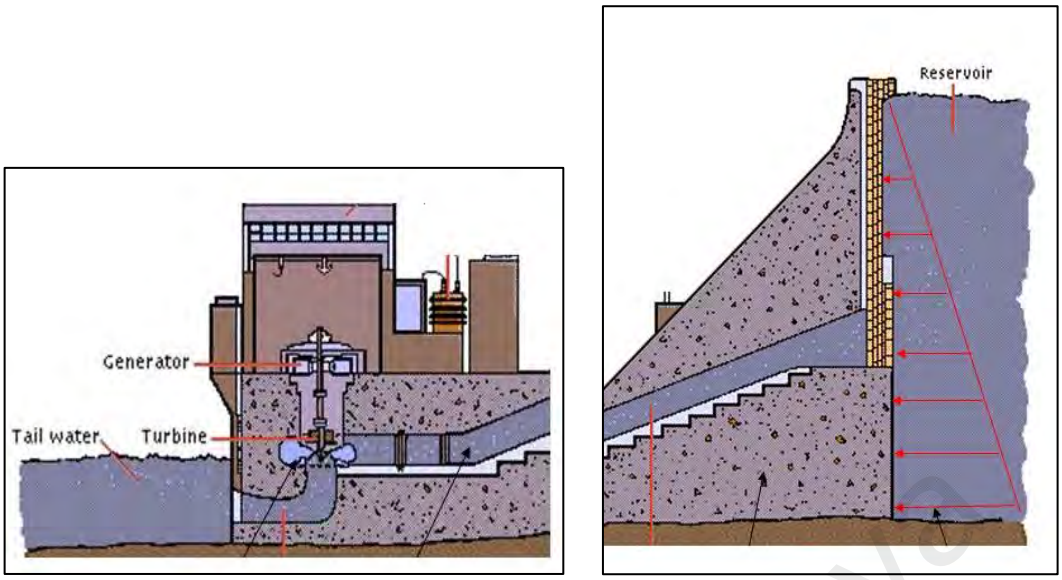

(a) The powerhouse (b) Dam body only

Figure 2.14: The dam body only separated from the Power house (Rahman (2003))

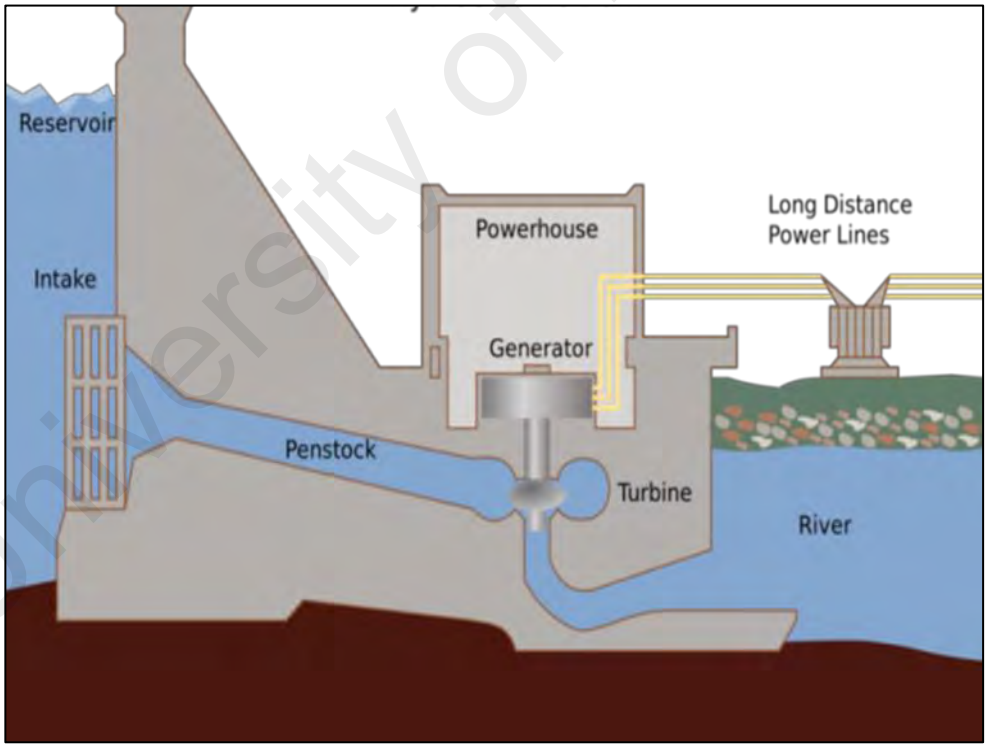

Figure 2.15: The dam included the power house (Nicolet (2007))

CHAPTER 3: METHODOLOGY

3.1 Introduction

This Chapter includes 3D numerical modeling based on finite element technique to assess the dynamic behavior of two selected embankment dams while the hydraulic performance of reaction turbines in the powerhouses of the selected embankment dams was assessed using 3D numerical modeling based on finite volume technique. The first selected dam is an earth-fill dam and located in Iraq. The dam is called Haditha dam. The second dam is a rockfill dam and located in Malaysia. This dam is called Temenggor dam. Figure 3 1 shows a flowchart that summarizes the research methodology.

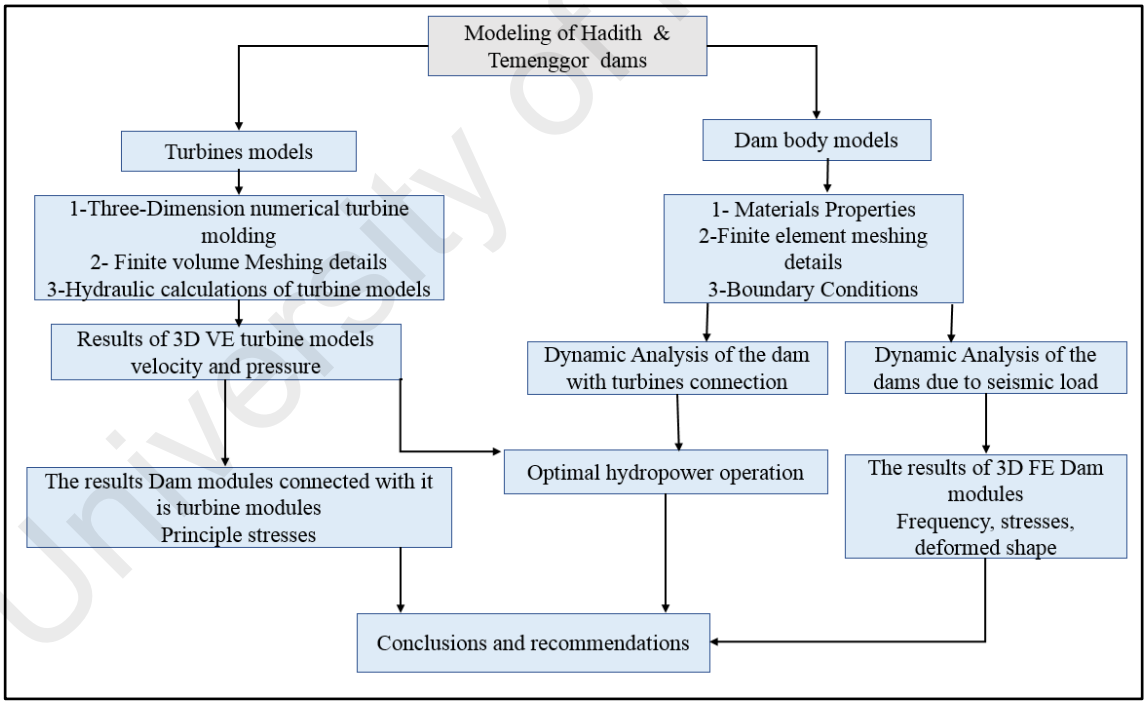

Figure 3.1: The full details of the flow chart of the proposed methodology

3.2 The case studies

In this study, two embanked dams were selected as a case study, the first one is Haditha dam which is located at Haditha city, Ambar Governorate, Iraq while Temenggor dam is located at the state of Perak, Malaysia.

3.2.1 Haditha dam

Haditha dam is outlined in Figure 3.2a and 3.2b and it is an earth-fill dam. It is located at a narrow stretch of the Euphrates river north of Haditha city, Iraq. Haditha dam represents a multipurpose structure, its used for powerhouse generation, regulate the flow of the Euphrates river and provide water for irrigation. It is the second-largest source of electric power in Iraq after the Mosul Dam.

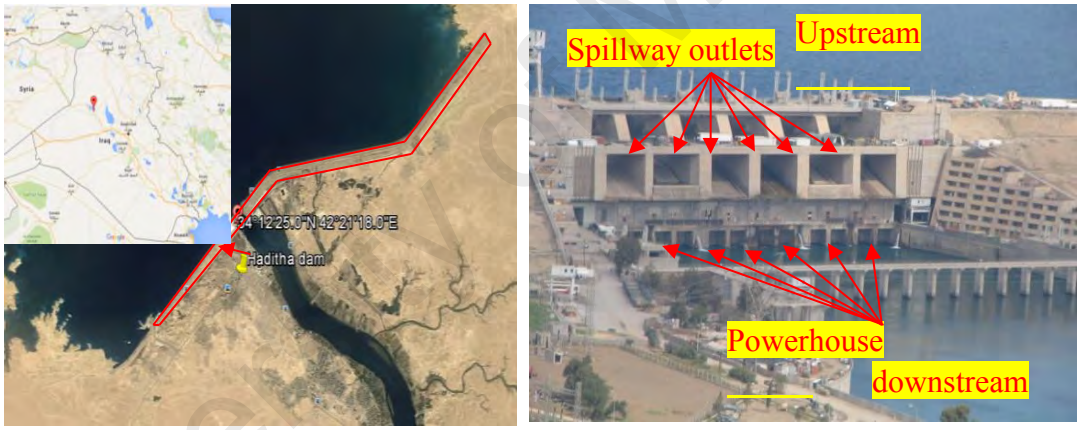

a: Top view of Haditha dam

b: Concrete part of Haditha dam include the spillway and

Figure 3.2: An important view of Haditha dam

The powerhouse in Haditha dam is designed to be an integral part of the dam. The powerhouse in Haditha dam contains six vertical Kaplan turbines capable of generating 660 MW. The turbines were installed in a hydro combine unit that comprises of both the spillway and the powerhouse plant in one structure (Lavrov et al. (2017)). Figure 3.3 shows the downstream parts of Haditha dam with 6 openings in the spillway outlet and 12 openings in the powerhouse outlet (two opening for each turbine unit).

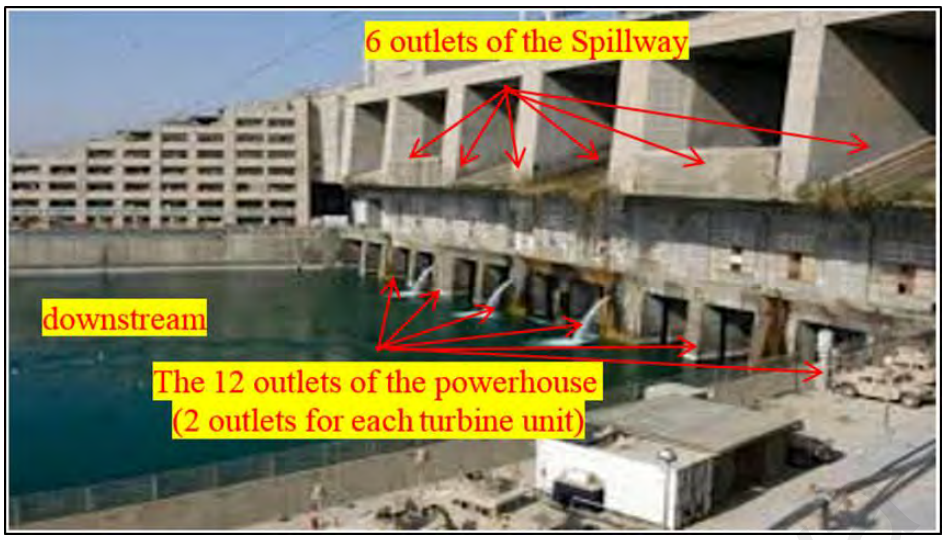

Figure 3.3: Downstream of Haditha dam with spillway and outlet of powerhouse

Table 3.1 outlines the important information pertaining to the Haditha dam which is crucial towards the construction of the 3-D dam model.

Table 3.1: The hydraulic information's of Hadith power stations

Specifications	**unit**	**Haditha**
location		34° 12′ 25″ N, 42° 21′ 18″ E
Power house type		Integral part of dam body
Height	m	57
Length	m	9000
Crest width	m	60
Type of turbines		Vertical Kaplan
Number of units		6
Install capacity	MW	6×110 = 600
Length of unit	m	67.35
Maximum U/S water level	m	150.2
Minimum U/S water level	m	129
Downstream water level (D/S)	m	107.3
Maximum powerhouse discharge	m^3/s	6×339 = 2034

3.2.2 Temenggor Dam

Temenggor dam shown in Figure 3.4 is a rockfill dam located in a narrow valley in Sungai Perak about 200 km northeast of Ipoh in Gerik, state of Perak, Malaysia. The powerhouse in Temenggor dam contains four vertical Francis turbines with installed capacity of 348 MW and it was constructed separately and away from dam body (Javadi & Nilsson (2014)).

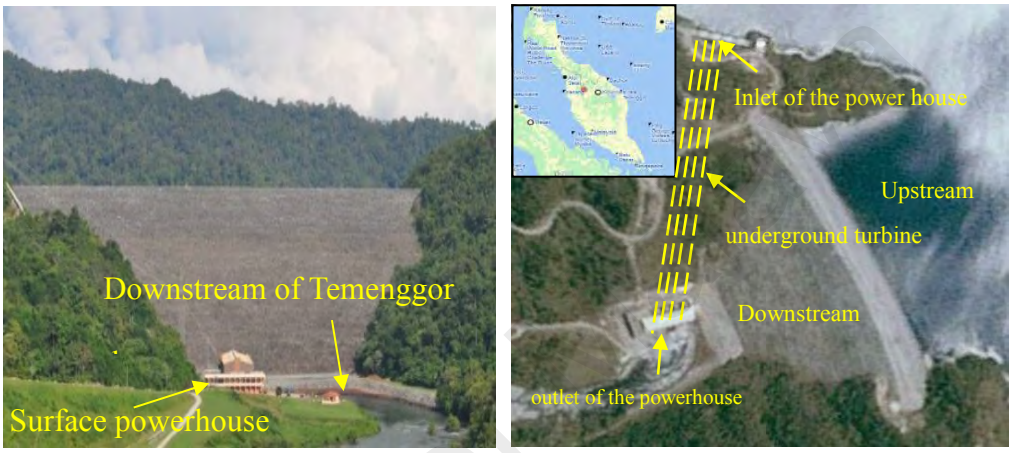

a: D/S of Temenggor dam include the powerhouse

b: Top view of Temenggor dam

Figure 3.4: An important view of Temenggor dam

The 3-D evaluation of the dam behavior under dynamic loading is crucial. Table 3.2 and Figure 3.5 outlined the important information on Temenggor dam which is crucial for the construction of a 3-D dam and turbine models.

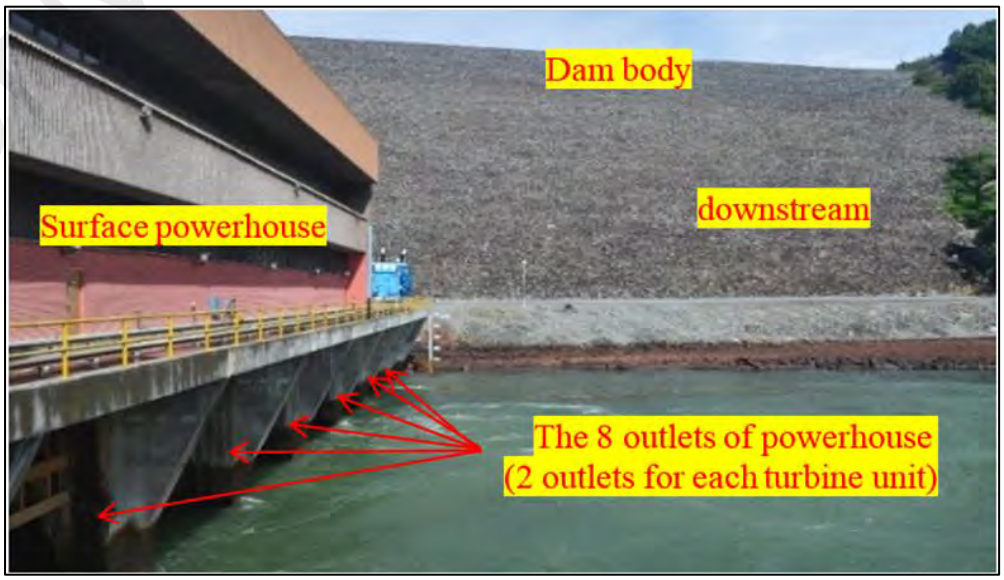

Figure 3.5: D/S of Temenggor dam with surface powerhouse

Table 3.2: The hydraulic information's of Temenggor power stations

Specifications	unit	Temenggor
location		5° 24′ 24″ N, 101° 18′ 4″ E
Power house type		surface power house
Height	m	127
Length	m	256
Crest width	m	20
Type of turbines		Vertical Francis
Number of units		4
Install capacity	MW	4×87 = 348
Length of unit	m	260
Penstock diameter	m	5.5
Maximum U/S water level	m	248.42
Minimum U/S water level	m	236.5
Downstream water level (D/S)	m	142
Maximum powerhouse discharge	m^3/s	4×100 = 400

The variables needed to perform the 3-D FE models for these two embanked dams can be categorized into three groups and as follows:

1. Geometric variables: concerning the details in Table 3.1 and Table 3.2.
2. Properties variables: concerning domains properties such as modulus of density, elasticity, material, and Poisson's ratio of the three domains coupled (water, concrete dam body and soil foundation) listed in Table 3.3.
3. Critical variables: concerning the critical influencing earthquake variables such as time-accelerations data, rang of upstream water and downstream water levels, discharge range, the velocity of flow, and the rotational speed of turbines. A sample of the data is shown in Appendix A.

Table 3.3: The dam-reservoir-foundation system materials properties

	unite	concrete	water	Soil 1	Soil 2	Soil 3
Modulus of Elasticity	GPa	25	-	12.5	25	50
Bulk Modulus of Elasticity	GPa	2.07	-	-	-	-
Mass density	Kg/m^3	2400	1000	2100	2400	2700
Poisson's Ratio	-	0.2	0.49	0.3	0.3	0.3
Damping Coefficient	-	0.05	1	0.05	0.05	0.05

Where Soil 1 is the homogeneous soil of Haditha dam body (left and right embankment and the homogeneous Temenggor dam body), Soil 2 is the homogeneous soil of Haditha bed foundation and the embankment sides of Temenggor dam and Soil 3 is the homogeneous soil of the Temenggor bed foundation.

Figure 3.8 shows the details of Haditha and Temenggor dam models with the details of dam-reservoir-foundation interaction.

3.3 Methods

Analytical solution of the governing equations of fluid flow dynamic is complicated because of its nonlinearity. The computational fluid dynamics (CFD), is a relevant approach to solve the fluid flow motion through the numerical models built in it. In this Chapter, the essential concepts used in the numerical simulations are discussed. These concepts include numerical methods, analytical procedures, fluid flow principles such as Navier-Stokes equations, finite volume method (FVM), and modeling procedure. In addition, this Chapter presents the general approach that focuses on the determination of forces acting on a body of embankment dam from turbines of the powerhouse (static and dynamic conditions) with time. The analysis is normally conducted using one or combination of methods such as theoretical analysis, field testing and FE method. This research focusses on using dynamic analysis which based on FE modeling. Worth to mention, ANSYS® environment software is adopted to conduct the numerical solution for the studied problems. In more describable presentation and in order to study the

vibrations and turbines operation on embanked dams with and without seismic effects, 3-D numerical models that consider different water levels in the dam reservoir are developed. The ANSYS software applied for the numerical models for several reasons:

1. The ANSYS commitment is to provide unequalled technical depth in any simulation domain. Whether it's structural analysis, fluids, meshing, or process & data management.
2. allows us to truly couple multiple physics in a single simulation. Technical depth in all fields is essential to understand the complex interactions of different physics.
3. ANSYS Workbench able to solve the most complex coupled physics analyses in a unified environment.
4. The ANSYS commitment to Simulation Driven Product Development is the same in any case.

3.4 Methodology of turbine modeling

The powerhouses represented one of the main parts of dams that used to generate hydroelectric power in low cost. The detection of the hydraulic characteristic in Kaplan and Francis turbine units that represent the main engine of the powerhouse is the key to find the effect of turbine operating in the other parts of the dam Pennacchi et al. (2015). The use of Kaplan or Francis turbines that classified as reaction turbines is difficult to use under part-load operation because of pressure oscillation.

This study includes a model for one-unit turbine existed at the powerhouse in the selected Dams as a case study to know the effect of powerhouse operating on dam's body. The hydraulic power of the turbines unit is given by Muis et al. (2015), Paish (2002), Samora et al. (2016), Sinagra et al. (2014) and Yah et al. (2017):

$$P = \rho . Q . gH . \eta \tag{3.1}$$

where P is the generated electric power (watt), ρ is the water mass density (kg/m^3), Q is water discharge (m^3/s), g is the acceleration gravity (9.81 m/s^2), H is the water head (m), and η is the efficiency of the hydropower.

The energy of the turbine is defined as follows (Temiz (2013)):

$$E = gH_n = (\frac{p_1 - p_2}{\rho}) + (\frac{V_1^2 - V_2^2}{2}) + g.(z_1 - z_2) + head\ loss_{1-2} \quad (3.2)$$

Where Hn is the water head of turbine (m), g is the acceleration gravity (9.81 m/s^2), p_1 is the upstream pressure (pa), p_2 is the downstream pressure (pa), V1 is the upstream velocity (m/s), V2 is the downstream velocity (m/s), z_1 is the upstream elevation (m), z_2 is the downstream elevation (m).

The sections 1 and 2 are defined the upstream and downstream measurement of the turbine. Depending on the statistical study that established the correlation between the specific speed and the net head for Kaplan as follow (Temiz (2013)):

$$n_{QE} = \frac{2.294}{(Hn)^{0.486}} \quad (3.3)$$

Where n is the rotational speed of turbine runner, and H_n is the net head of the turbine. The parameter n_{QE} is known as the specific speed which is a general relationship that combines main parameters governing geometrically similar turbines operating under dynamic conditions.

And the statistical study of the established correlation between the specific speed and the net head for Francis as follow:

$$n_{QE} = \frac{1.924}{(Hn)^{0.512}} \quad (3.4)$$

Then the rotational speed is defined as:

$$n = \frac{E^{3/4} \times n_{QE}}{\sqrt{Q}} \tag{3.5}$$

Where E is the specific hydraulic energy of machine which can be calculated via:

$$E = H_n \times \mathrm{g} \tag{3.6}$$

Where g is the acceleration gravity (9.81 m/s^2):

$$H_n = H_g \times \eta \tag{3.7}$$

In this thesis, two reaction hydraulic turbines were selected as a cases study including vertical Kaplan that is used in Haditha Power station and the other is a vertical Francis that is used in Temenggor power station.

The formulation of the models for Haditha earth-fill and Temenggor rock-fill dams integrated with their turbines presented and the procedure is implemented using ANSYS® software. Analyzing models acquired several steps to find the different parameters in which are summarized below:

1. ANSYS-modal used to analyze the 3-D dam models to find the natural frequencies in different water levels and foundation depths.

2. The seismic effect on the dam models in different upstream water levels and foundation depth was implemented depending on ANSYS-Harmonic response.

3. The 3-D numerical turbine models created and analyzed depending on the upstream water level and discharge ranges using ANSYS-CFX to find the hydraulic performance for one turbine unit of Haditha and Temenggor powerhouses.

4. By connecting the ANSYS-Static Structural part that represents the 3-D embanked dam model with ANSYS-CFX part included one turbine unit of the powerhouse that represents main part of the dam. This combination used to find the effect of operating turbine to the Dam body.

3.4.1.1 Three-Dimension numerical turbine models

To find the turbines operating effect of the powerhouse on the embanked dams, one vertical Kaplan turbine from Haditha powerhouse and one vertical Francis turbine from Temenggor surface powerhouse were selected as a case study to be investigated. The ANSYS-CFX used to simulate the three-dimensional numerical finite volume turbine models. The turbine includes the runner with blades, and shaft was defined as a submerged rotational body. The water field includes the inlet, penstock, spiral part, draft tube, and outlet were defined. Taking into consideration the boundary conditions include the range of discharges, operating head, rotational speed of turbines, and the gravity force effect. Then After, the two models run with three submerged weirs suggestion at the downstream of turbine units. Figure 3.6 outlined turbine model's dimensions' details of Haditha and Temenggor turbine units.

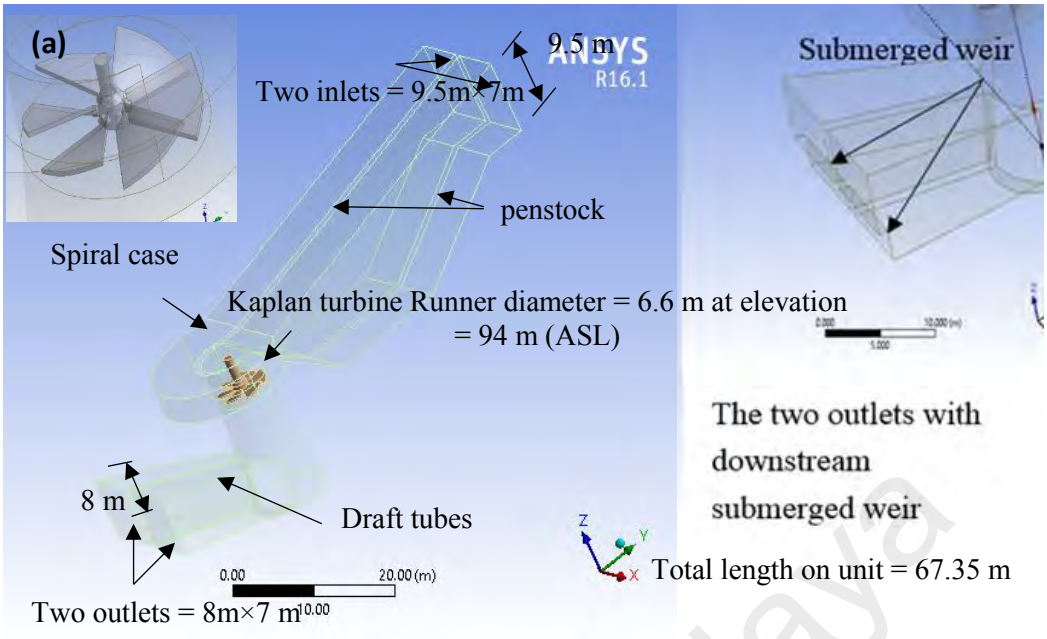

(a) 3-D model of vertical Kaplan unit

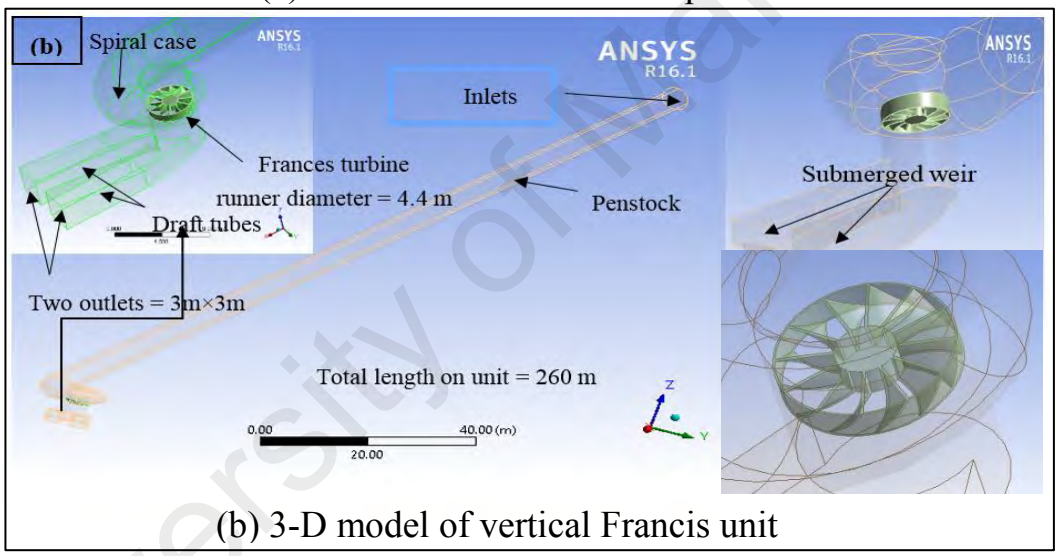

(b) 3-D model of vertical Francis unit

Figure 3.6: 3-D model of Haditha and Temenggor turbine units with dimensions

The second step in turbine modeling involves selection of a suitable finite volume mesh. The flow simulation of the turbines was employed by using several meshes to test the grid independence and it converges after many iterations. The grid independence of the turbine is made using tetrahedral elements after performing several trials to determine the smallest possible aspect ratio under 150 and the minimum orthogonal over 0.15 as recommended by ANSYS-CFX code. Whereas, hexahedral elements analysis performed for the walls boundary layers. To obtain the required pressure fluctuation, the final mesh satisfied y^+<200 around the boundary wall and this is in agreement with the previous

research conducted by. The runner, guide vanes, and draft tube interactions were counted by using slip meshes. This slipping of meshes are toured each other in the interface sides. But it is important to ensure that the velocity components, pressure, and flow flux are harmonious after interpolation. The meshing details used in the Haditha Kaplan turbine model and Temenggor Francis turbine model are shown in Table 3.4. (The number of elements and nodes used in Temenggor turbine meshing is higher than the Haditha turbine model because the Temenggor turbine unit is longer than the Haditha turbine unit). The Francis runner with 12 blades has several fine details represented by small elements, whereas the Kaplan runner includes only 6 blades with details larger than those of the Temenggor runner turbine. Figure 3.7 illustrated the meshing details of the two turbine models.

Table 3.4: The meshing details of Haditha Kaplan turbine unit and Temenggor Francis turbine unit

Mesh details		nodes	Elements	maximum Aspect Ratio	minimum orthogonal Quality
Haditha Kaplan					
without weir	water	2475877	483251	10.706	0.23896
	turbine	302504	66998	10.706	0.23896
weir height = 1.333 m	water	2538602	51216	11.216	0.2315
	turbine	303550	67980	11.216	0.2315
weir height =2.667 m	water	2542563	51753	12.012	0.2325
	turbine	305156	68284	12.012	0.2325
weir height = 4 m	water	2552615	52312	12.214	0.2385
	turbine	306521	68325	12.214	0.2385
Temenggor Francis					
without weir	water	2368529	432191	14.561	0.17684
	turbine	331131	77886	14.561	0.17684
weir height = 0.5 m	water	2461567	448575	14.263	0.18043
	turbine	331091	77846	14.263	0.18043
weir height =1 m	water	2462371	448865	14.202	0.18022
	turbine	330388	77792	14.202	0.18022
weir height = 1.5 m	water	2471293	450536	13.94	0.19626
	turbine	330783	77872	13.94	0.19626

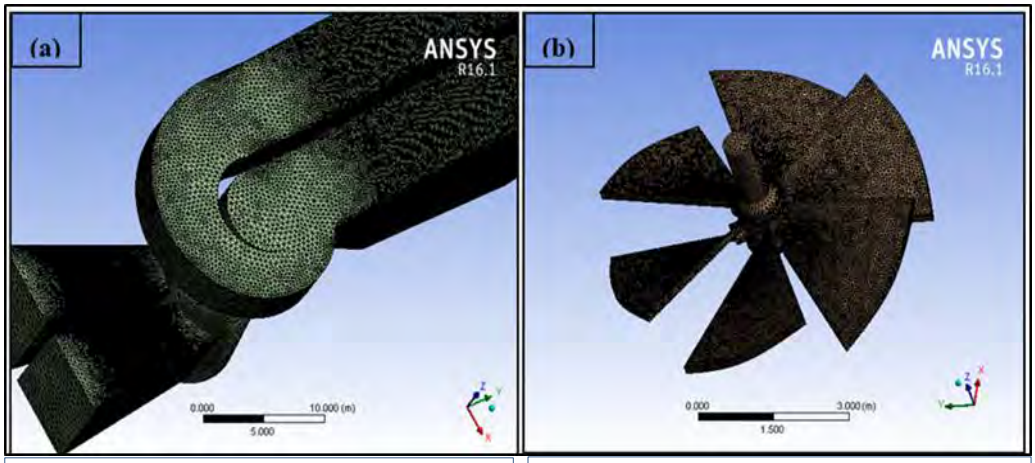

(a) 3-D model of vertical Kaplan unit with mesh details

(b) FV-Meshing of Haditha turbine runner model

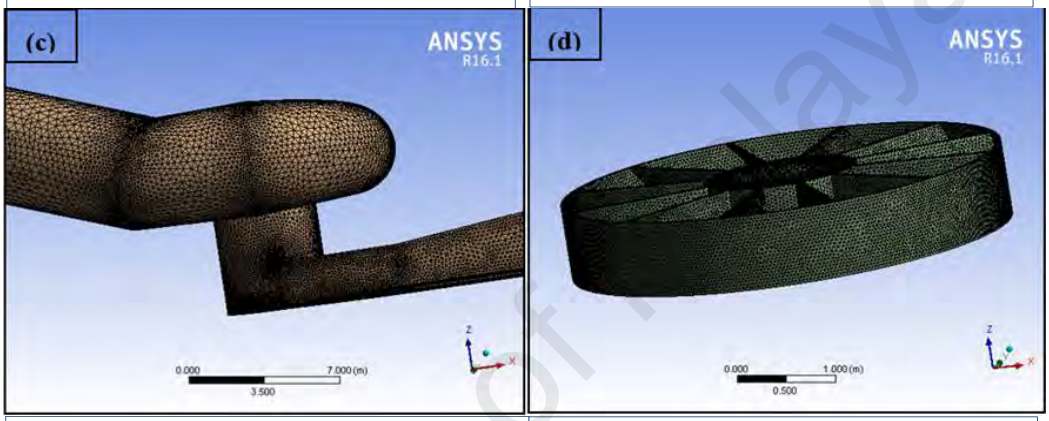

(c) 3-D model of vertical Frances unit with mesh details

(d) FV-Meshing of Temenggor turbine runner model

Figure 3.7: Turbine components mesh details

3.4.1.2 Computations of inputs for turbine models

The k-ε turbulence 3-D model is used to distinguish the unsteady in-compressible flow inside the turbine units (Anup et al. (2014)). All hydraulic turbines run under a limited range of head and discharge. The hydrological data (U/S and D/S water levels with discharges) needed for operating model was allocated from the site visit. Table 3.5 and 3.6 shows the hydrological data of Haditha and Temenggor powerhouses and the specific speed (column 3) calculated by applying Equations (3.3) and (3.4) at first trial, respectively. Equation (3.1) is used to calculate the hydraulic input power by using efficiency for Haditha Kaplan (that got from dam site visiting and the engineering reports) and Temenggor Francis turbines 71.1% and 83.4%, respectively. The inlet velocity

calculated by applying the continuity equation and the rotational speed found by applying Equation (3.5).

Table 3.5: Hydraulic calculations for Haditha turbine

No.	U/S.W. L (m)	Net head (m)	N_{QE}	Q (m^3/s)	P (kW)	V_{inlet} (m/s)	N (rad/s)
Haditha turbine							
1	129	18.5	0.6779	100	25807	1.5038	3.3520
2	134.3	25.5	0.5800	118	41975	1.7744	3.3586
3	139.6	32.5	0.5155	136	61658	2.0451	3.3353
4	144.9	39.5	0.4689	151	83204	2.2707	3.3326
5	150.2	46.5	0.4331	169.5	109949	2.5489	3.2839

Table 3.6: **Hydraulic calculations for Temenggor turbine**

No.	U/S.W. L (m)	Net head (m)	NQE	Q (m3/s)	P (kW)	V_{inlet} (m/s)	N (rad/s)
Temenggor turbine							
1	236.5	94.50	0.2058	50.0	38658	2.1045	3.1687
2	239.48	97.48	0.2068	65.0	51840	2.7359	3.3551
3	242.46	100.46	0.2036	75.0	61644	3.1568	3.6091
4	245.44	103.44	0.2006	88.0	74474	3.7040	3.8491
5	248.42	106.42	0.1977	100.0	87068	4.2090	4.2671

The Kaplan and Francis numerical models run to find the pressure distribution by input the inlet velocity for different upstream water levels and the rotational speed of turbines listed in Table 3.5 and 3.6, and outlet pressure equal to one atmosphere. This was conducted by several trials to find the pressure that gives total head closest to the upstream water level. This model simulation represents the process to calculate the hydraulic turbine performance runs under real headwater level. This implies that the turbines supported is of considerable rigidity. In normal working conditions the number of revolutions of the turbines is 1.666 HZ according to the contract documents and manuals.

3.4.2 Three-Dimension numerical dam models

The following steps are conducted in this research to develop the 3-D FE numerical dam models to analyze the vibration effects on embanked dams:

1. Building a database for different cases, i.e. different sets of input-output variables using the ANSYS ®.
2. In the first case, the 3-D FE numerical model used to find the dynamic behaviors of Haditha and Temenggor embanked dams due to seismic effect and different upstream water levels and foundation depths. This is the case of excluding the effect of turbines operation (the powerhouse is not operated and the gates of turbine units were closed). Due to the shapes of Haditha and Temenggor dams, their 3-D form behaves on the base of linear appearance. The 3-D model was developed using an ANSYS-Harmonic coupling with ANSYS-model to calculate the dynamic behaviours of the dam-reservoir-foundation system. The models considered for this analysis are as follows (Fenves & Chopra (1985)):

- Shallow bed foundation with a full and an empty reservoir.
- Deep bed foundation with a full and an empty reservoir.
- Fixed base with a full and an empty reservoir.

Where the first and second the dam models were constructed with shallow and deep foundations outlined in Figure 3.8..

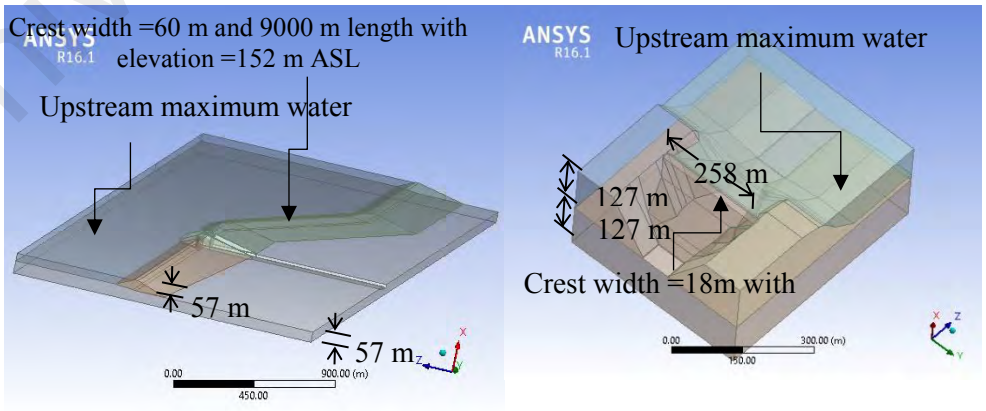

a: 3D model of the Haditha dam bed foundation (d = 57 m)

b: 3D model of the Temenggor dam rock-bed foundation (d = 127 m)

Figure 3.8: 3-D models of Haditha and Temenggor dam-reservoir-foundation systems with shallow and deep foundation.

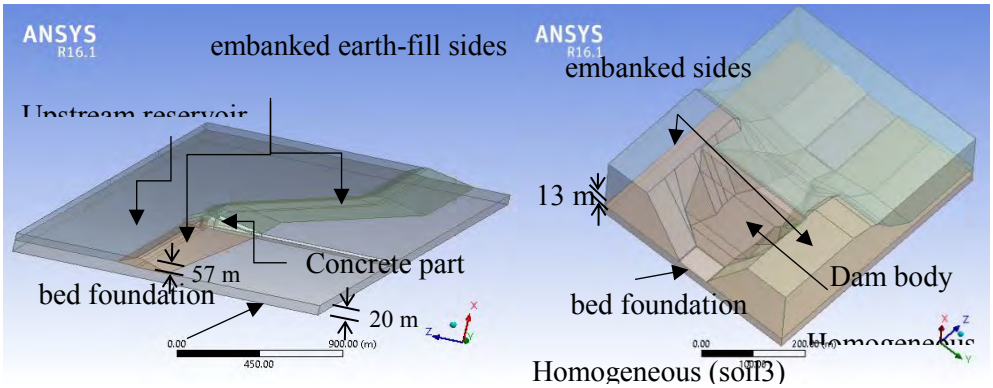

c: 3D model of the Haditha dam bed foundation (d = 20 m)

d: 3D model of the Temenggor dam rock-bed foundation (d = 13 m)

Figure 3-8: continued

The third case the dams were constructed with fixed based and neglecting the foundation (see Figure 3.9).

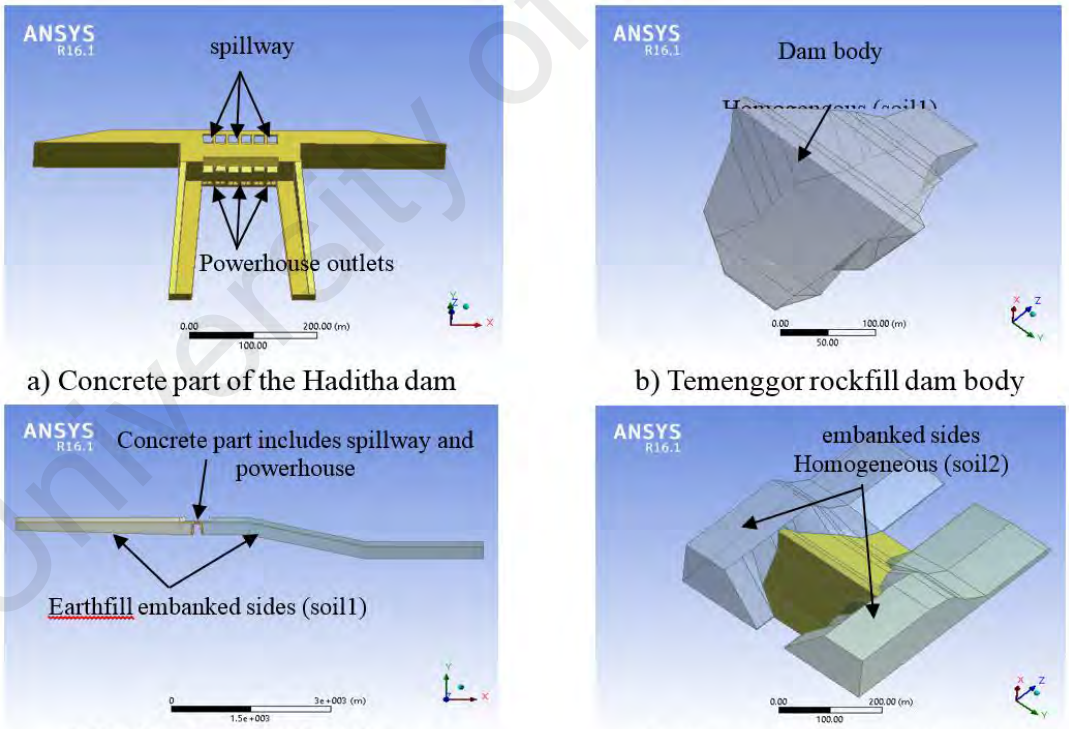

a) Concrete part of the Haditha dam

b) Temenggor rockfill dam body

c) Haditha Dam body with empty reservoir

d) Temenggor dam body with empty reservoir

Figure 3.9: 3-D models of Haditha and Temenggor dam-reservoir-foundation systems with fixed base condition.

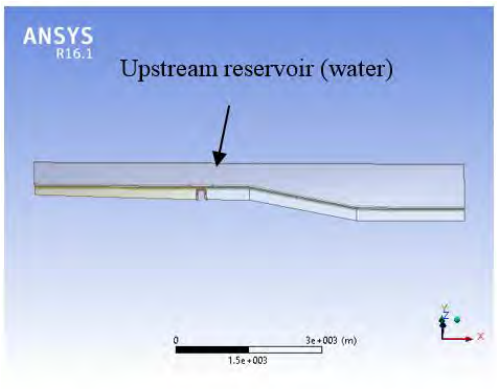

e) Haditha dam filled with water

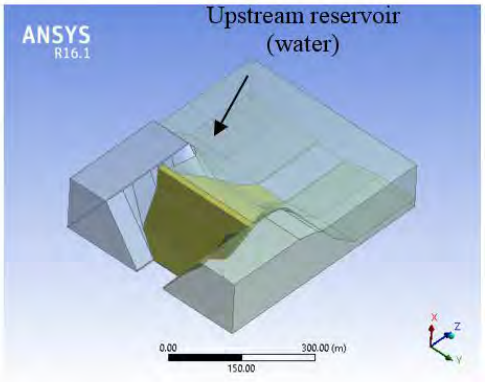

f) Temenggor dam filled with water

Figure 3-9: continued

The model developed to analyze the operation turbines effects on dams in accordance with different water levels by transforming the boundary pressure results of the turbine model to the interface area connection between dam body and turbines units. In order, the system to be analyzed, the embanked dam which impounds reservoir is extending to truncation line in the upstream direction and rests on a bounded foundation. The dynamic analysis is needed to identify the other variables in addition to those geometric variables. Based on the shape of the Haditha earth-fill dam and Temenggor rockfill dam, the models used 57 m for Haditha dam and 127 m for Temenggor dam assumptions of the foundation depth with minimum and maximum upstream water levels listed in Table 3.1 and Table 3.2. Figure 3.10 and 3.11 outlined the 3-D models of Haditha and Temenggor dams with its foundations base and connection with turbine units.

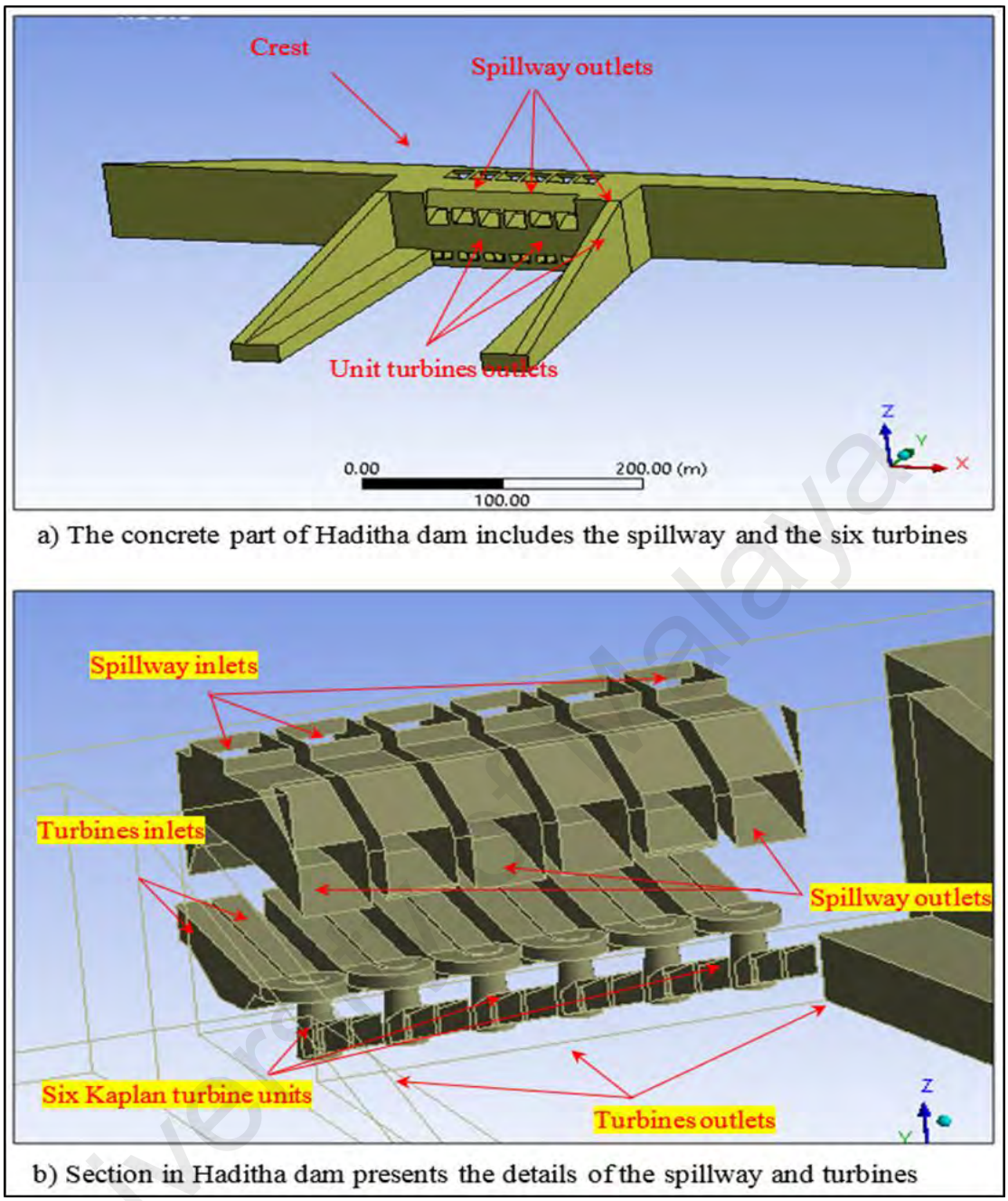

Figure 3.10: Views of the 3-D models of Haditha dam with turbine units and spillway

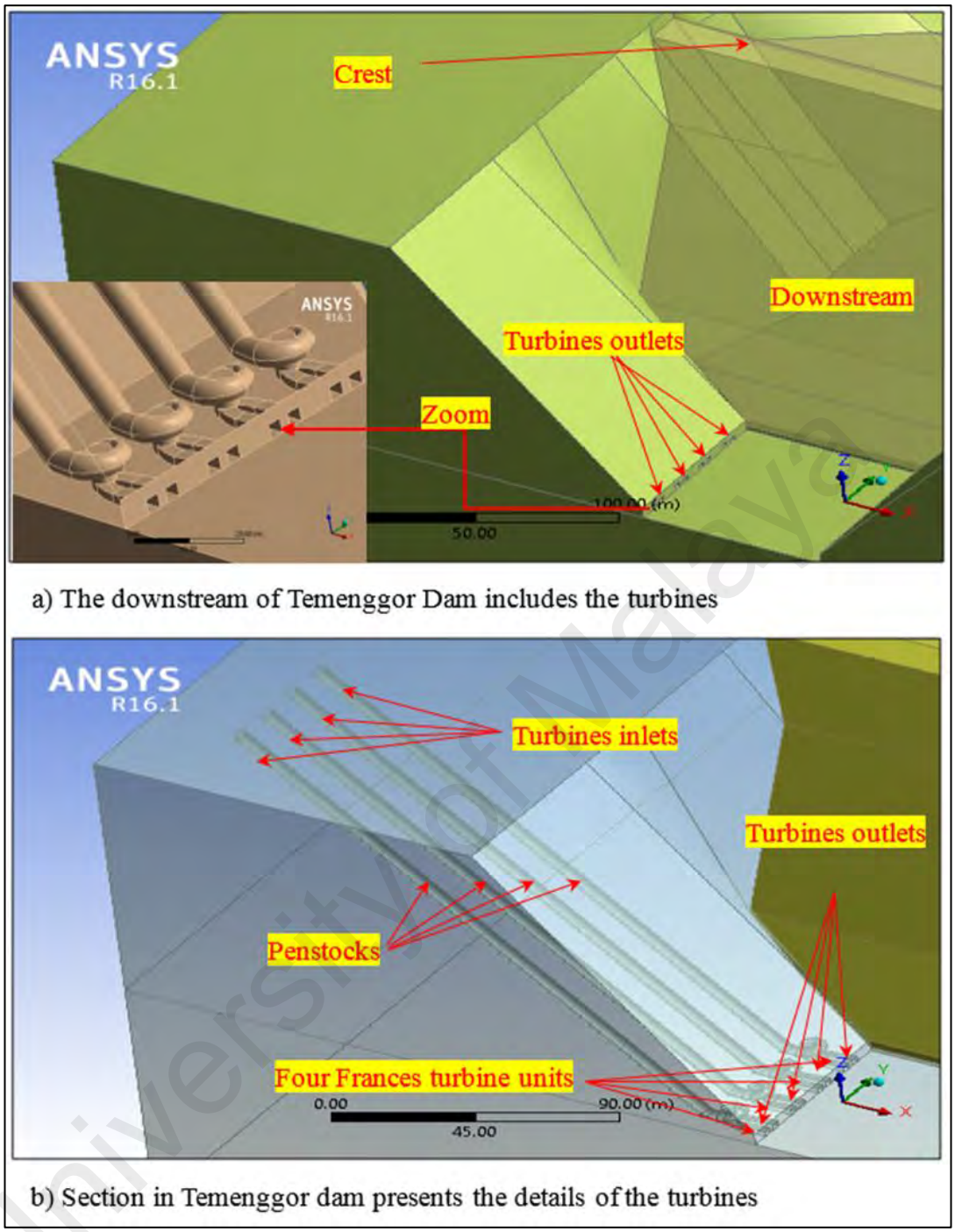

Figure 3.11: Views of the 3-D models of Temenggor dam with turbine units

3.4.2.1 Assumptions in dam models

For the requirements of creating the 3-D FE dam models, the concrete is assumed homogeneous and isotropic, the water is considered as incompressible, un-viscous fluid and the dam-foundation treated as homogeneous and isotropic. Table 3.3 outlined the

dam-reservoir-foundation system materials properties were estimated from engineering reports.

3.4.2.2 Boundary Conditions of reservoir domain

The 3-D numerical reservoir domain exists six boundaries. By applying the appropriate boundary condition to define the hydrodynamic aspects of these boundary interactions. The boundary conditions used for the fluid medium in this study appeared below. The boundary conditions used for the dam-reservoir-foundation system in the ANSYS analysis are shown in Figure 3.12.

The free surface boundary condition to consider the effects of surface waves in the fluid is taken as (Attarnejad & Kalateh (2012)):

$$\frac{\partial p}{\partial n} + \frac{1}{g} . \frac{\partial 2p}{\partial t^2} = 0 \tag{3.8}$$

In this study, by neglecting the surface waves of water effect, the value of the pressure applied is equal to zero on the boundary of the free surface of the reservoir.

The far-end truncated boundary condition has been presented by Maity (2005). The far-end truncated boundary condition applied in present case is based on the theory presented by Demirel (2015):

$$\frac{\partial p}{\partial n} + \frac{1}{C_\circ} \frac{\partial p}{\partial t} = 0 \tag{3.9}$$

The foundation–reservoir interface boundary condition applied in the present case is (Samii & Lotfi (2012)):

$$\frac{\partial p}{\partial n} + \rho_w a_n^s + q \frac{\partial p}{\partial t} = 0 \tag{3.10}$$

Related to the reflection ratio (α) at this boundary (LI et al. (2008)).We can write the formula used in foundation-reservoir boundary as:

$$\frac{\partial p}{\partial n} + \rho_w a_n^r - \left(\frac{1}{C_\circ}\frac{1+\alpha_\circ}{1-\alpha_\circ}\right)\frac{\partial p}{\partial t} = 0 \tag{3.11}$$

The Dam–Reservoir Interface boundary condition applied in the present case (Wang et al. (2011)):

$$\frac{\partial p}{\partial n} + \rho_w a_n^s = 0 \tag{3.12}$$

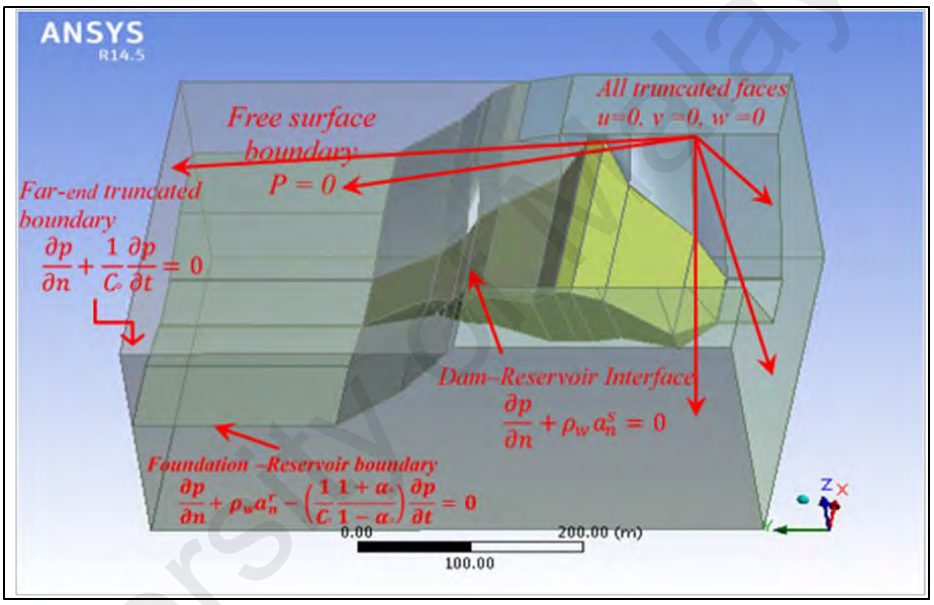

Figure 3.12: The boundary conditions of the Dam-reservoir-foundation system

3.4.2.3 Meshing details for 3 D dam models

3-D finite element models are created for Haditha and Temenggor dams. The elements used for ANSYS ® analysis are as follows:

1. Fluid volume element: This is nodes 3-D element with a second degree of freedom (2DOF) for pressure (Singh (2017)), suitable for model acoustic fluid for modeling water of the reservoir, with the options of the structure present and structure absent. For structure, present elements, each node has three degrees of freedom (3DOF), which account for water particles displacement in horizontal and vertical direction and pressure.

2. Space element: This is used for modeling both concrete dam body and foundation bed soil. This 3-D element has nodes with three degrees of freedom (3-DOF) for each, which accounts for solid particles 3-D displacements.

3. Fluid-solid connection element: This element is adopted for the interface surface between two different domains, fluid and solid elements.

4. Different materials connection element: This element is adopted for the interface surface between two solid domains with different properties, concrete dam and soil elements.

Figure 3.13 outlined the 3-D FE models of the Haditha and Temenggor dams with a fixed base in full and empty reservoirs cases, respectively.

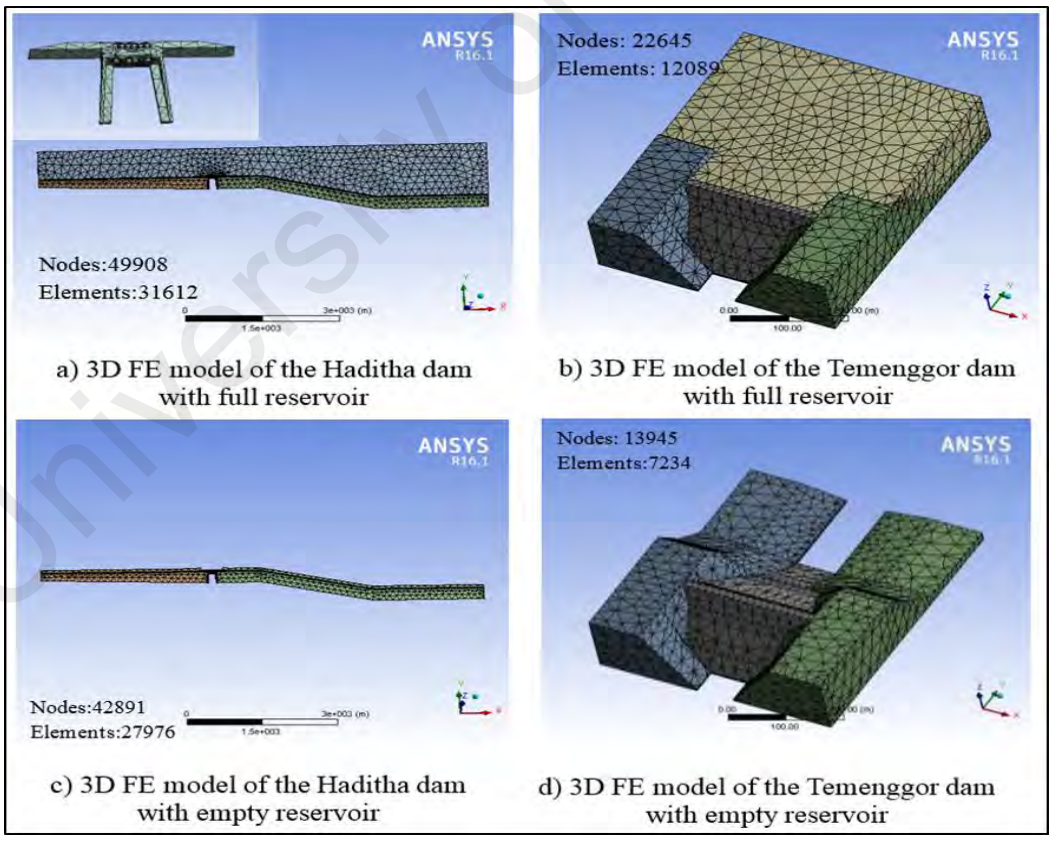

Figure 3.13: 3-D FE models of the Haditha and Temenggor dams with fixed base in full and empty reservoirs cases

Figure 3.14 and Figure 3.15 showed the 3-D FE models for the Haditha and Temenggor dams with empty reservoir and bed foundation 57 m and 127 m, respectively.

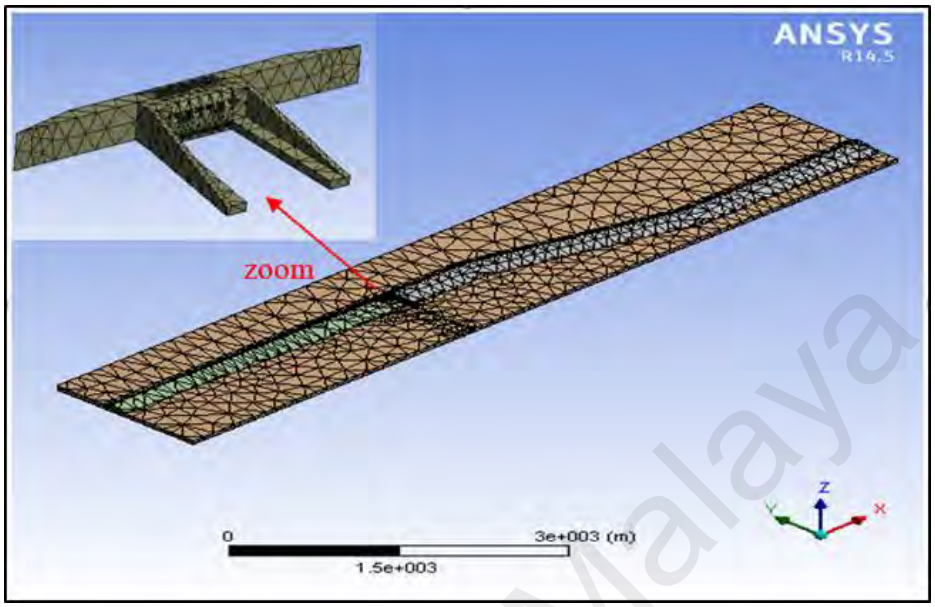

Figure 3.14: 3-D FE models for the Hadith dam-reservoir-foundation system with empty reservoir and deep bed foundation (57m)

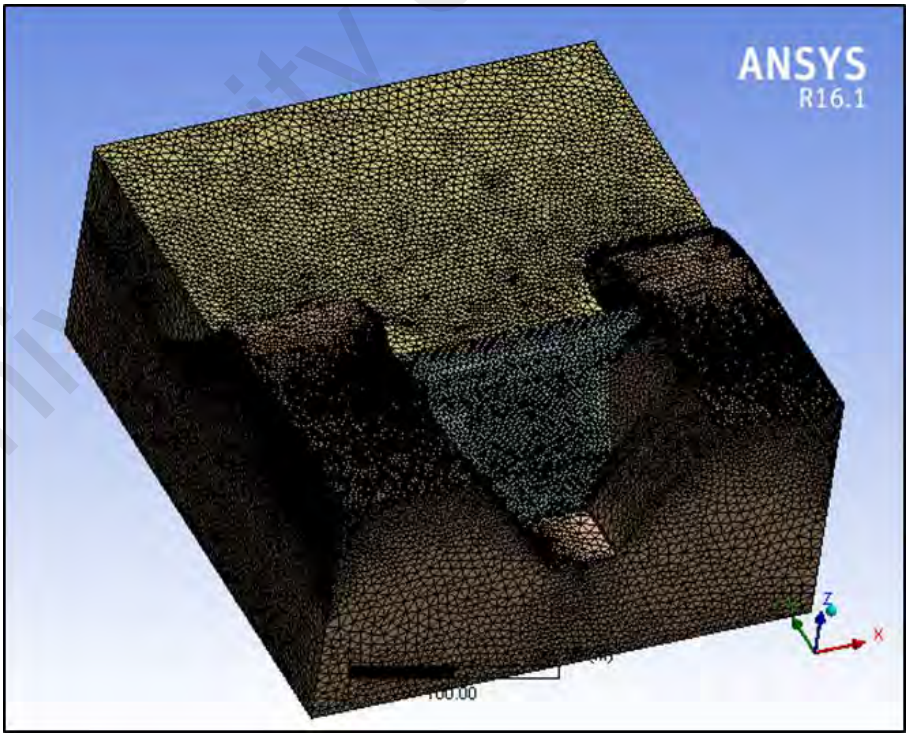

Figure 3.15: 3-D FE models for the Temenggor dam-reservoir-foundation system with empty reservoir and deep bed foundation (127 m)

3.4.2.4 Analysis of seismic effects

The data of strong earthquake of magnitude 7.8 M (struck the island of Sumatra in Indonesia) was used to calculate the response of the embanked dams. Its loading was analyzed by using the prediction of this response, i.e. transforming the governing data from a time domain to frequency domain using ARTeMIS®, as shown in Figure 3.16 and 3.17.

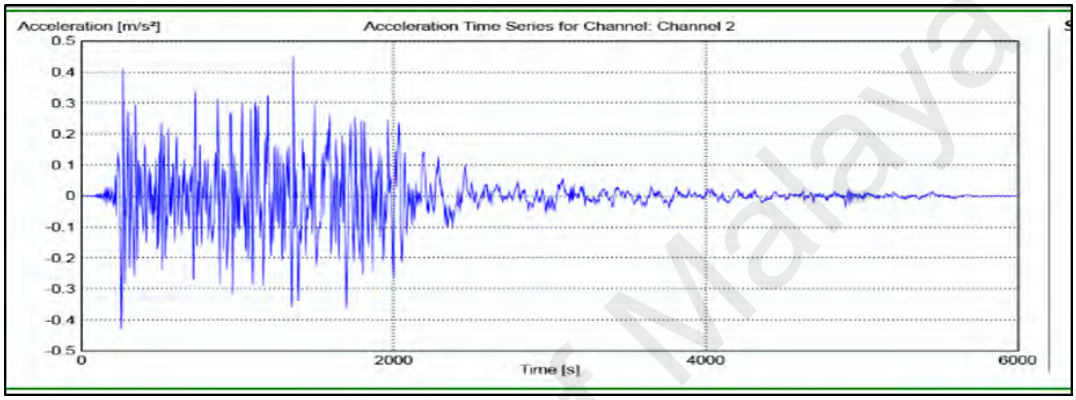

Figure 3.16: The earthquake time–acceleration data

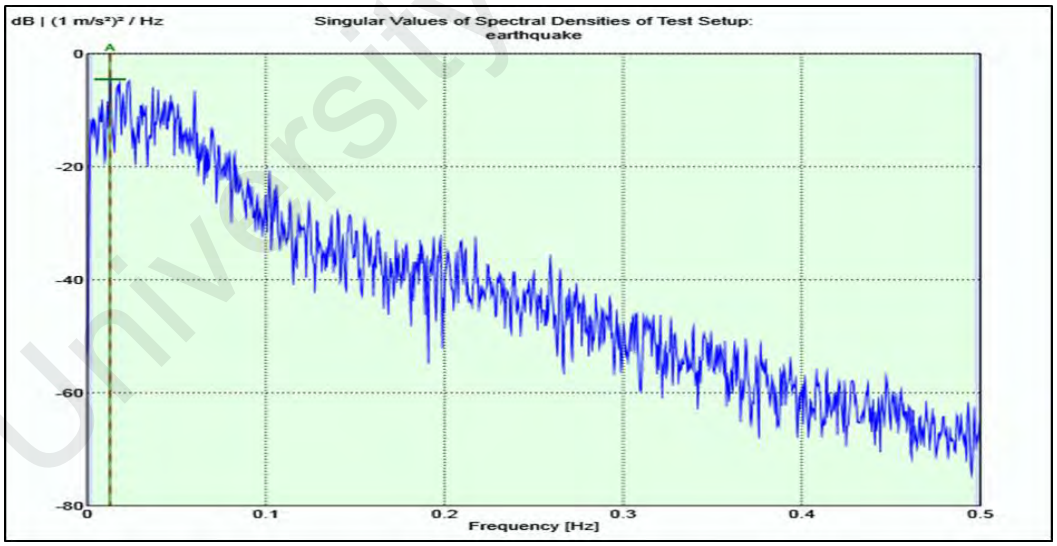

Figure 3.17: The earthquake data transformed from time domain to frequency domain

The vertical axis in Figure 3.17 represents the logarithmic expiration $dB|(1\,m/s^2)^2/Hz|$. The acceleration can be calculated by using the formula Altunişik et al. (2015):

$$dB = 10log\{(1\ m/s^2)^2/Hz\} \quad (3.13)$$

The acceleration representing the frequency Hz can be calculated from:

$$a_{\left(m/s^2\right)} = \left\{Hz \times 10^{dB/10}\right\}^{0.5} \quad (3.14)$$

The earthquake used for analysis the seismic load depends on 0.2g acceleration in the direction of flow and 0.15g in the vertical direction (Ahmed et al. (2014)).

The model was also used to estimate the dynamic properties with the change of water levels from maximum drawdown to the flood level by taking into consideration the empty case. The soil properties of the dam-foundation were estimated from engineering reports and seismic reflection investigation listed in Table 3.3. Generally, the accepted damping ratio range for the dams is between 2% to 5% (Lotfi (2003)). The material damping properties involved in this work are listed in Table 3.3. The model run on three inertial dam-foundation properties (massless, complete mass, and decreasing mass 50%). The natural frequencies for four modes of 3-D FE in empty and maximum water levels and three assumptions of reactions are fixed, with two shallow and deep depths of foundations were presented.

3.4.3 Turbine models and fluid structure interaction

The dynamic motion of a continuous fluid medium is done by the principles of mechanics and thermodynamics. In a Cartesian coordinate frame of reference, they can be expressed in the incompressible Navier-Stokes equations forms for mass and momentum (Ahn et al. (2017)) and (Chen et al. (2017)):

$$\nabla . u = 0 \quad (3.15)$$

$$\rho_f \frac{\partial u}{\partial t} + \rho_f u . \nabla u - \nabla . \tau_f = f_{\mathrm{f}} \quad (3.16)$$

The general equations for the displacement and hydrodynamic pressure fields are uncoupled. The continuous pressure field satisfies Laplace's equation and the distribution of hydrodynamic pressures can be obtained from the equation (Burman et al. (2012) and Rikui et al. (2009)).

$$\nabla^2 P = 0 \tag{3.17}$$

For a compressible and in viscid fluid, the hydrodynamic pressure P resulting from the ground motion of the rigid dam satisfies the wave equation in the form (Cetin & Mengi (2003) and Olson & Bathe (1983)):

$$\nabla^2 \mathrm{P} = \frac{1}{\mathrm{C}_\circ{}^2} \frac{\partial^2 \mathrm{p}}{\partial \mathrm{t}^2} \tag{3.18}$$

The reason of gradual significant concern in discussing the vibration effect on dams due to reducing the danger of this phenomena while it is coupling with machines and structures especially large structures like high buildings and large dams.

3.4.4 Dynamic analysis and dam turbines models integration

The 3-D FE numerical dam model was developed to calculate the principal stress and mode shape of the dam-reservoir-foundation system with the change of water levels from maximum drawdown to the flood level. The hydrostatic pressure and gravity were defined according to the water level and foundation depths and the dam-reservoir-foundation interaction. The concrete and soil physical properties of the dam-foundation were estimated from engineering reports and water physical properties listed in Table 3.3.

Figure 3.18 illustrated the ANSYS-CFX solution connection with the STATIC-STRUCTURAL setup that used to import the pressure pattern results of turbine model to the connection area between of the dam body and turbine units. The framework included two models: The Dam and turbine model. ANSYS-CFX was used to model the transformation of the pressure to the dam model. ANSYS-Static Structural facilities were

used to convert the pressure from the turbine units to the common area between the dam and powerhouse for the purpose of simulating the principal stresses at selected locations (nodes) in the dam body.

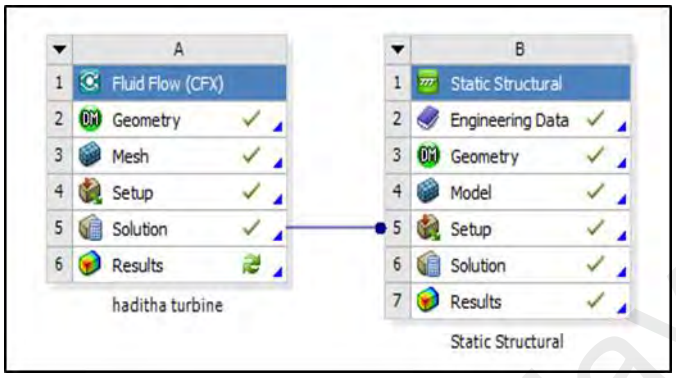

Figure 3.18: The connection between ANSYS-CFX solution and STATIC-STRUCTURAL setup

By operating the dam-turbines framework in maximum drawdown and flood upstream water levels taking into account all possibilities of operating the turbines in full load. This is for the purpose to find the suitable procedure to operate the powerhouse that guarantees to minimize the principal stresses in the dam body. Figure 3.19 sketched the concrete part of Haditha dam and Temenggor rockfill dam with numbering the turbine units.

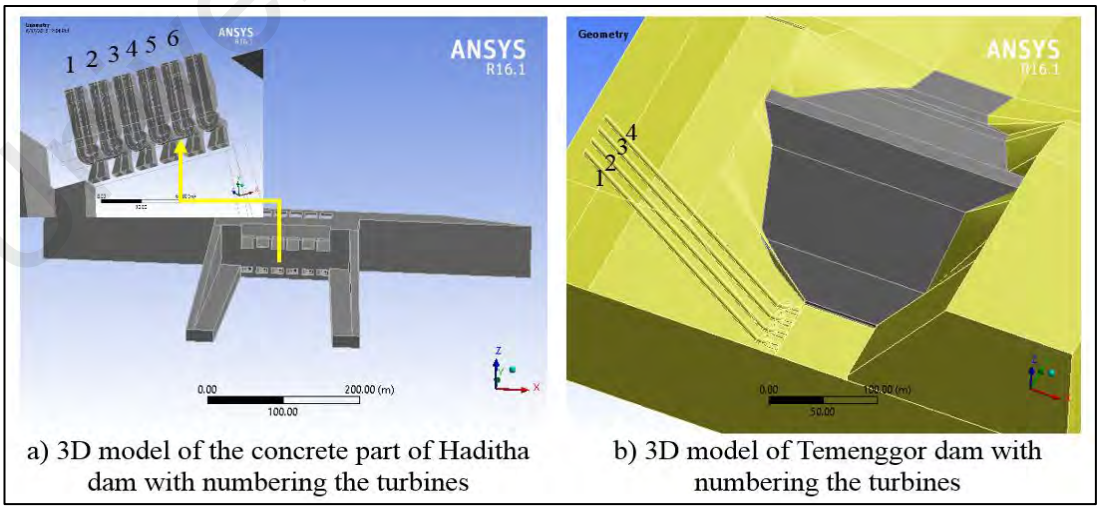

a) 3D model of the concrete part of Haditha dam with numbering the turbines

b) 3D model of Temenggor dam with numbering the turbines

Figure 3.19: 3-D dam models with turbine units numbering

Figure 3.20 showed the selected points in the Dam bodies used for measuring the principal stress according to the numbers of operating turbine.

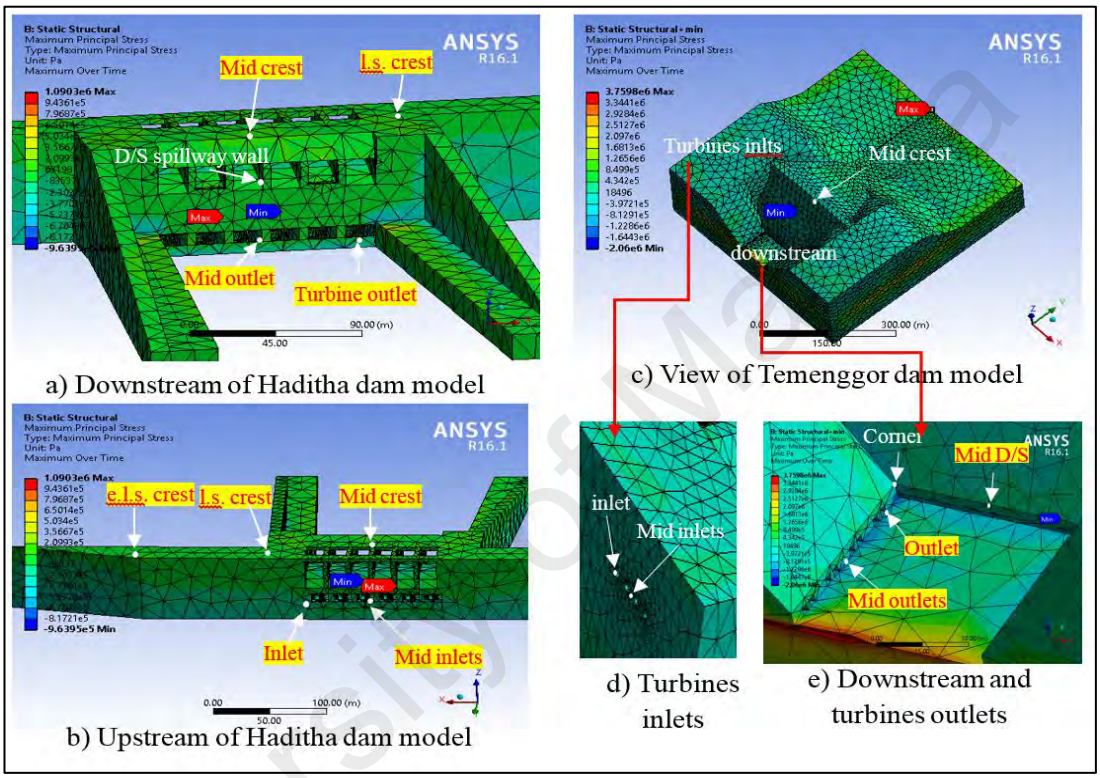

Figure 3.20: 3-D FE model of Haditha dam and Temenggor dam with the locations of the selected points used to measure the principal stress

3.4.5 Models validation

Validation of ANSYS-CFX model was conducted in three stages. In the first stage, the pressure pattern and velocity distribution in a selected turbine unit were predicted by ANSYS-CFX model and compared with the predicted values obtained from Newmark numerical method. The comparison is shown in Table 3.7. Data used in running ANSYS-CFX model were adopted from Wel & Zhang (2010). In the second stage, the predicted dam stability due to vibration effect was conducted by using ANSYS dam-powerhouse model and the results were compared with the forced

vibration test conducted by Jafari & Davoodi (2004) on the Masjed-Soleiman (MS) embankment dam and the results are shown in Table 3.7.

Table 3.7:ANSYS-CFX turbine model validation compared with Newmark numerical method results and ANSYS dam model validation compared with Masjed-Soleiman (MS) embankment dam (forced vibration test).

ANSYS-CFX	Newmark numerical method	ANSYS-CFX	Newmark numerical method	ANSYS	forced vibration test)
Velocity vector V (m/sec)	Velocity vector V′ (m/sec)	Pressure distribution P (kPa)	Pressure distribution P′(kPa)	Frequency f (Hz)	Frequency f′ (Hz)
0	0	-475	-480	3.58	3.5
4.9375	5	-160	-160	3.91	3.9
9.875	10	155	160	4.38	4.4
14.8125	15	470	480	4.75	4.7
19.75	20	785	800	6.21	6.1
24.6875	25	1100	1120	7.02	6.9
29.625	30	1415	1440	8.17	8.1

In the third stage, the rotational speeds N for Haditha Kaplan turbine and Temenggor Francis turbine that listed in Table 3.5 and Table 3.6 and compared with the predicted values obtained from (Punmia et al. (2009) and Hamill, (2001)) that shows the range of specific speed and the rotational speed for each type listed in Table 3.8.

Table 3.8:The turbines rotational speed ranges

Type of turbine	Specific speed	Head (m)	Q (m^3/s)	Rotational speed rang for Haditha Kaplan turbine	Head (m)	Q (m^3/s)	Rotational speed rang for Temenggor turbine
Pelton wheel	12 to 60						
Francis turbine	60 to 500				94.5	50	2.8 to 6.04
					106.4	100	2.2 to 18.3
Kaplan turbine	280 to 800	18.5	100	2.1 to 6.04			
		48.5	169.8	3.2 to 9.26			

CHAPTER 4: RESULTS AND DISCUSSION

4.1 Introduction

The results obtained from the application of 3-D FE numerical models for both Haditha and Temenggor embankment dams integrated with turbine models can be categorized into three summarized groups as listed below:

1. The first group of hydraulic performance results are related to the application of 3-D numerical finite volume turbine models by considering the operation of one vertical Kaplan turbine unit in the powerhouse of Haditha dam and also the operation of one vertical Francis turbine unit in the powerhouse of Temenggor dam that run in different water levels and discharges range. The results include velocity flow lines, pressure distribution in the turbines, and total estimated head at turbine inlet compared with the upstream water level.
2. The second group of the results is related to the application of 3-D numerical finite element dam models by considering the seismic influence on Haditha and Temenggor dams respectively. The dam models considered the interaction effects of the dam-reservoir-foundation system in different water levels and foundation depths. The results include principal stresses, normal stress in the direction of flow, vertical stress, total displacement, displacement in the direction of flow, vertical displacement, and the natural frequency.
3. The third group of the results is that obtained from the integration of 3-D numerical finite element dam models with 3-D numerical finite volume turbine models. The results cover all the possibilities that may arise from the operation of the powerhouses including maximum and minimum water levels for the case of full inlet gates openings. The results of the 3-D dam models include the principal stresses distributions in both dams and powerhouses.

4.2 Simulation results from 3-D turbine models (first group)

The simulation results include that related to total head at turbine inlet, velocity and pressure distribution, shear stress distribution and pressure fluctuation in turbine draft tube.

4.2.1 Simulation of total head at turbine inlet

Table 4.1 shows the calculated results of the total head at the inlet of Haditha and Temenggor turbine units, by operating the turbine models in according to different water levels listed in Table 3.5. This procedure conducted by investigating several runs for the turbine models with changing the rotational speed of turbine to find the inlet pressure that gives the inlet total head closest to the upstream water level.

Table 4.1: Total Head and percent of error calculation at the inlet of Haditha turbine unit and Temenggor turbine unit

Haditha turbine									
No.	**U/S.W.L (m)**	**Q (m^3/s)**	**V_{inlet} (m/s)**	**P_{inlet} (kPa)**	**$v^2/2g$ (m)**	**p/γ (m)**	**Z (m)**	**$H_t = v^2/2g+p/\gamma+Z$**	**error %**
1	129	100	1.504	232.61	0.115	23.71	105	129.08	0.06
2	134.3	118	1.774	284.32	0.160	28.98	105	134.39	0.07
3	139.6	136	2.045	338.15	0.213	34.47	105	139.93	0.24
4	144.9	151	2.271	368.30	0.263	37.54	105	143.06	1.27
5	150.2	169.5	2.549	469.50	0.331	47.86	105	153.44	2.16
Temenggor turbine									
No.	**U/S.W.L (m)**	**Q (m^3/s)**	**V_{inlet} (m/s)**	**P_{inlet} (kPa)**	**$v^2/2g$ (m)**	**p/γ (m)**	**Z (m)**	**$H_t = v^2/2g+p/\gamma+Z$**	**error %**
1	236.5	50	2.105	208.98	0.226	21.30	215	236.53	0.01
2	239.48	65	2.736	236.04	0.382	24.06	215	239.44	0.02
3	242.46	75	3.157	261.53	0.508	26.66	215	242.17	0.12
4	245.44	88	3.704	293.85	0.699	29.95	215	245.65	0.08
5	248.42	100	4.209	326.38	0.903	33.27	215	249.17	0.30

Figure 4.1 display the consistency between the total head estimated from numerical models with the upstream reservoir water levels runs from minimum to maximum upstream water levels.

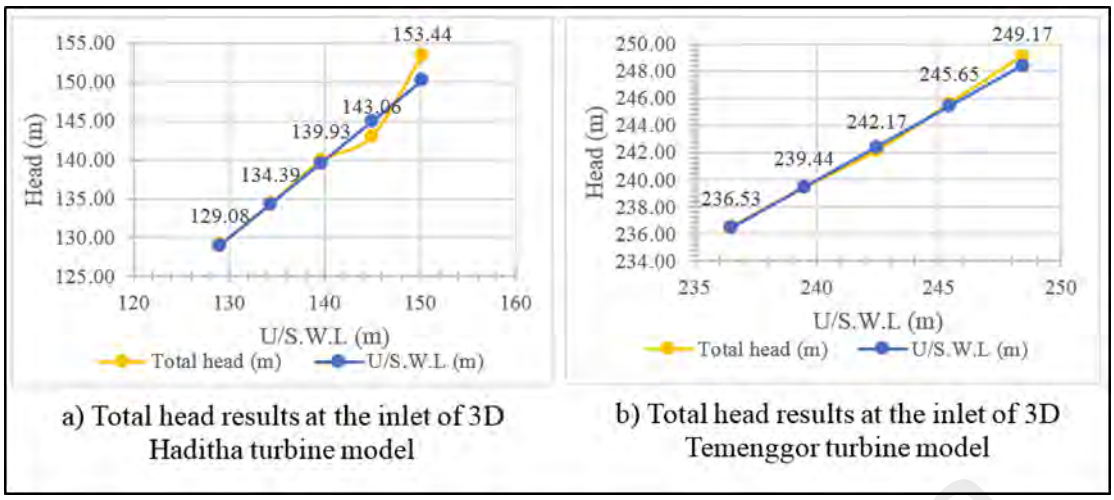

a) Total head results at the inlet of 3D Haditha turbine model

b) Total head results at the inlet of 3D Temenggor turbine model

Figure 4.1: The total head estimated from operating the numerical models of Haditha and Temenggor turbine units

The results showed that the maximum difference between the total head estimated at the inlet of the model and upstream water level of Haditha and Temenggor turbine models equal to 3.24 m, and 0.75 m, respectively. This is because of the head loss varies according to multiple forms of turbulent flow and the types of pipes (smooth or rough). On other hands, the rotational speed of turbine varies according to two variables (the head and discharge) that obtained from data in which they are not evidenced by clear relationship. The comparison of the total head at the turbine model inlets with the upstream water level represent a practical way to find the accuracy of the model results.

4.2.2 Simulation of velocity and pressure distribution in the turbines

Figure 4.2a outlines the velocity distribution in the Haditha turbine model with the maximum head = 150.2 m from the entrance up to the spiral casing. It varies because of the change in the cross-sectional area based on the continuity equation. The maximum velocities occurred around the turbine because of the contraction of the cross-sectional area. The flow is limited to the lower part of the draft tube and the outlet based on the amount of water flow. Figure 4.2b illustrates a constant velocity distribution at the penstock of the Temenggor turbine model with the maximum head 248.42 m because of the constant cross-sectional area. The velocity gradually increased from the spiral casing

to the turbine runner because of the contraction of the cross-sectional area. The velocity is consistently distributed across the draft tube because of the rotational motion and turbulent flow incident that occurred after the turbine is operating. The results evidenced that the maximum water velocity appeared at the location of the turbine runner. In quantitative term, 27.3 m/s for a discharge of 165.5 m^3/s (Haditha turbine) and 40 m/s for a discharge of 100 m^3/s (Temenggor turbine). Although the discharge rate in Haditha turbine is more than Temenggor turbine, the cross-sectional area of Haditha turbine is larger than Temenggor turbine.

Figure 4.2c and 4.2d indicate that the boundary pressure distributions of Haditha and Temenggor turbine models which are proportional to the inverse of the velocity distribution, based on the energy equation. The minimum pressure values achieved after the turbines operated; yet, not reached the cavitation pressure. The velocity and pressure results were similar in distribution shape to the results obtained by Javadi & Nilsson (2017) and Muis et al. (2015).

The net turbine head is determined by calculating the energy difference between the two points before and after the turbine runner. Figure 4.3 showed the pressure difference between the two points. The elevation difference ($\Delta z = 2$ m) above and below the turbine runner is considered. The maximum drop in pressure up and down the runner turbines allocated to be at 145 m and 248.4 m for Haditha and Temenggor turbine model, respectively. This is representing the best water level elevation for operating the turbines with the maximum efficiency.

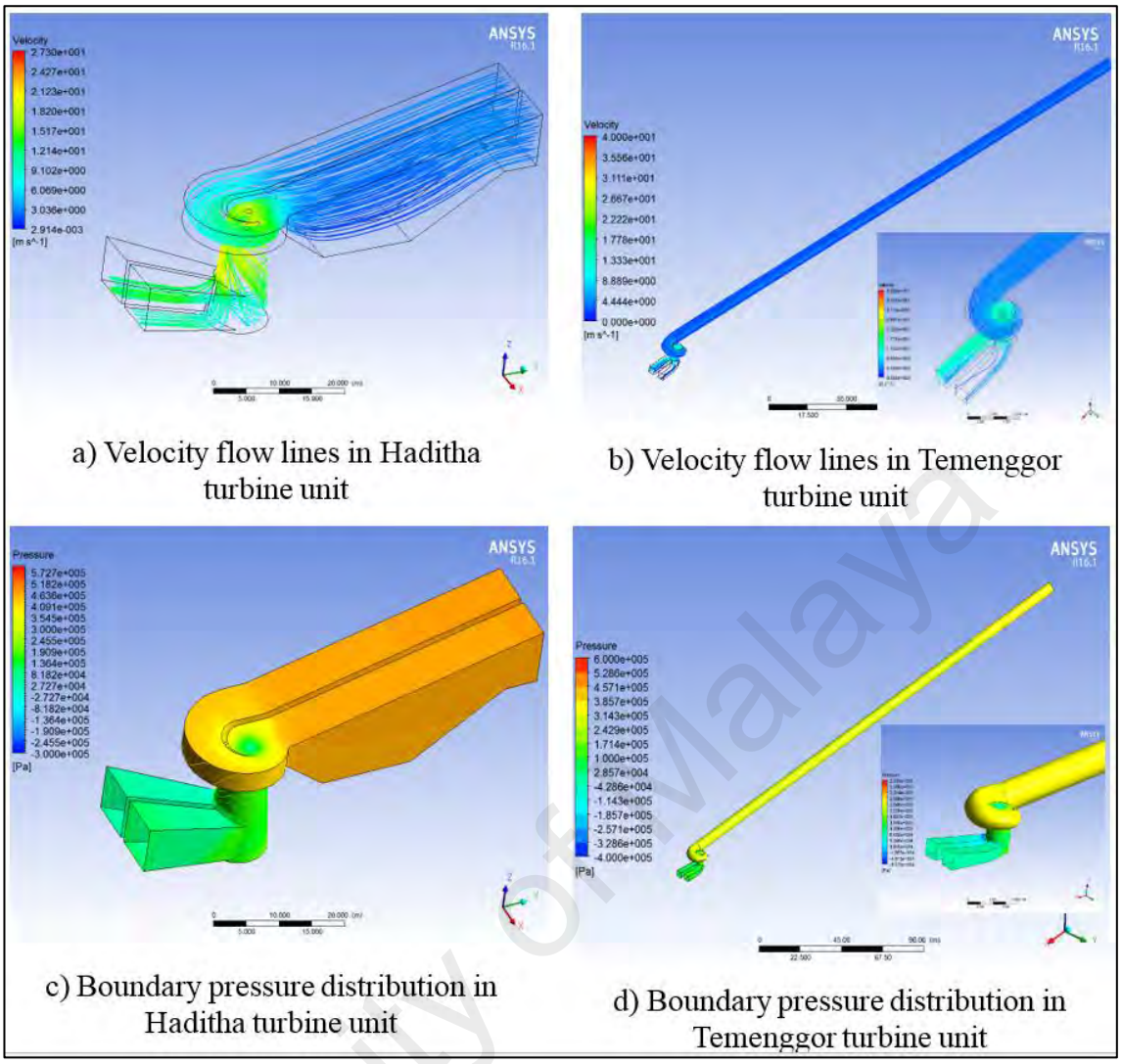

Figure 4.2: The velocity and pressure distribution in Haditha and Temenggor turbine units

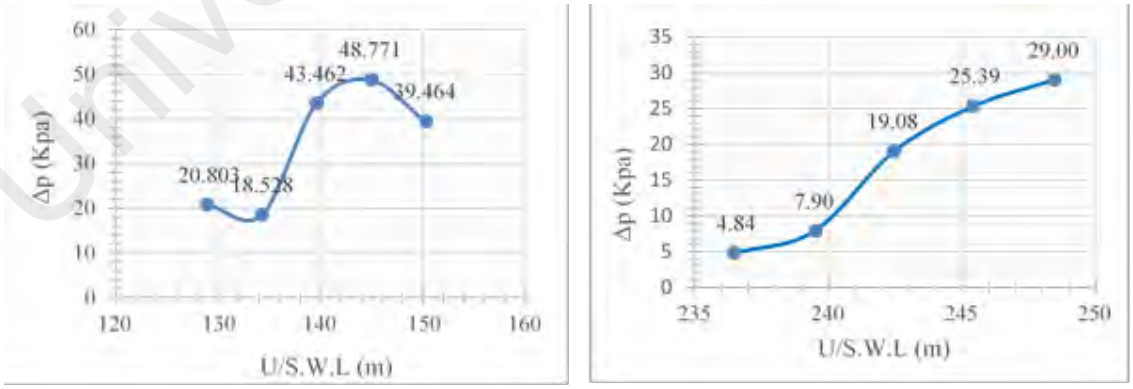

a: The pressure difference up and down the runner of Haditha turbine model

b: The pressure difference up and down the runner of Temenggor turbine model

Figure 4.3: The pressure difference between in two points, up and down the runner of turbine

4.2.3 Simulation of shear stresses and their distribution in the turbines

Figure 4.4 illustrates the wall shear stress distribution of the Haditha and Temenggor turbine units operating under the maximum head. The maximum wall shear stress values are 0.56 kPa and 1.5 kPa, which account for 0.1% and 0.25% of the maximum wall pressure value, respectively. Consequently, wall shear stress values are ignored in transporting boundary pressure from the turbine models. The dam models have determined the effect of operating the turbine on the dynamic behavior of the embankment dams due to their values which are small compared to the pressure values. Moreover, they depended on the pipe type (smooth or rough) and flow rate, which cannot be clearly identified.

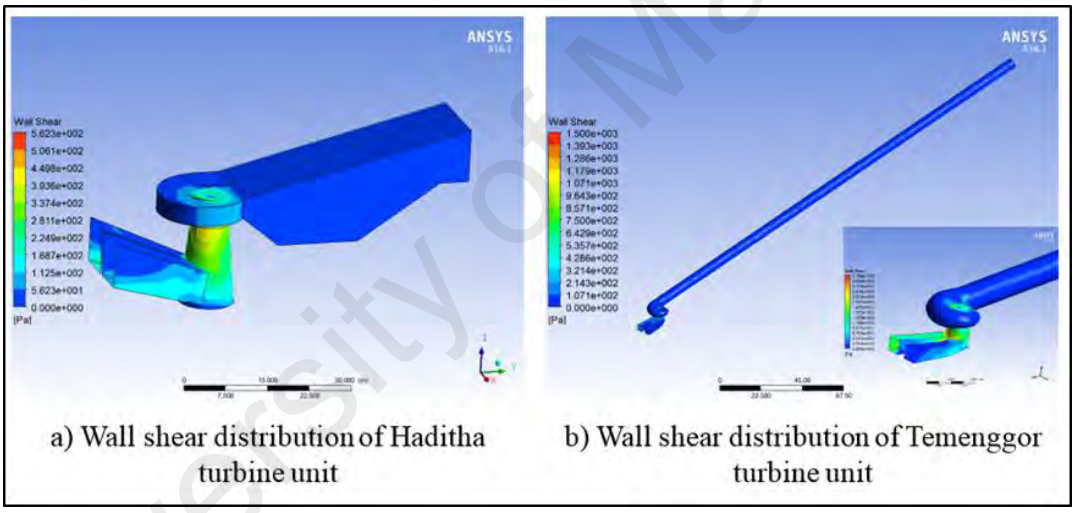

a) Wall shear distribution of Haditha turbine unit

b) Wall shear distribution of Temenggor turbine unit

Figure 4.4: Wall shear stress distribution of Haditha and Temenggor turbine units runs under the maximum heads

Calculating the wall pressure results for the 3-D FV turbine models within the range of the upstream water levels represent a preliminary step to determine the effect of operating the turbine on its boundary walls. This is representing the connection with dam body and that will be transferred to the subsequent steps on the dam model to find the turbine operating influence on the dynamic behavior of the dams.

4.2.4 Simulation of pressure fluctuations in the turbines draft tubes

To have comprehensive details visualization of the attained results of the pressure fluctuation, Table 4.2 and 4.3 outlines the pressure fluctuation results on the left side and

right-side draft tubes. The results were obtained with operating Haditha and Temenggor turbine models with three weir heights suggestion and without a weir. The maximum differences in pressure above and below the turbine runner exist at the following heads 144.9 m and 248.4 m for the Haditha and Temenggor turbine models, respectively. In which represents the best water level elevations to operate the turbines with the highest efficiency. Tables tabulated the pressure fluctuation results on both side draft tube (i.e., left and right). The attained results were determined based on operating Haditha and Temenggor turbine models (i) without a weir as a first case, and (ii) with three weir heights suggestions as a second case. The results showed a reasonable depth of the submerged weir that represents a 16.7% and 33.33% from the actual draft tube opening high for Haditha and Temenggor turbine. The optimal height allocated were reduced the fluctuation of the pressure.

Table 4.2: Draft tube pressure results in different weir height suggestion in Haditha Kaplan turbine units

The top surface of cone and draft tube connection			Left side		Right side		Difference in pressure head between L & R sides (m)
	U/S.W. L (m)	Head (m)	p (Pa)	p/γ (m)	p (Pa)	p/γ (m)	
without weir	150.2	46.5	-37526	-3.825	-1878	-1.914	1.9108
	139.6	32.5	-14033	-1.430	-2298	-0.234	1.1962
	129	18.5	-5679	-0.578	-699	-0.071	0.5076
weir height = 1.333 m*	150.2	46.5	-12411	-1.265	-5916	-0.603	0.6621
	139.6	32.5	-20255	-2.064	-1589	-1.620	0.4440
	129	18.5	-5905	-0.601	-6039	-0.615	0.0137
weir height =2.667 m	150.2	46.5	33013	3.3652	-3930	-4.006	7.3719
	139.6	32.5	11481	1.1703	-2337	-2.382	3.5530
	129	18.5	-12293	-1.253	-1850	-0.188	1.0645
weir height = 4 m	150.2	46.5	-42998	-4.383	60855	6.203	10.5864
	139.6	32.5	-46978	-4.788	66184	6.746	11.5354
	129	18.5	-22010	-2.243	35709	3.640	5.8837

* Indicate the perfect weir dimension.

Table 4.3: Draft tube pressure results in different weir height suggestion in Temenggor Francis turbine units

The top surface of cone and draft tube connection			Left side		Right side		difference in pressure head between L & R sides (m)
	U/S.W. L (m)	Head (m)	p (Pa)	p/γ (m)	p (Pa)	p/γ (m)	
without weir	248.42	106.42	-1329	-13.553	-2650	-2.701	10.8517
	242.46	100.46	-7935	-8.0889	-6917	-7.051	1.0377
	236.5	94.5	-3449	-3.5167	-2722	-0.277	3.2392
weir height = 0.5 m	248.42	106.42	-1319	-13.451	-3059	-3.118	10.3319
	242.46	100.46	-4942	-5.038	-1457	-1.485	3.5523
	236.5	94.5	-2425	-2.472	-7019	-0.715	1.7565
weir height =1 m*	248.42	106.42	-3980	-4.0576	-4360	-4.444	0.3869
	242.46	100.46	-2217	-2.26	-2370	-2.415	0.1559
	236.5	94.5	-1219	-1.243	-5728	-0.583	0.6591
weir height = 1.5 m	248.42	106.42	56042	5.71274	-2156	-2.198	7.9113
	242.46	100.46	10345	1.05454	-7566	-0.771	1.8258
	236.5	94.5	2867	0.29225	-1572	-0.160	0.4525

* Indicate the perfect weir dimension.

In more representable manner, the flow velocity (Figure 4.5 and 4.7) and flow pressure (Figure 4.6 and 4.8) on the left and right side of draft tubes was displayed graphically for Haditha and Temenggor turbine models, respectively. In Figure 4.5 the flow velocity phenomenon of Haditha turbine was simulated in accordance two different components dam up-stream water level and submerged weir depth. Based on Figure 4.5 , it can be recognized that the velocity distribution on both sides of the draft tube became more regular with increasing the submerged weir height. The maximum velocity range located in the turbine runner region affected by operating turbine at minimum and maximum upstream water levels with changing submerged weir height varies 7.6% and 4.1%, respectively. On another aspect, which is the water pressure value, Figure 4.6indicates the water pressure fluctuation with the same regards dam up-stream water level and submerged weir depth. Based on the obtained results, it was attained that building 1.333 m submerged weirs in the downstream of Haditha turbine units with operating the turbine

model in minimum (129 m) and maximum upstream water level (150.2 m) reduce of the pressure difference range between left and right side 23% and 1% of the total head, respectively.

On the other case, Temenggor turbine modeled to investigate the same two interesting measures water velocity and pressure. Figure 4.7: Flow velocity at Temenggor turbine. presents the influence of the upstream water level and the proposed weir height to optimize the suitable steady water flow. The graphical visualization defined that the optimal velocity distribution attained when 1 m submerged weir built in the downstream of turbine outlet. The maximum velocity range located in the turbine runner region affected by operating turbine in minimum (236.5 m) and maximum (248.42 m) upstream water levels with changing built submerged weir height varies 26.7% and 10.9%, respectively. Water flow pressure presentation was demonstrated in Figure 4.8 Revealing this figure conclude that operating the turbine model in minimum (236.5 m) and maximum upstream water level (248.42 m) reduce of the range pressure difference between left and right side of 8.5% and 15.9% from the total head, respectively.

In conclusion, results showed that reducing pressure fluctuation provides uniform velocity distribution according to the Reynolds-averaged Navier–Stokes equations at the draft tubes, especially in high discharges. This fluctuation is more visible in the Temenggor Francis turbine than the Haditha Kaplan turbine because it runs under a high upstream water level that is greater than the Haditha Kaplan turbine. The recommended submerged weir construction at the outlet draft tube was owing to the uneven distribution of water flow and particularly in diffuser section. The findings indicated an essential approach that can be implemented practically in the powerhouse system operation to maintain a steady draft tube water flow with balanced water pressures on both side outlet.

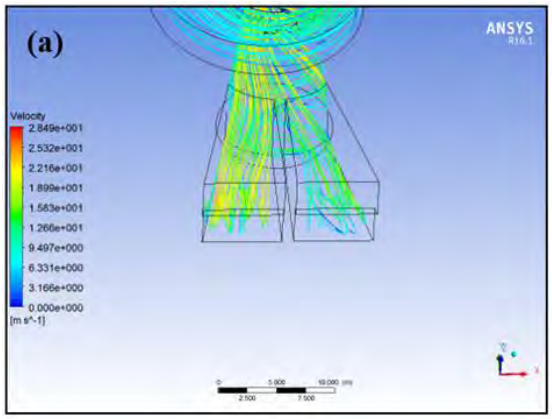

weir depth = 4 m and U/S.W.L. = 129 m

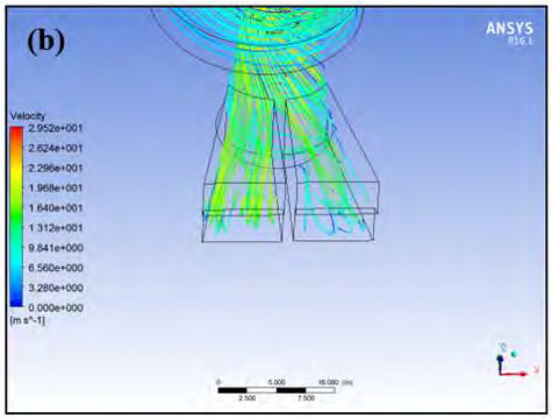

weir depth = 4 m and U/S.W.L. = 150.2 m

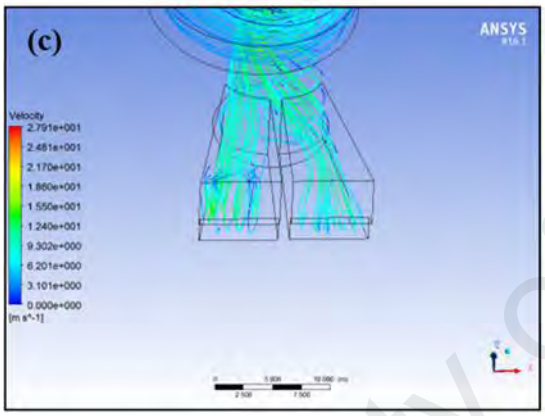

weir depth = 2.667 m and U/S.W.L. = 129 m

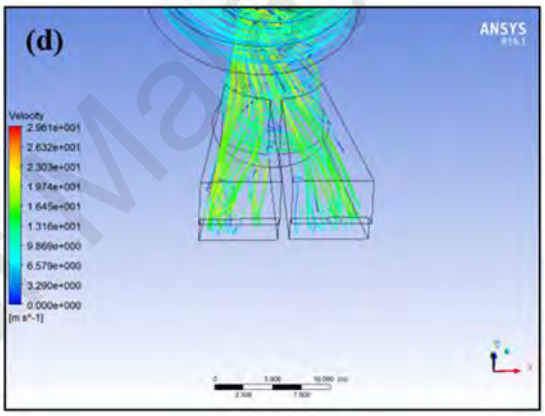

weir depth = 2.667 m and U/S.W.L. = 150.2 m

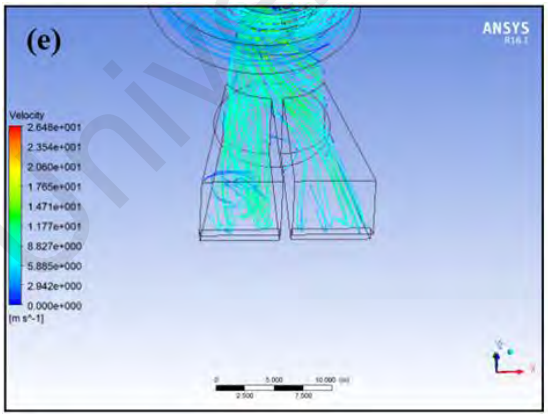

weir depth = 1.333 m and U/S.W.L. = 129 m

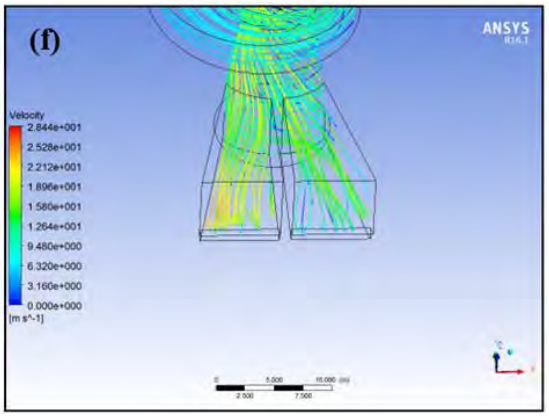

weir depth = 1.333 m and U/S.W.L. = 150.2 m

Figure 4.5: Flow velocity at Haditha turbine.

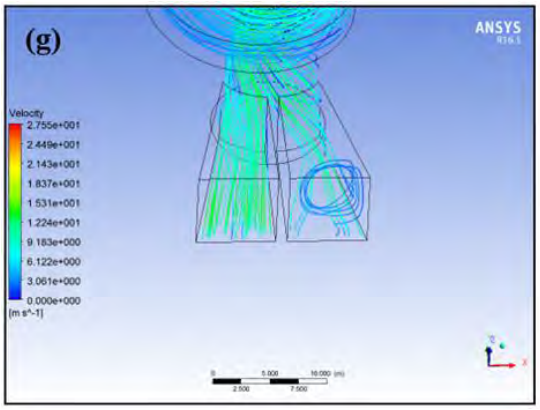

weir depth = 0 m and U/S.W.L. = 129 m

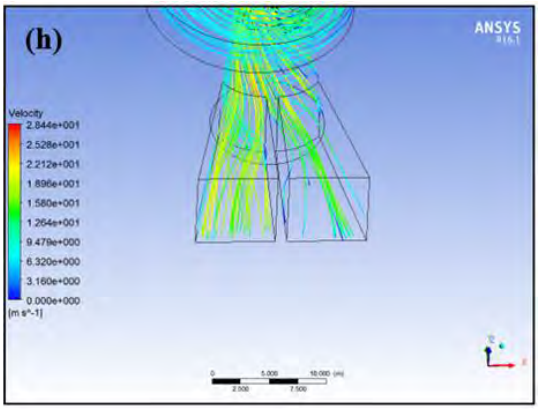

weir depth = 0 m and U/S.W.L. = 150.2 m

Figure 4-5: Continued.

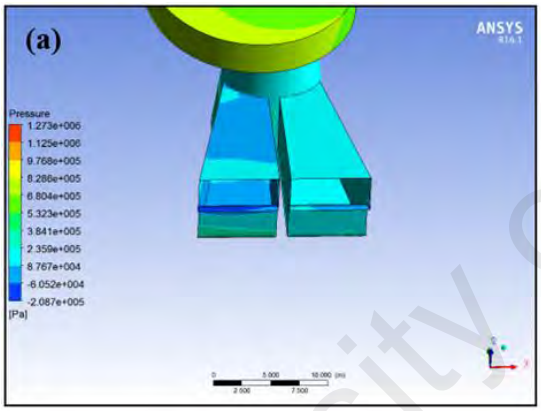

weir depth = 4 m and U/S.W.L. = 129 m

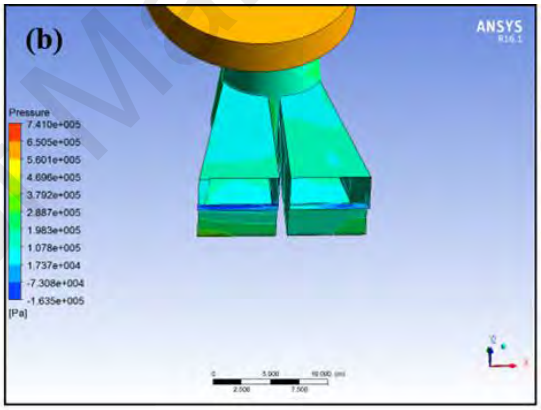

weir depth = 4 m and U/S.W.L. = 150.2 m

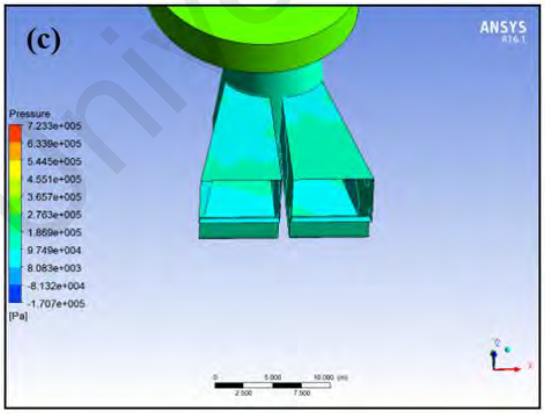

weir depth = 2.667 m and U/S.W.L. = 129 m

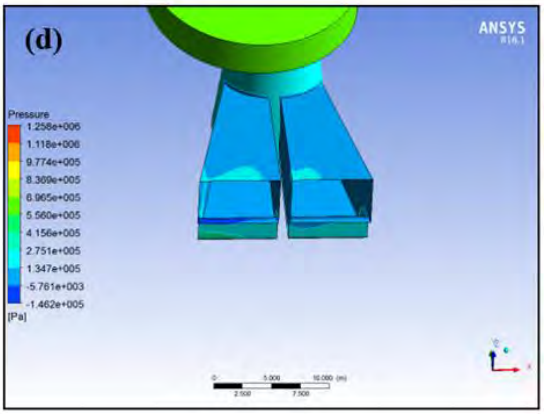

weir depth = 2.667 m and U/S.W.L. = 150.2 m

Figure 4.6: Flow pressure at Haditha turbine.

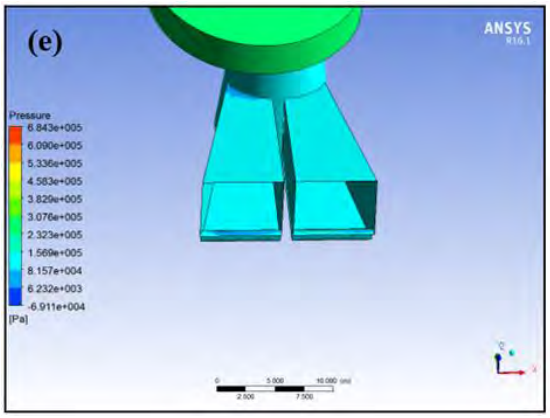

weir depth = 1.333 m and U/S.W.L. = 129 m

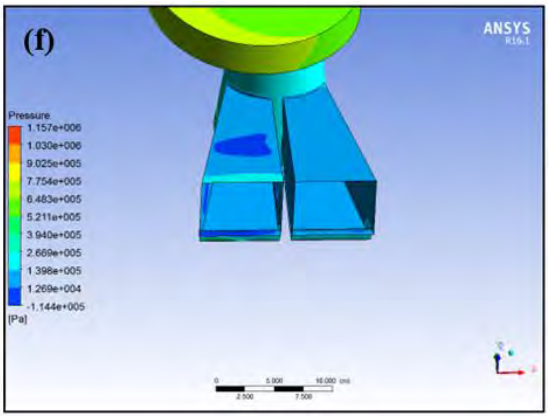

weir depth = 1.333 m and U/S.W.L. = 150.2 m

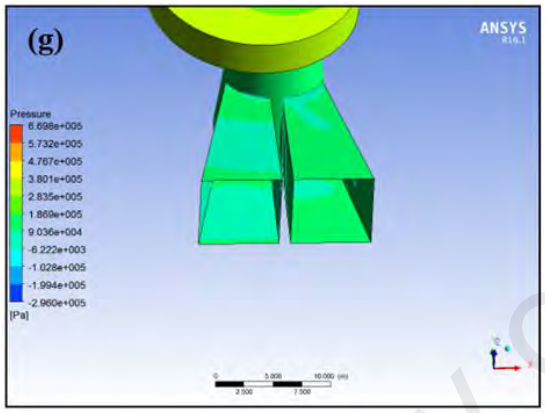

weir depth = 0 m and U/S.W.L. = 129 m

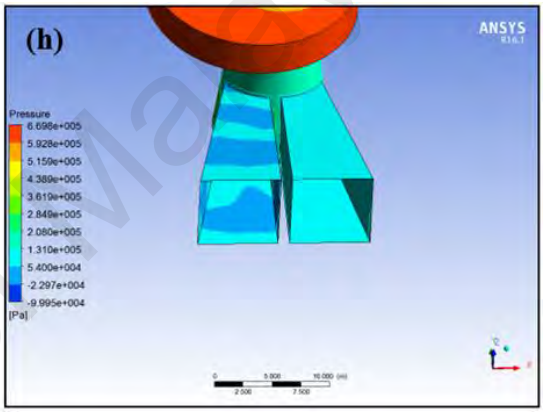

weir depth = 0 m and U/S.W.L. = 150.2 m.

Figure 4-6: continued

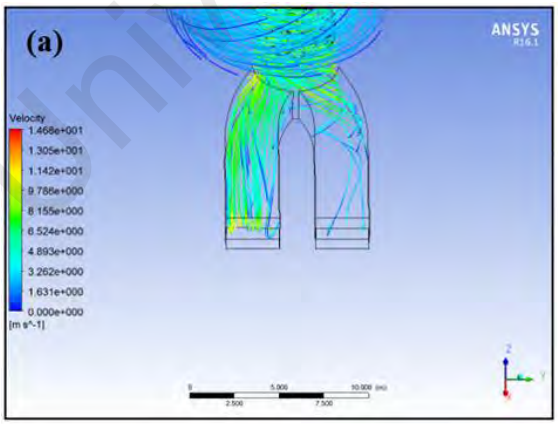

weir depth = 1.5 m and U/S.W.L. = 236.5 m

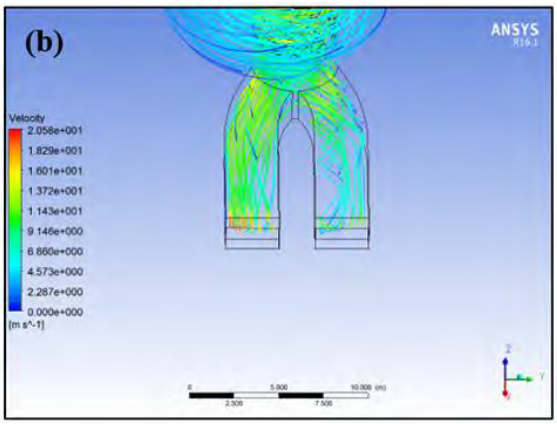

weir depth = 1.5 m and U/S.W.L. = 248.42 m

Figure 4.7: Flow velocity at Temenggor turbine.

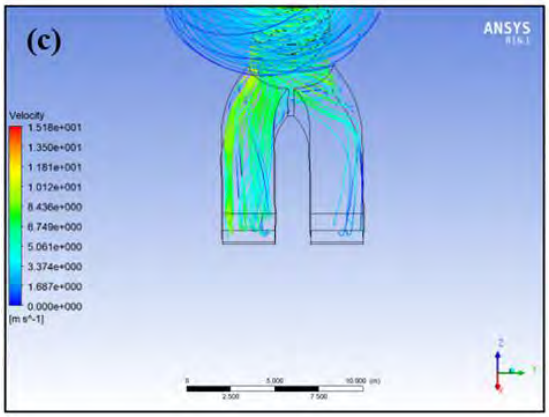

weir depth = 1 m and U/S.W.L. = 236.5 m

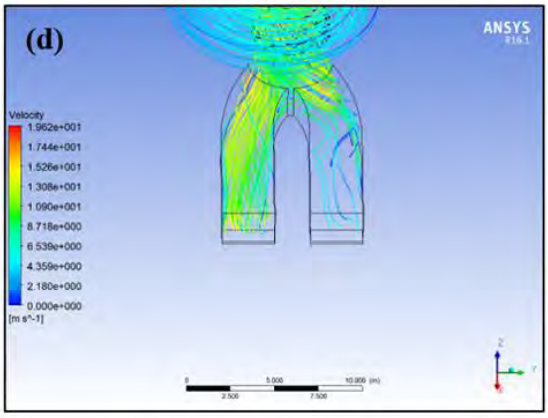

weir depth = 1 m and U/S.W.L. = 248.42 m

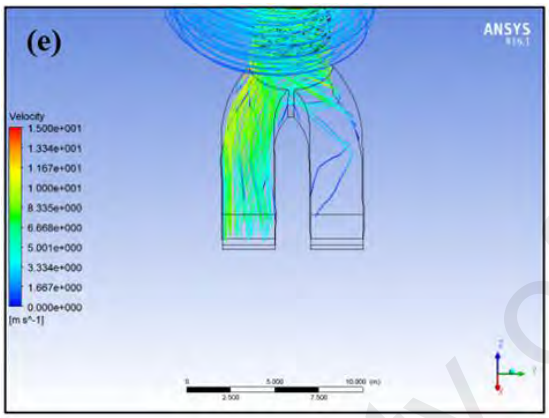

weir depth = 0.5m and U/S.W.L. = 236.5 m

weir depth = 0.5 m and U/S.W.L. = 248.42 m

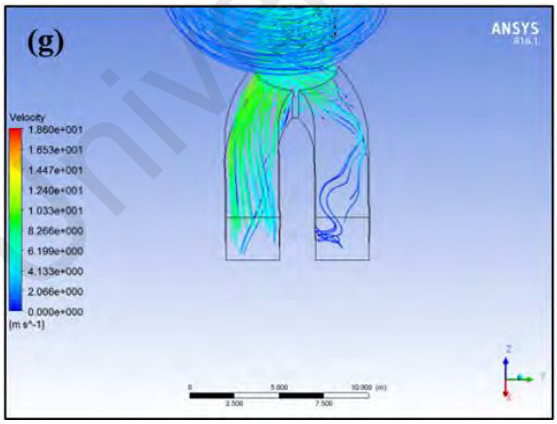

weir depth = 0 m and U/S.W.L. = 236.5 m

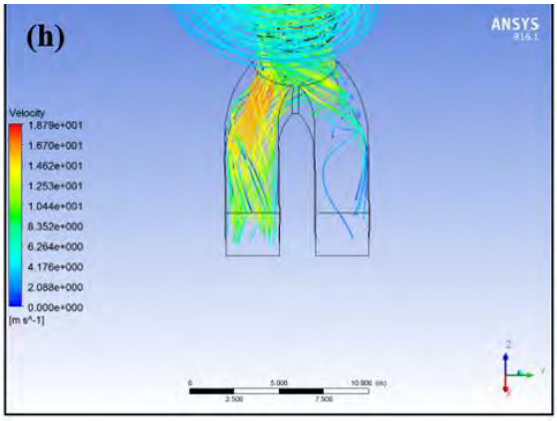

weir depth = 0 m and U/S.W.L. = 248.42 m

Figure4-7: continued

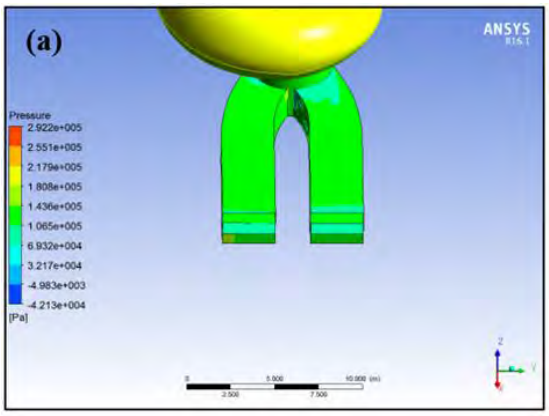

weir depth = 1.5 m and U/S.W.L. = 236.5 m

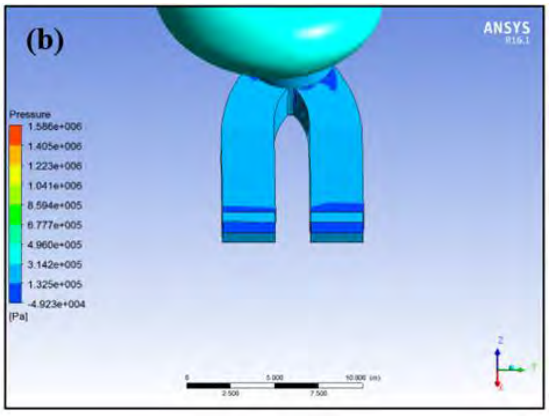

weir depth = 1.5 m and U/S.W.L. = 248.42 m

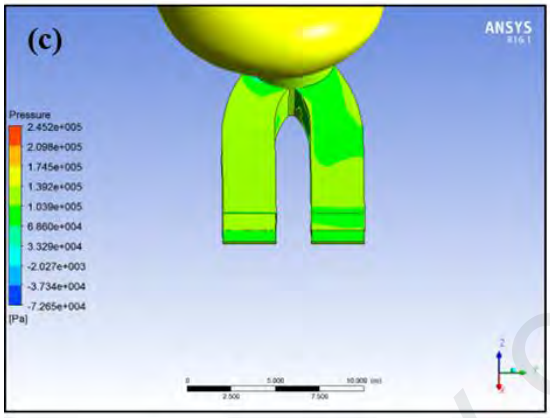

weir depth = 1 m and U/S.W.L. = 236.5 m

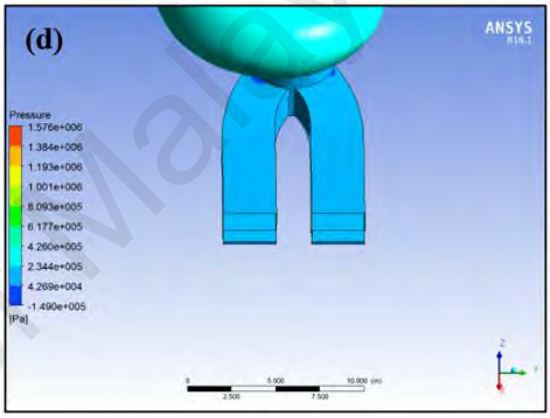

weir depth = 1 m and U/S.W.L. = 248.42 m

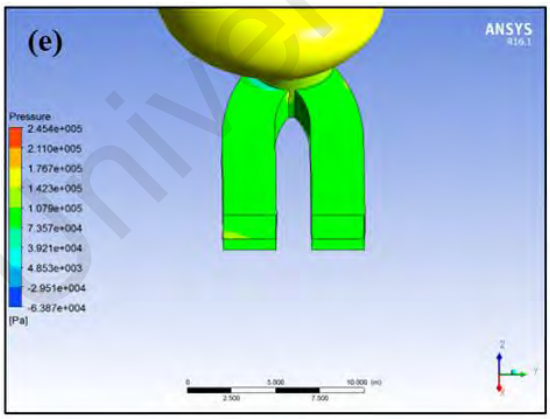

weir depth = 0.5m and U/S.W.L. = 236.5 m

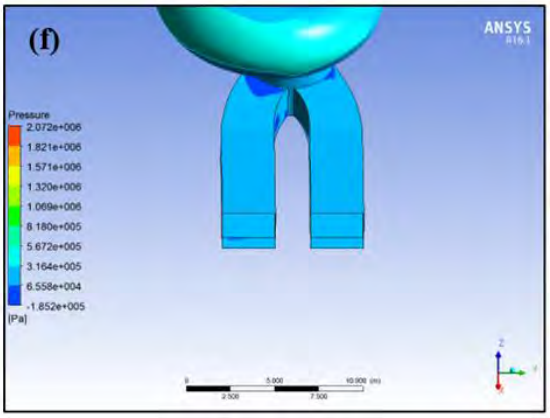

weir depth = 0.5 m and U/S.W.L. = 248.42 m

Figure 4.8: Flow pressure at Temenggor turbine

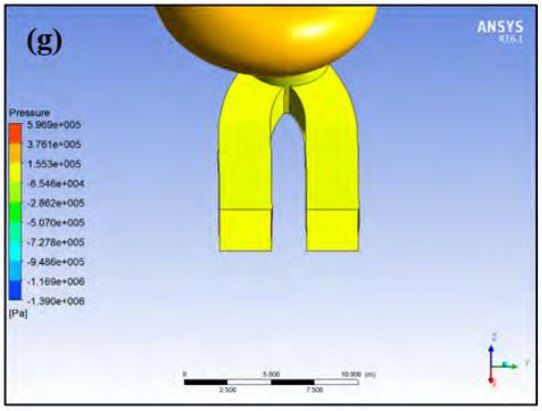

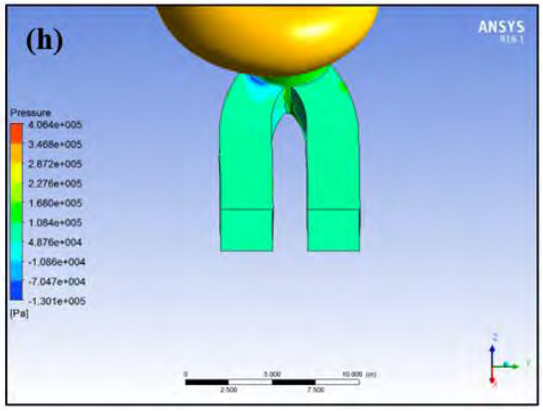

weir depth = 0 m and U/S.W.L. = 236.5 m	weir depth = 0 m and U/S.W.L. = 248.42 m

Figure 4-8: continued

4.3 Simulation results from 3-D FE dam models (second group)

The dynamic behavior results founded by applying strong earthquake on the Haditha and Temenggor dam models taking into consideration the effect of the dam-reservoir-foundation interaction in different foundation depths and water levels. By connecting the ANSYS-model with ANSYS-HARMONIC RESPONSE as explained in Figure 4.9 and run 3-D FE dam models to compute the parameters that included principal stresses, normal stress in the direction of flow, vertical stress, total displacement, the displacement in the direction of flow, vertical displacement, and the natural frequency.

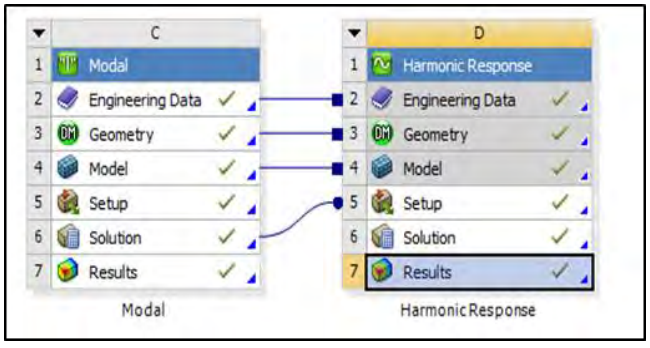

Figure 4.9: The connection between ANSYS-Model and ANSYS-Harmonic Response

4.3.1 Simulation of natural frequency and mode shapes results of 3-D FE

The natural frequencies result of Haditha and Temenggor embanked dams with the case of empty and maximum water levels with three assumptions of reactions fixed, sallow, and deep depths of the foundation, are presented in Table 4.4 and Table 4.5. This assumption was found similar to the results by Watanabe et al. (1996).

Table 4.4: Natural Frequencies for Haditha earth-fill dam of different models

	Fixed base	Earth bed d = 20 m	Earth bed d = 57 m	Fixed base	Earth bed d = 20 m	Earth bed d = 57m
	Empty reservoir			**Full reservoir**		
Mode	Model 1	Model 2	Model 3	Model 1'	Model 2'	Model 3'
1	5.8699	5.6111	4.8606	4.9663	4.6695	4.2612
2	6.7163	6.1159	5.0983	4.9707	4.6783	4.2791
3	7.2138	6.4624	5.1475	4.9720	4.6835	4.2950
4	7.3014	6.5821	5.1742	4.9759	4.6845	4.2957

Table 4.5: Natural Frequencies for Temenggor rock-fill dam of different models

	Fixed base	Rock bed d = 13m	Rock bed d = 127m	Fixed base	Rock bed d = 13m	Rock bed d = 127m
	Empty reservoir			**Full reservoir**		
Mode	Model 1	Model 2	Model 3	Model 1'	Model 2'	Model 3'
1	4.917	4.697	3.210	1.9204	1.900	1.863
2	5.462	5.190	4.130	2.0748	2.094	1.954
3	5.818	5.635	4.253	2.2793	2.223	2.150
4	5.992	5.779	4.583	2.3741	2.349	2.329

Adding the water effect and increasing the foundation depth to the Hadith and Temenggor dam models of the dam-foundation-reservoir system led to increasing the mass in which decreased the natural frequencies of the system; yet, not more than 41.6% and 68.9%, respectively (in Empty reservoir**)**. Figure 4.10 outlined the decreasing of the natural frequency values with the increasing of the foundation depth in full reservoir case in Haditha dam and empty reservoir case in Temenggor dam.

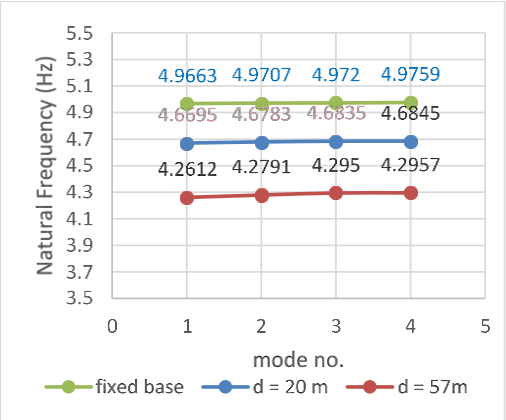

a: The natural frequencies for Haditha dam of 3D FEM with full reservoir

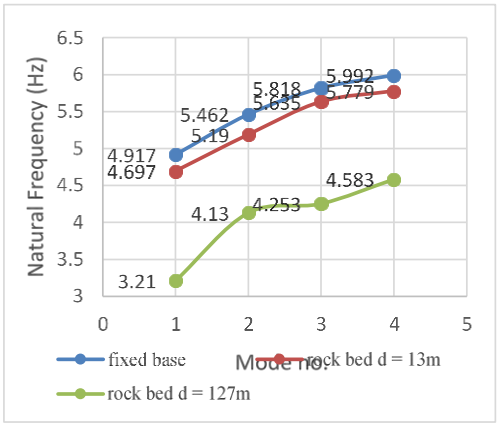

b: The natural frequencies for Temenggor dam of 3D FEM with empty reservoir

Figure 4.10: The natural frequency values with the increasing of foundation depth

The 3-D FE mode shapes results of Haditha and Temenggor dams of an empty reservoir with deep bed foundation 57 m and 127 m, respectively are presented in Figure 4.11 and 4.12.

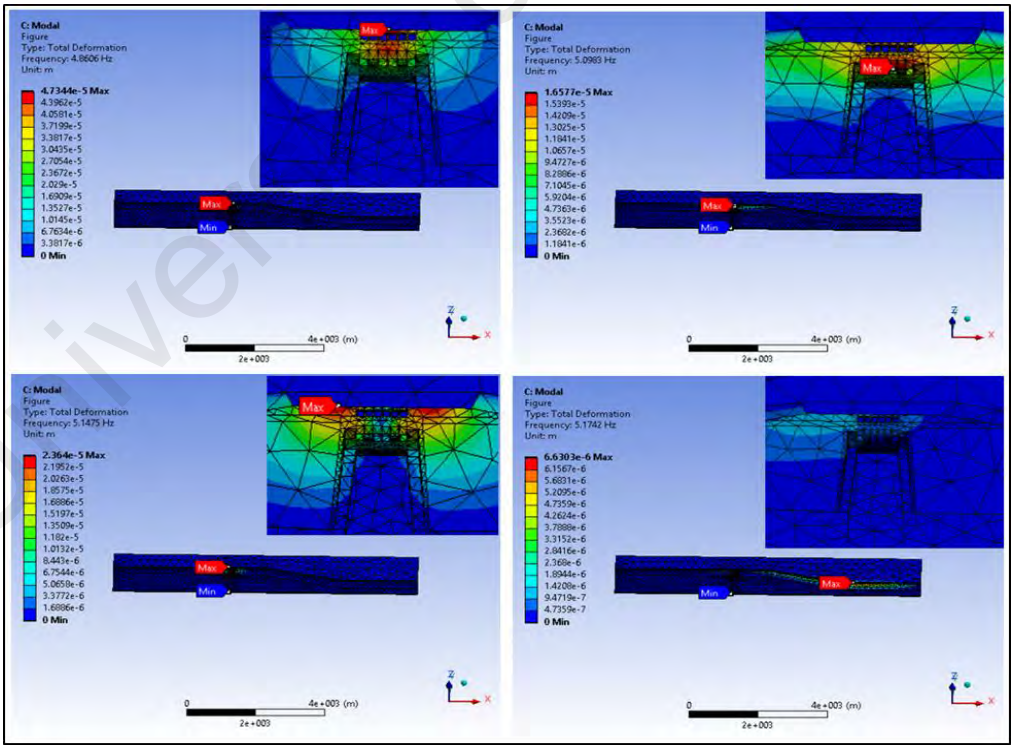

Figure 4.11: Four mode shapes of Haditha dam empty reservoir with 57 m bed foundation

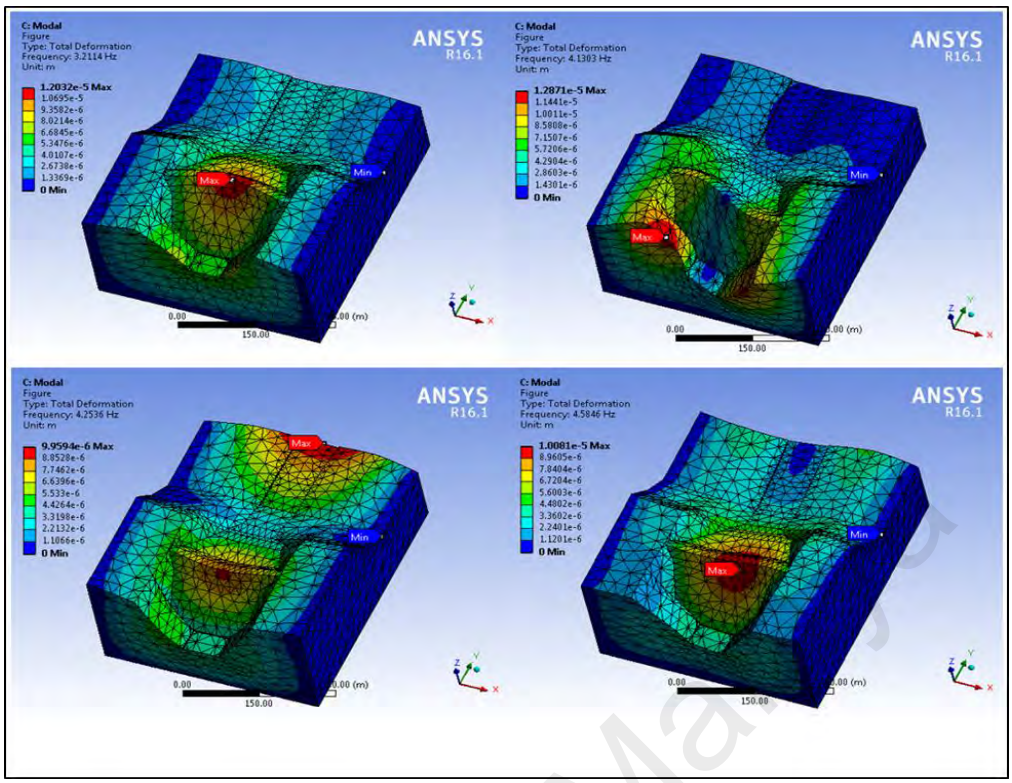

Figure 4.12: Four mode shapes of Temenggor dam of empty reservoir with 127 m rock-bed foundation

And the 3-D FE mode shapes results for the dams of a full reservoir with the fixed base are presented in Figure 4.13 and 4.14.

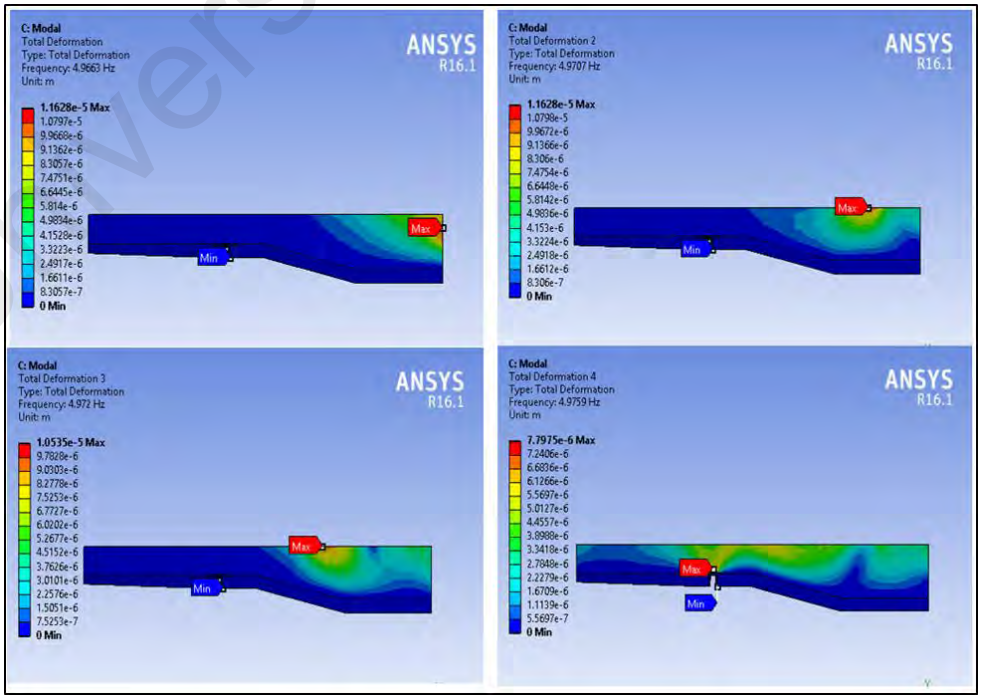

Figure 4.13: Four mode shapes of Haditha full reservoir dam with fixed base

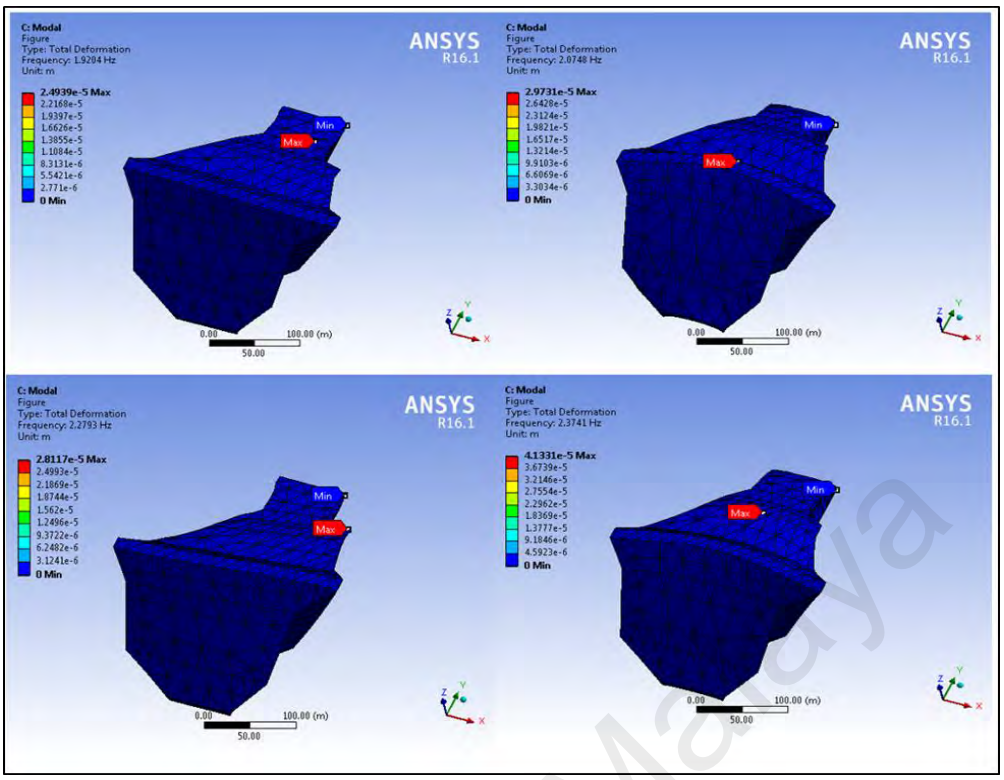

Figure 4.14: Four mode shapes of Temenggor dam of full reservoir with fixed base

4.3.2 Simulation of seismic effect with fixed base

The determination of the set of stresses (principal stress, normal stress in the flow direction and vertical stress) and deformed shapes (total deformation, deformation in the flow direction, and vertical deformation) are an important parameter in interpreting the dynamic behaviours of the embanked dam. Assuming the dam has a fixed base, the influence of empty and full reservoir to seismic effects will be discussed. The results of the analysis are listed in Table 4.6 and Table 4.7. The critical results for principal stresses are shown in Figure 4.15.

Table 4.6: The set of stresses results and deformed shapes of 3-D FE Haditha model

Fixed base			Principal Stress		Stress in flow direction		Vertical stress	
			min.	max.	min.	max.	min.	max.
	Hz	time(sec)	units (kPa)					
Full-reservoir	0.1	10	-17.85	140.7	-96.63	65.596	-150	80.101
	2	0.5	-0.939	7.386	-5.071	3.443	-7.8	4.212
Empty-reservoir	0.1	10	-116.8	1510.7	-454.6	490.7	-972	1500.1
	2	0.5	-9.242	120.93	-35.87	39.690	-80	120.11
Fixed base			total deformation		deformation in flow direction		vertical deformation	
			min.	max.	min.	max.	min.	max.
	Hz	time(sec)	units (mm)					
Full-reservoir	0.1	10	0	4.012	-0.04	3.797	-1.39	1.538
	2	0.5	0	0.3	-0.003	0.284	-0.10	0.115
Empty-reservoir	0.1	10	0	2.608	-0.034	2.3895	-1.07	0.941
	2	0.5	0	0.212	-0.003	0.1932	-0.08	0.075

Table 4.7: The set of stresses results and deformed shapes of 3-D FE Temenggor model

Fixed base			Principal Stress		Stress in flow direction		Vertical stress	
			min.	max.	min.	max.	min.	max.
	Hz	time(sec)	units (kPa)					
Full-reservoir	0.1	10	-1843	1996	-2989	1796	-6974	3685
	2	0.5	-1.5	1.1	-2.0	0.9	-4.7	0.7
Empty-reservoir	0.1	10	-191	1637	-439	619.9	-455	1360
	2	0.5	-4.3	37.5	-10.1	14.2	-10.5	31.2
Fixed base			total deformation		deformation in flow direction		vertical deformation	
			min.	max.	min.	max	min.	max
	Hz	time(sec)	units (mm)					
Full-reservoir	0.1	10	0.00	18.74	-0.03	16.97	-8.75	2.21
	2	0.5	0.00	0.03	0.00	0.02	-0.01	0.00
Empty-reservoir	0.1	10	0.00	4.50	0.00	4.43	-0.36	1.57
	2	0.5	0.00	0.10	0.00	0.10	-0.01	0.04

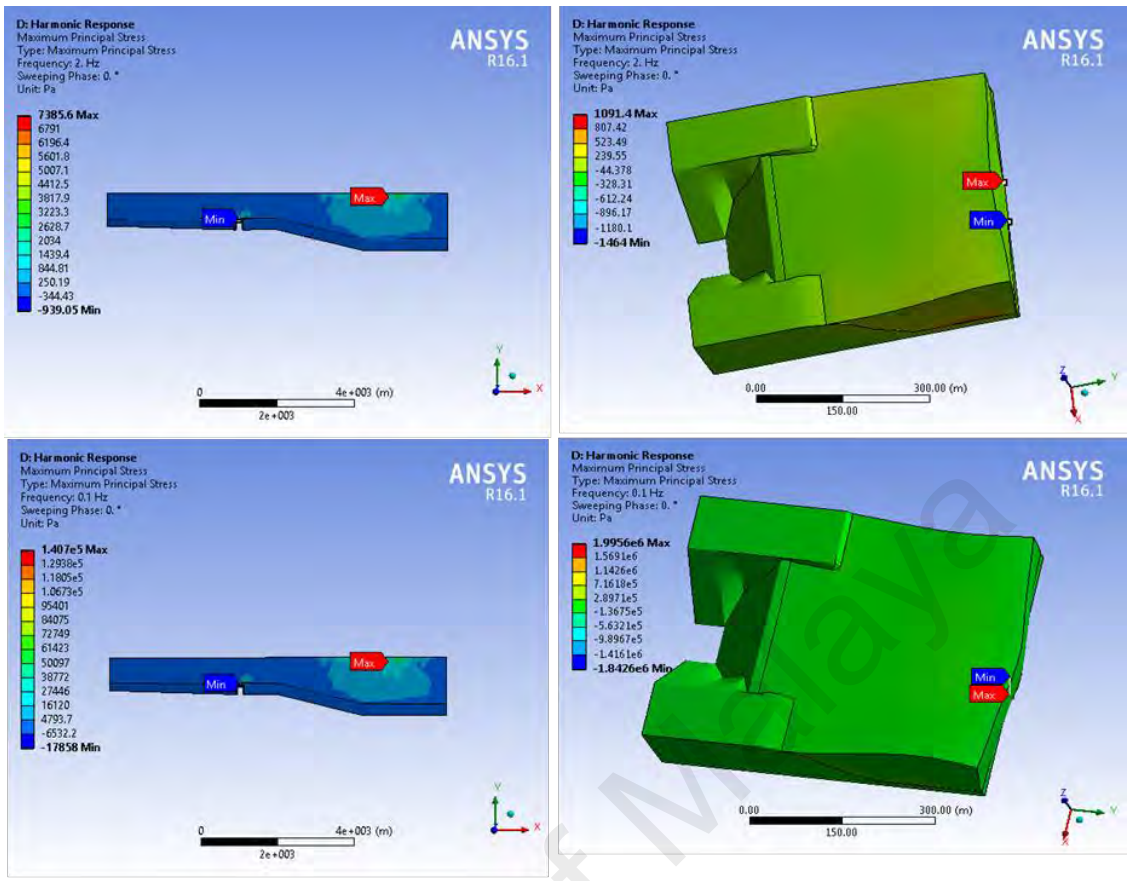

a) Principal stress distribution in the Haditha dam-reservoir system

b) Principal stress distribution in the Temenggor dam-reservoir system

Figure 4.15: The principal stresses 3-D FE model results of Haditha and Temenggor dams for the 0.1 and 2 Hz frequencies

The results of the seismic analysis showed that the ranges of principal stress increased by 92.5% and 99.98% for Haditha and Temenggor dams respectively (for the case of full reservoir). This is due to the effect of the earthquake was gradually increased with the time in the shock waves form. The percentages of stress reduction inconsistent with the results undertaken by Jain et al. (2015).

The range of displacements in Haditha and Temenggor dam-reservoir-foundation system varies from (-1.394 to 4.012 mm) and (-8.75 to 18.74 mm) in full reservoir condition, respectively. Figure 4.16 shows that the highest maximum displacement values were located in the reservoir region, implying that the range of displacements in the dam

bodies exceeds 0.13 mm and 4.31 mm as shown in Figure 4.17, although it remained less than 4.012 mm and 18.74 mm.

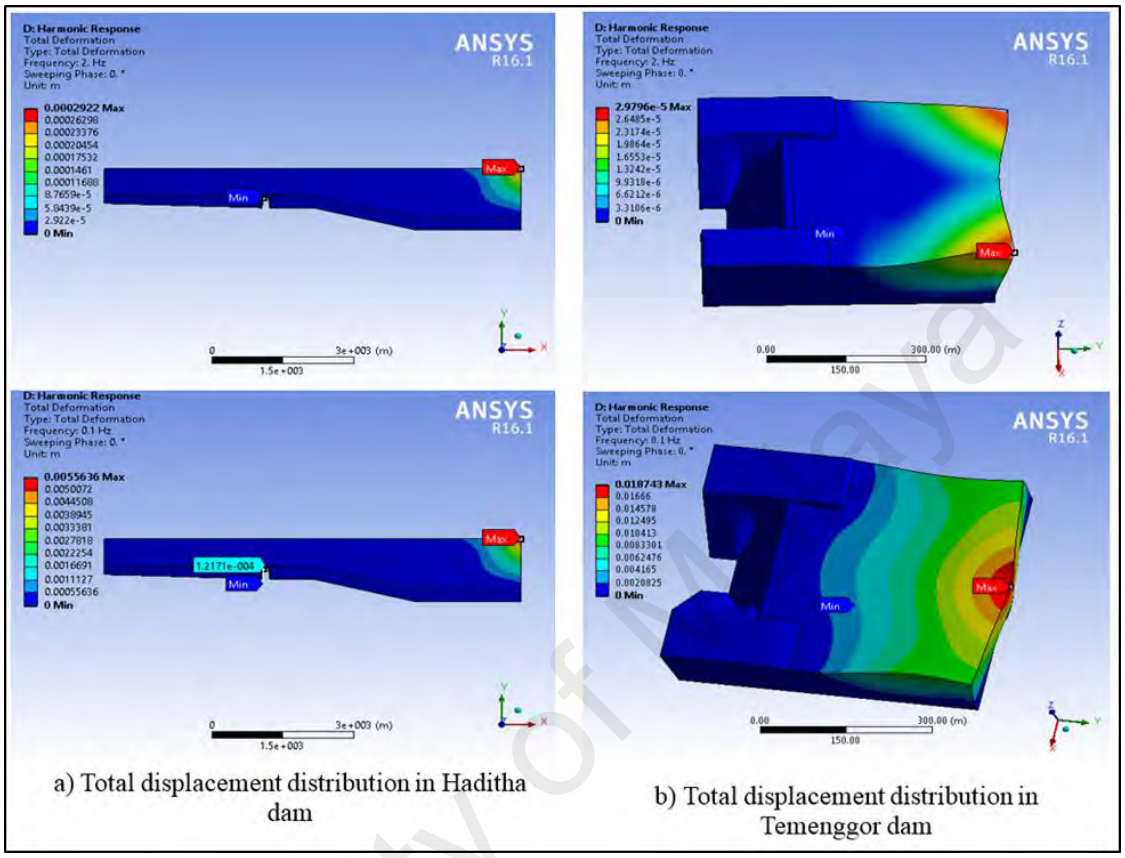

a) Total displacement distribution in Haditha dam

b) Total displacement distribution in Temenggor dam

Figure 4.16: Total displacement distribution in the dam-reservoir system models for 0.1 and 2Hz frequencies

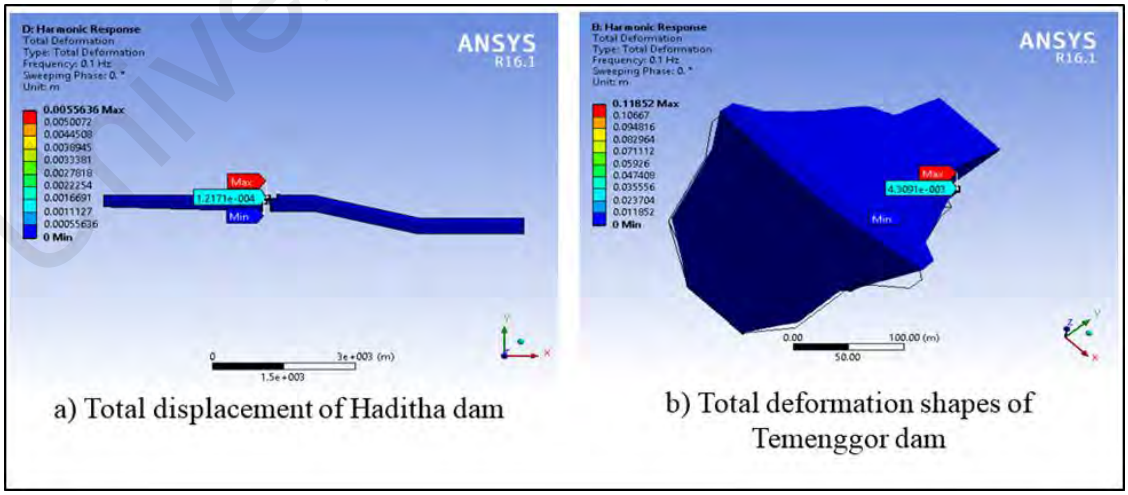

a) Total displacement of Haditha dam

b) Total deformation shapes of Temenggor dam

Figure 4.17: Total displacement distribution in the dam body models for 0.1 Hz

4.3.3 Simulation of seismic effect with shallow bed foundation

The foundation-dam interaction of Haditha and Temenggor dam-foundation-reservoir system were investigated by taking a foundation depth 20 m and 13 m, respectively with three assumptions of inertia properties (massless, 50% mass and complete mass model). The results of critical stresses and deformed shapes are listed in Table 4.8, Table 4.9, Table 4.10 and Table 4.11. The principal stress distribution and deformation shape in the direction of flow in both cases of empty and full reservoir at the same frequency are shown in Figure 4.18 and 4.19.

Table 4.8: The set of stresses results of 3-D numerical Haditha Dam-Reservoir-Foundation system

Earth- bed =20 m				Principal Stress		Stress in flow direction		Vertical stress	
				min.	max.	min.	max	min.	max
	Hz	Time (sec)	Mass coef.	n = 0.5, units (kPa)					
Full	0.1	10	0	-98.46	123.11	-244	40.26	-103.7	48.614
	2	0.5		-1.778	2.22	-4.416	0.727	-1.875	0.878
	0.1	10	0.5	-98.44	123.08	-244.3	40.25	-103.7	48.603
	2	0.5		-1.778	2.224	-4.416	0.727	-1.875	0.878
	0.1	10	1	-98.42	123.05	-244.3	40.24	-103.7	48.592
	2	0.5		-1.771	2.21	-4.398	0.724	-1.867	0.8745
Empty	0.1	10	0	-206.4	1449.7	-330	481.8	-1094	1441.6
	2	0.5		-4.899	32.871	-7.393	11.28	-26.0	32.690
	0.1	10	0.5	-206.4	1449.4	-330.5	481.7	1094	1441.3
	2	0.5		-4.89	32.80	-7.37	11.2	-25.9	32.62
	0.1	10	1	-206.3	1449.1	-330	481.6	-1094	1441.1
	2	0.5		-4.886	32.747	-7.36	11.25	-25.9	32.567
	Hz	Time (sec)	Mass coef.	n = 0.25, units (kPa)					
Full	0.1	10	0	-106.6	133.39	-264.8	43.62	-112.4	52.674
	2	0.5		-5.573	6.968	-13.83	2.279	-5.875	2.751
	0.1	10	0.5	-106.6	133.37	-264.8	43.61	-112.4	52.667
	2	0.5		-5.554	6.943	-13.78	2.271	-5.854	2.7415
	0.1	10	1	-106.6	133.35	-264.7	43.61	-112.4	52.66
	2	0.5		-5.534	6.919	-13.7	2.263	-5.83	2.7318
Empty	0.1	10	0	-221.5	1556.1	-354.9	517.1	-1174	1547.4
	2	0.5		-18.17	122.11	-27.47	41.86	-96.4	121.44
	0.1	10	0.5	-0.022	1555.9	-354.8	517.1	-1174	1547.3
	2	0.5		-18.1	121.68	-27.37	41.75	-96.2	121.02
	0.1	10	1	-221.5	1555.8	-354.8	517	-1174	1547.1
	2	0.5		-18.0	121.25	-27.27	41.6	-95.9	120.59

Table 4.9: The deformed shape results of 3-D numerical Haditha Dam-Reservoir-Foundation system

Earth- bed =20 m				Total deformation		Deformation in flow direction		Vertical deformation	
				min.	max.	min.	max	min.	max
	Hz	time(sec)	Mass coef.	n= 0.5, units (mm)					
Full	0.1	10	0	0	4.600	-0.104	4.499	-0.940	0.073
	2	0.5		0	0.083	-0.002	0.081	-0.017	0.001
	0.1	10	0.5	0	4.598	-0.104	4.498	-0.940	0.073
	2	0.5		0	0.083	-0.002	0.081	-0.017	0.001
	0.1	10	1	0	4.597	-0.104	4.497	-0.940	0.073
	2	0.5		0	0.083	-0.002	0.081	-0.016	0.001
Empty	0.1	10	0	0	3.192	-0.029	2.935	-1.251	0.840
	2	0.5		0	0.077	-0.000	0.070	-0.03	0.02
	0.1	10	0.5	0	3.192	-0.029	2.935	-1.252	0.840
	2	0.5		0	0.076	-0.000	0.070	-0.03	0.02
	0.1	10	1	0	3.191	-0.029	2.934	-1.252	0.840
	2	0.5		0	0.076	-0.000	0.070	-0.030	0.019
	Hz	time(sec)	Mass coef.	n = 0.25, units (mm)					
Full	0.1	10	0	0	4.984	-0.113	4.875	-0.102	0.079
	2	0.5		0	0.260	-0.006	0.255	-0.053	0.004
	0.1	10	0.5	0	4.983	-0.113	4.874	-1.019	0.079
	2	0.5		0	0.259	-0.005	0.254	-0.053	0.004
	0.1	10	1	0	4.982	-0.113	4.873	-1.018	0.0787
	2	0.5		0	0.253	-0.059	0.253	-0.053	0.004
Empty	0.1	10	0	0	3.426	-0.031	3.149	-1.345	0.902
	2	0.5		0	0.284	-0.003	0.261	-0.111	0.072
	0.1	10	0.5	0	3.425	-0.031	3.149	-1.344	0.902
	2	0.5		0	0.283	-0.002	0.260	-0.111	0.072
	0.1	10	1	0	3.425	-0.031	3.149	-1.343	0.902
	2	0.5		0	0.282	-0.003	0.259	-0.110	0.072

Table 4.10: The set of stresses results of 3-D numerical Temenggor Dam-Reservoir-Foundation system

Rock- bed =13 m				Principal Stress		Stress in flow direction		Vertical stress	
				min.	max.	min.	max	min.	max
	Hz	time(sec)	Mass coef.	n = 0.5, units (kPa)					
Full	0.1	10	0	-437.4	1783.3	-481.7	1430.0	-1579	301.0
	2	0.5		-0.7	2.8	-0.8	2.2	-2.5	0.7
	0.1	10	0.5	-436.9	1781.0	-481.1	1428.2	-1577	300.7
	2	0.5		-0.7	2.7	-0.8	2.2	-2.4	0.7
	0.1	10	1	-436.3	1778.7	-480.5	1426.3	-1575	300.3
	2	0.5		-0.7	2.7	-0.8	2.2	-2.4	0.7
Empty	0.1	10	0	-203.7	1707.8	-476.2	645.8	-405.7	1373.8
	2	0.5		4.5	38.4	-10.9	14.5	-9.2	30.9
	0.1	10	0.5	-203.7	1707.5	-476.1	645.6	-405.6	1373.6
	2	0.5		-4.5	38.4	-10.9	14.5	-9.2	30.8
	0.1	10	1	-203.7	1707.2	-476.0	645.5	-405.5	1373.3
	2	0.5		-4.5	38.3	-10.9	14.5	-9.2	30.8
	Hz	time(sec)		n = 0.25, units (kPa)					
Full	0.1	10	0	-443.0	2324.3	-500.2	1840.4	-1899	289.0
	2	0.5		-0.9	4.5	-1.1	3.5	-3.7	0.8
	0.1	10	0.5	-442.4	2321.4	-499.5	1838.1	-1897	288.6
	2	0.5		-0.9	4.4	-1.1	3.5	-3.6	0.8
	0.1	10	1	-441.9	2318.5	-498.9	1835.8	-1894	288.3
	2	0.5		-0.9	4.4	-1.1	3.5	-3.6	0.8
Empty	0.1	10	0	-231.6	1978.6	-531.3	748.4	-412.3	1552.1
	2	0.5		-5.6	48.1	-13.1	18.2	-10.0	37.8
	0.1	10	0.5	-231.6	1978.4	-531.3	748.3	-412.2	1552.0
	2	0.5		-5.5	48.1	-13.1	18.2	-10.0	37.8
	0.1	10	1	-231.6	1978.2	-531.2	748.2	-412.2	1551.8
	2	0.5		-5.5	48.0	-13.1	18.2	-10.0	37.8

Table 4.11: The deformed shape results of 3-D numerical Temenggor Dam-Reservoir-Foundation system

Rock- bed =13 m				Total deformation		Deformation in flow direction		Vertical deformation	
				min.	max.	min.	max	min.	max
	Hz	time(sec)	Mass coef.	n= 0.5, units (mm)					
Full	0.1	10	0	0.00	18.11	-0.03	17.12	-5.93	2.03
	2	0.5		0.00	0.03	0.00	0.03	-0.01	0.00
	0.1	10	0.5	0.00	18.09	-0.03	17.10	-5.92	2.03
	2	0.5		0.00	0.03	0.00	0.03	-0.01	0.00
	0.1	10	1	0.00	18.06	-0.03	17.08	-5.92	2.03
	2	0.5		0.00	0.03	0.00	0.03	-0.01	0.00
Empty	0.1	10	0	0.00	4.96	0.00	4.89	-0.35	1.72
	2	0.5		0.00	0.11	0.00	0.10	-0.01	0.04
	0.1	10	0.5	0.00	4.96	0.00	4.89	-0.35	1.72
	2	0.5		0.00	0.11	0.00	0.10	-0.01	0.04
	0.1	10	1	0.00	4.95	0.00	4.89	-0.35	1.72
	2	0.5		0.00	0.11	0.00	0.10	-0.01	0.04
	Hz	time(sec)		n = 0.25, units (mm)					
Full	0.1	10	0	0.00	17.04	-0.03	16.14	-5.50	2.08
	2	0.5		0.00	0.03	0.00	0.03	-0.01	0.01
	0.1	10	0.5	0.00	17.02	-0.03	16.12	-5.49	2.07
	2	0.5		0.00	0.03	0.00	0.03	-0.01	0.01
	0.1	10	1	0.00	17.00	-0.03	16.10	-5.49	2.07
	2	0.5		0.00	0.03	0.00	0.03	-0.01	0.01
Empty	0.1	10	0	0.00	3.70	0.00	3.69	-0.22	0.96
	2	0.5		0.00	0.08	0.00	0.08	-0.01	0.02
	0.1	10	0.5	0.00	3.70	0.00	3.69	-0.22	0.96
	2	0.5		0.00	0.08	0.00	0.08	-0.01	0.02
	0.1	10	1	0.00	3.70	0.00	3.69	-0.22	0.96
	2	0.5		0.00	0.08	0.00	0.08	-0.01	0.02

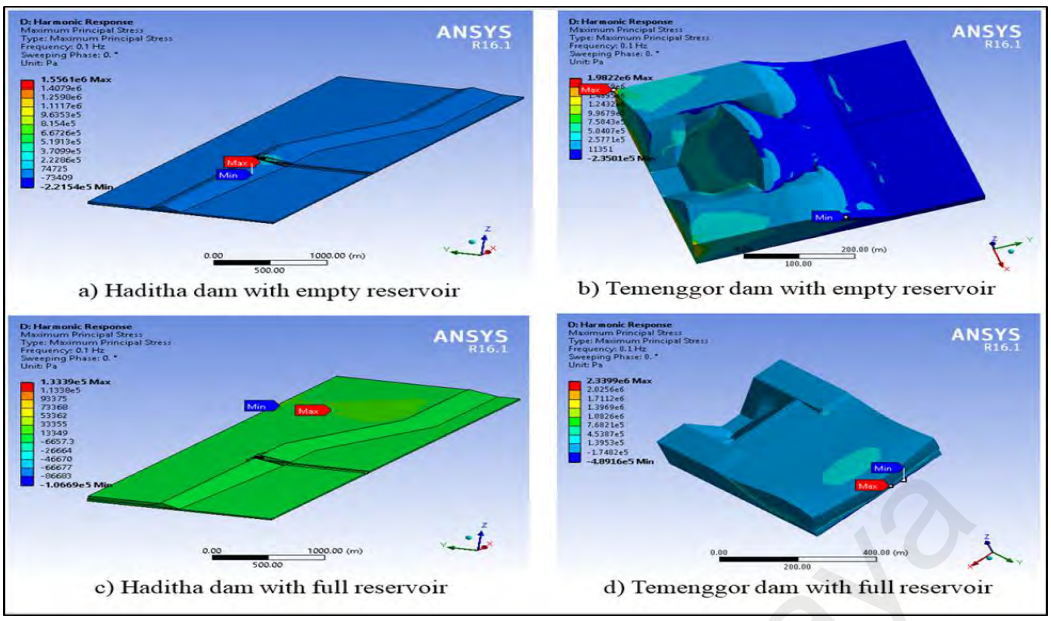

Figure 4.18: Principal stress distribution in Haditha and Temenggor dams for the cases of empty and full reservoir for Hz =0.1

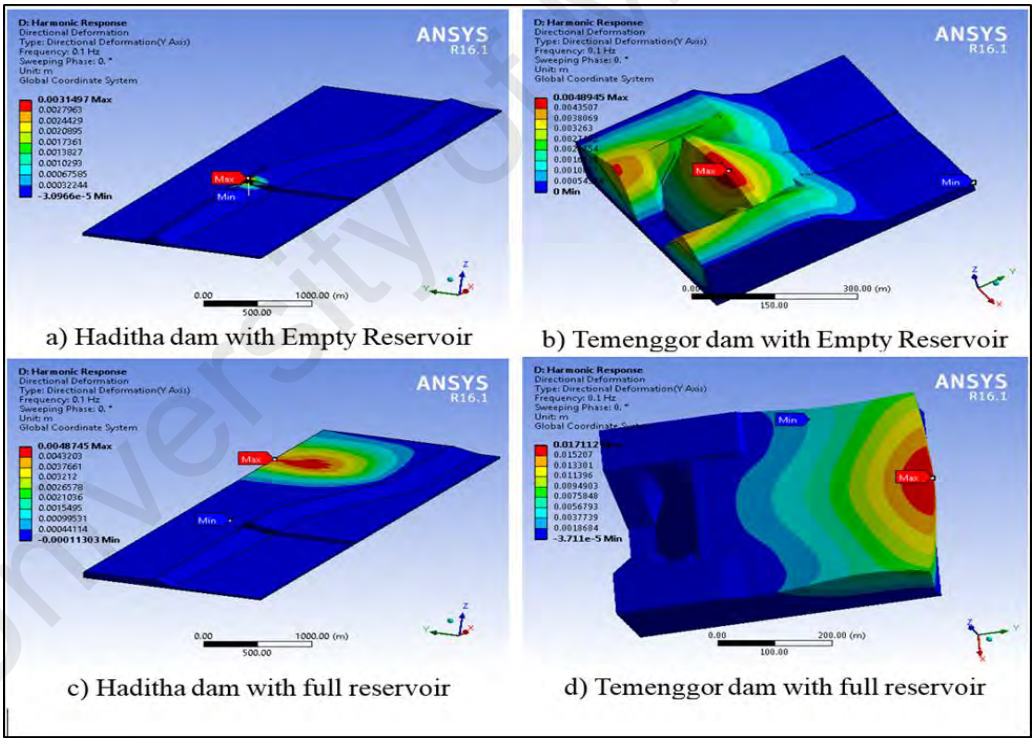

Figure 4.19: Deformed shape in flow direction for Haditha and Temenggor dams for the cases of empty and full reservoir for Hz=0.1

After analyzing the results, it appeared that the critical values of principal, the direction of flow, and vertical stresses of Haditha dam-reservoir-foundation system happened with the empty case for n = 0.25 (1556.1, 517, and 1547.9 kPa), respectively. Whereas, the critical stress values of Temenggor dam-reservoir-foundation system happened with the full reservoir case with n = 0.25 (2324.3, 1840.4, and 1899.4 kPa), respectively. The differences of critical values of these parameters of Haditha and Temenggor dam-reservoir-foundation system between empty and full cases are (1422.71, 473.5, and 1494 kPa) and (345, 1092, and 1487.1kPa), respectively. However, the locations of critical values were different in both cases. The results showed that the different percentages of (principal, the direction of flow, and vertical) stress at the midpoint of the crest of Haditha and Temenggor dams were (72%,101%, and 164%) and (60%, 79%, and 72%), respectively.

The analysis results of the fixed base assumption and shallow rock bed appeared to have difference of critical total deformation values 0.9 mm in Haditha dam- reservoir-foundation system, while the same maximum deformation ≅ 18 mm in Temenggor dam-reservoir- foundation system, and the different percentages of critical values between empty and full cases for total, direction of flow, and vertical displacements for Haditha and Temenggor dam- reservoir- foundation system were (31.3%, 35.4%, and 92.4%) for n= 0.25 and (73%, 71.4%, and 94%) for n = 0.25, respectively. However, the displacement results at the midpoint of the crest show that the values of the empty case were larger than the full case was closest to the results of Albano et al. (2015) and Yilmazturk et al. (2015).

4.3.4 Simulation of seismic effect with deep bed foundation

The Haditha and Temenggor dam-foundation interaction were investigated by taking the foundation depth to be 57m and 127 m, respectively to compare between the shallow

and deep foundation effects on the dynamic behaviours of the earth and rock-fill dams. The results of critical stresses and deformed shapes are listed in Table 4.12, 4.13, 4.14, and 4.15.

Table 4.12: The set of stresses results of 3-D numerical Haditha Dam-Reservoir-Foundation system

Earth- bed =57 m				Principal Stress		Stress in flow direction		Vertical stress	
				min.	max.	min.	max	min.	max
	Hz	time(sec)	Mass coef.	n = 0.5, units (kPa)					
Full	0.1	10	0	-93.98	256.21	-224.1	82.794	-96.05	25.442
	2	0.5		-1.68	4.5797	-4.006	1.479.9	-1.716	0.45474
	0.1	10	0.5	-93.96	256.14	-224.0	82.772	-96.02	25.435
	2	0.5		-1.675	4.5685	-3.99	1.4763	-1.71	0.4536
	0.1	10	1	-93.9	256.07	-224	82.75	-95.9	25.428
	2	0.5		-1.671	4.557	-3.986	1.4727	-1.085	0.4525
Empty	0.1	10	0	-373	5097.4	-1655	1381.7	-2040	5058.2
	2	0.5		-8.28	113.11	-36.74	30.670	-45.29	112.24
	0.1	10	0.5	-373	5096.4	-1655	1381.4	-2040	5057.2
	2	0.5		-8.271	112.88	-36.6	30.606	-45.1	112.01
	0.1	10	1	-373	5095.4	-1655	1381.1	-2039	5056.2
	2	0.5		-8.25	112.64	-36.5	30.543	-45.1	111.77
	Hz	time(sec)	.	n=0.25, units (kPa)					
Full	0.1	10	0	-101.6	277.17	-242.4	89.568	-103.9	27.523
	2	0.5		-5.419	14.774	-12.92	4.774	-5.538	1.4671
	0.1	10	0.5	-101.6	277.13	-242.4	89.554	-103.8	27.519
	2	0.5		-5.396	14.71	-12.86	4.7537	-5.514	1.461
	0.1	10	1	-101.6	277.09	-242.3	89.539	-103.8	27.514
	2	0.5		-5.372	14.647	-12.81	4.732	-5.491	1.454
Empty	0.1	10	0	-400.9	5471.9	-1777	1483.2	-2190	5429.8
	2	0.5		-30.81	420.56	-136	114.03	-168.3	417.32
	0.1	10	0.5	-400.9	5471.3	-1777	1483	-2.19	5429.2
	2	0.5		-30.69	418.91	-136.0	113.59	-167.7	415.69
	0.1	10	1	-400.8	5470.7	-177.7	1482.9	-2190	5428.6
	2	0.5		-30.57	417.28	-135.5	113.15	-167	414.06

Table 4.13: The deformed shape results of 3-D numerical Haditha Dam-Reservoir-Foundation system

Earth-bed =57m				Total deformation		Deformation in flow direction		Vertical deformation	
				min.	max.	min.	max	min.	max
	Hz	time(sec)	Mass coef.	n= 0.5, units (mm)					
Full	0.1	10	0	0	7.404	-0.068	7.395	-0.843	0.361
	2	0.5		0	0.132	-0.001	0.132	-0.015	0.006
	0.1	10	0.5	0	7.402	-0.068	7.393	-0.843	0.361
	2	0.5		0	0.132	-0.001	0.132	-0.015	0.006
	0.1	10	1	0	7.4	-.068	7.391	-0.842	0.361
	2	0.5		0	0.132	-0.001	0.132	-0.015	0.006
Empty	0.1	10	0	0	9.637	-0.013	9.040	-3.453	3.176
	2	0.5		0	0.139	-0.000	0.201	-0.077	0.071
	0.1	10	0.5	0	9.635	-0.013	9.039	-3.452	3.176
	2	0.5		0	0.213	-0.000	0.200	-0.076	0.070
	0.1	10	1	0	9.633	-0.013	9.037	-3.452	3.175
	2	0.5		0	0.213	-0.000	0.1998	-0.076	0.070
				n = 0.25, units (mm)					
Full	0.1	10	0	0	8.009	-0.074	8.000	-0.912	0.391
	2	0.5		0	0.427	-0.004	0.426	-0.049	0.021
	0.1	10	0.5	0	8.008	-0.074	7.998	-0.912	0.391
	2	0.5		0	0.425	-0.004	0.425	-0.048	0.021
	0.1	10	1	0	8.007	-0.074	7.997	-0.912	0.391
	2	0.5		0	0.423	-0.004	0.423	-0.048	0.021
Empty	0.1	10	0	0	10.345	-0.013	9.705	-3.707	3.41
	2	0.5		0	0.795	-0.001	0.746	-0.285	0.2621
	0.1	10	0.5	0	10.344	-0.013	9.704	-3.706	3.4091
	2	0.5		0	0.792	-0.001	0.743	-0.284	0.2611
	0.1	10	1	0	10.343	-0.013	9.703	-3.706	3.409
	2	0.5		0	0.789	-0.010	0.740	-0.283	0.2601

Table 4.14: The set of stresses results of 3-D numerical Temenggor Dam-Reservoir-Foundation system

Rock- bed =127 m				Principal Stress		Stress in flow direction		Vertical stress	
				min.	max.	min.	max	min.	max
	Hz	time(sec)	Mass coef.	n = 0.5, units (kPa)					
Full	0.1	10	0	-373.2	1822.4	-571.9	1448.6	-2094	385.42
	2	0.5		-0.190	1.840	-1.13	0.450	-0.270	1.630
	0.1	10	0.5	-372.7	1819.8	-571.0	1446.5	-2091	384.87
	2	0.5		-0.19	1.82	-1.12	0.44	-0.27	1.610
	0.1	10	1	-372.1	1817.1	-570.2	1444.4	-2088	384.31
	2	0.5		-0.190	1.810	-1.110	0.440	-0.270	1.590
Empty	0.1	10	0	-520.8	3200.7	-1037	1209.2	-1080	2821.5
	2	0.5		-8.69	53.14	-17.39	20.08	-16.15	46.85
	0.1	10	0.5	-520	3199.3	-1037	1208.7	-1079	2820.3
	2	0.5		-8.65	52.900	-17.31	19.990	-16.06	46.630
	0.1	10	1	-520.3	3197.9	-1036	1208.2	-1079	2819
	2	0.5		-8.61	52.66	-17.24	19.89	-15.97	46.42
	Hz	time(sec)	.	n=0.25, units (kPa)					
Full	0.1	10	0	-375	2080	-555.8	1640.2	-2221	318.97
	2	0.5		-0.4	1.86	-0.54	1.46	-2.01	0.49
	0.1	10	0.5	-375	2077	-555	1638	-2219	318.56
	2	0.5		-0.39	1.84	-0.54	1.45	-1.99	0.48
	0.1	10	1	-374	2075	-554	1636	-2216	318
	2	0.5		-0.39	1.83	-0.53	1.44	-1.97	0.48
Empty	0.1	10	0	-664.5	3881.2	-1019	1465	-1972	3419
	2	0.5		-14.24	82.67	-21.8	31.21	-42.64	72.82
	0.1	10	0.5	-664	3880	-1018	1465	-1971	3419
	2	0.5		-14.2	82.47	-21.75	31.13	-42.54	72.65
	0.1	10	1	-664	3879	-1018	1465	-1971	3418
	2	0.5		-14.17	82.27	-21.69	31.06	-42.45	72.47

Table 4.15: The deformed shape results of 3-D numerical Temenggor Dam-Reservoir-Foundation system

Rock- bed =127 m				Total deformation		Deformation in flow direction		Vertical deformation	
				min.	max.	min.	max	min.	max
	Hz	time(sec)	Mass coef.	n= 0.5, units (mm)					
Full	0.1	10	0	0.00	30.67	-0.05	28.15	-12.18	1.99
	2	0.5		0.00	0.02	-0.02	0.00	0.00	0.01
	0.1	10	0.5	0.00	30.62	-0.05	28.11	-12.16	1.99
	2	0.5		0.00	0.02	-0.02	0.00	0.00	0.01
	0.1	10	1	0.00	30.58	-0.05	28.07	-12.14	1.99
	2	0.5		0.00	0.02	-0.02	0.00	0.00	0.01
Empty	0.1	10	0	0.00	14.63	0.00	14.38	-1.13	3.43
	2	0.5		0.00	0.24	0.00	0.24	-0.02	0.06
	0.1	10	0.5	0.00	14.62	0.00	14.37	-1.13	3.43
	2	0.5		0.00	0.24	0.00	0.23	-0.02	0.06
	0.1	10	1	0.00	14.62	0.00	14.37	-1.12	3.43
	2	0.5		0.00	0.24	0.00	0.23	0.02	0.06
	Hz	time(sec)	.	n = 0.25, units (mm)					
Full	0.1	10	0	0.00	22.94	-0.04	21.38	-8.31	2.15
	2	0.5		0.00	0.02	0.00	0.02	-0.01	0.00
	0.1	10	0.5	0.00	22.91	-0.04	21.35	-8.30	2.14
	2	0.5		0.00	0.02	0.00	0.02	-0.01	0.00
	0.1	10	1	0.00	5.73	0.00	5.44	-1.22	3.26
	2	0.5		0.00	0.12	0.00	0.11	-0.03	0.08
Empty	0.1	10	0	0.00	5.73	0.00	5.44	-1.22	3.26
	2	0.5		0.00	0.12	0.00	0.11	-0.03	0.07
	0.1	10	0.5	0.00	5.73	0.00	5.43	-1.22	3.26
	2	0.5		0.00	0.12	0.00	0.11	-0.03	0.07
	0.1	10	1	0.00	22.94	-0.04	21.38	-8.31	2.15
	2	0.5		0.00	0.02	0.00	0.02	-0.01	0.00

The changes in mass coefficient resulted in little changes in stresses and deformed shape parameters because the dynamic analysis depends on the total mass. However, stiffness coefficient is greatly influential upon the dynamic behaviours because it changes the physical properties which are the constituent dam body and foundation. Most critical values of stresses and displacements in the dam-reservoir-foundation system are not necessarily equal to the critical values in the dam body. Figure 4.20 and 4.21 show the critical values of Principal stresses and vertical displacement locations in the Haditha and Temenggor dam-reservoir-foundation systems and on the dam bodies separately.

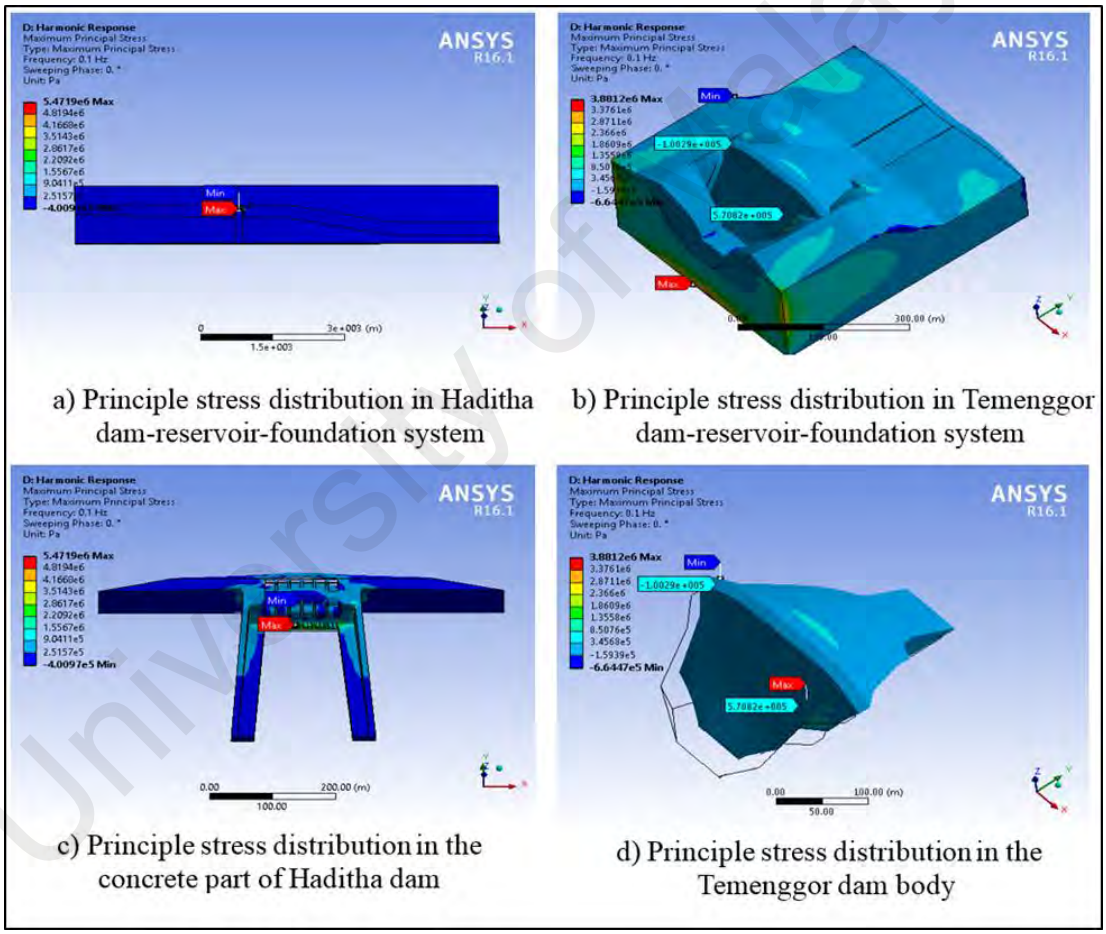

Figure 4.20: Ccritical values of principal stresses in the dams with empty reservoir condition for n = 0.25

The critical stress values located in the concrete part of Haditha dam body, while the results appeared that the different percentages of principal, in-flow direction and vertical

stresses between the Temenggor dam-reservoir-foundation system and dam body were only 85, 81, and 87%, respectively.

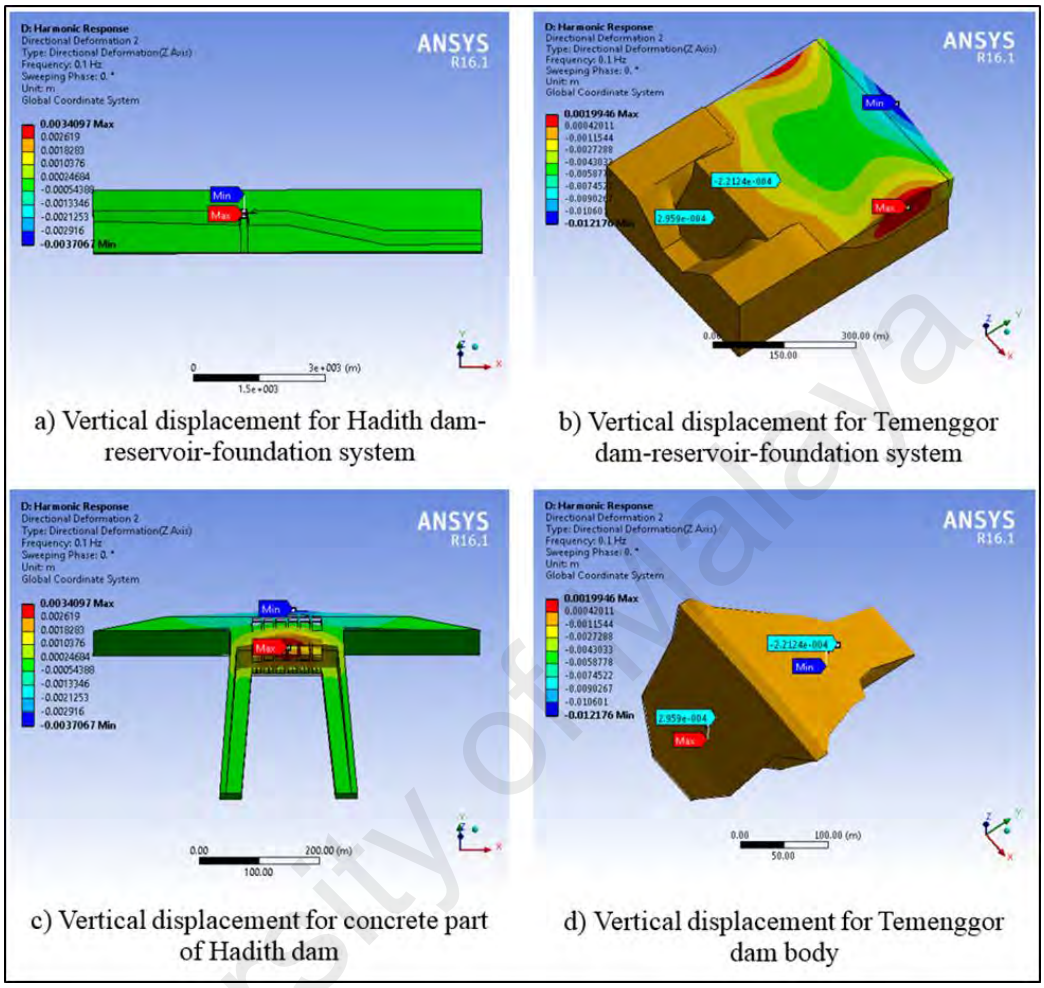

Figure 4.21: Maximum Vertical displacement for the dams with empty reservoir for the vales of n= 0.25 at Haditha dam and full reservoir condition for Temenggor dam with n = 0.5

The 3-D model analysis with deep foundation results outline that the total critical values, in-flow direction, and vertical displacements in the Haditha dam-reservoir-foundation system were (10.345, 9.704, and 3.707 mm), respectively and happen in empty case with n = 0.25, while the maximum values in Temenggor dam-reservoir-foundation system were (30.6, 28.15, and 2 mm), respectively and happen in full reservoir case with n = 0.5. because the height of water at Temenggor upstream reservoir is greater than the height of water in Haditha reservoir about three times. However, all these values were located in the reservoir region, meaning that the maximum values represent the water

movement in the reservoir only, and the real critical values of total, in-flow direction and vertical displacements were 2.43, 2.43, and 0.3 mm, respectively.

4.4 Optimal powerhouse operation (third group)

In every dam, hydropower generation must be optimally operated in according to the produced stresses and pressures on the dam body. This is highly vital for the purpose of obtaining reliable and practical processes in the hydropower system configuration. In addition, decision maker and hydraulic engineers are highly needed this optimization procedure to provide safe and sustainable dam operation. In Figure 4.22 and 4.23, a 3-D numerical presentation of Haditha and Temenggor dams were exhibited the powerhouse system pressure distribution on the dam body itself. As it can be seen in Figure 4.22, pressure distribution in the turbines number six that transformed from the CFX-turbine model to the ANSYS-Static structure dam model for Haditha dam; whereas, Figure 4.23 outlines the sequence and location of the four turbine units in Temenggor dam where their pressures were transformed from turbine model on the dam body.

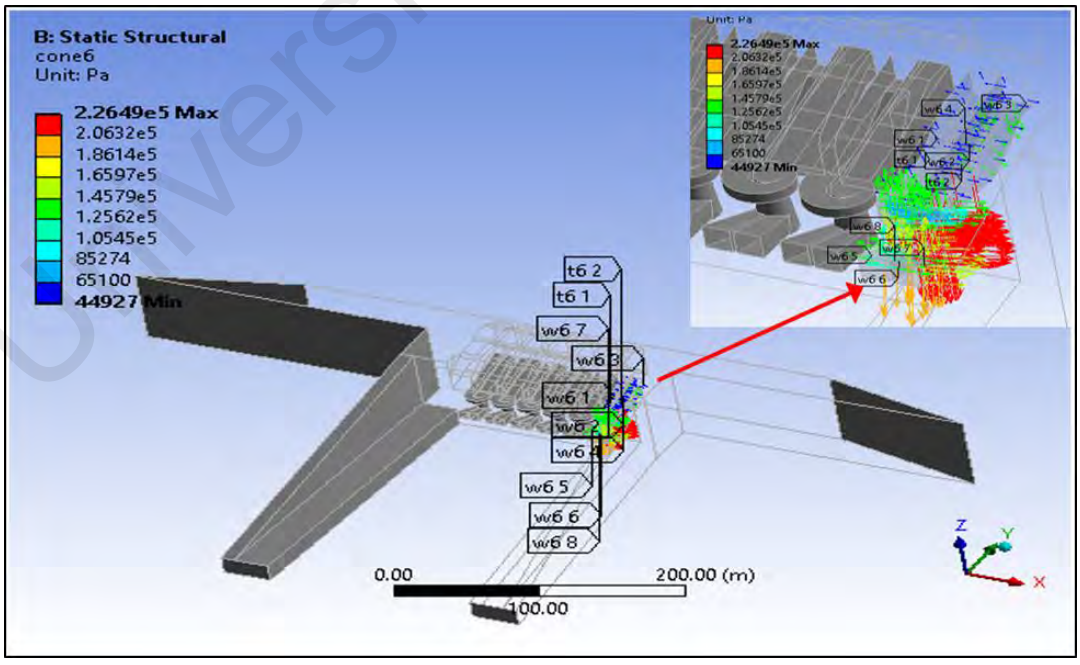

Figure 4.22: 3-D numerical Haditha model with pressure transformation pattern from turbine model for turbine unit number 6

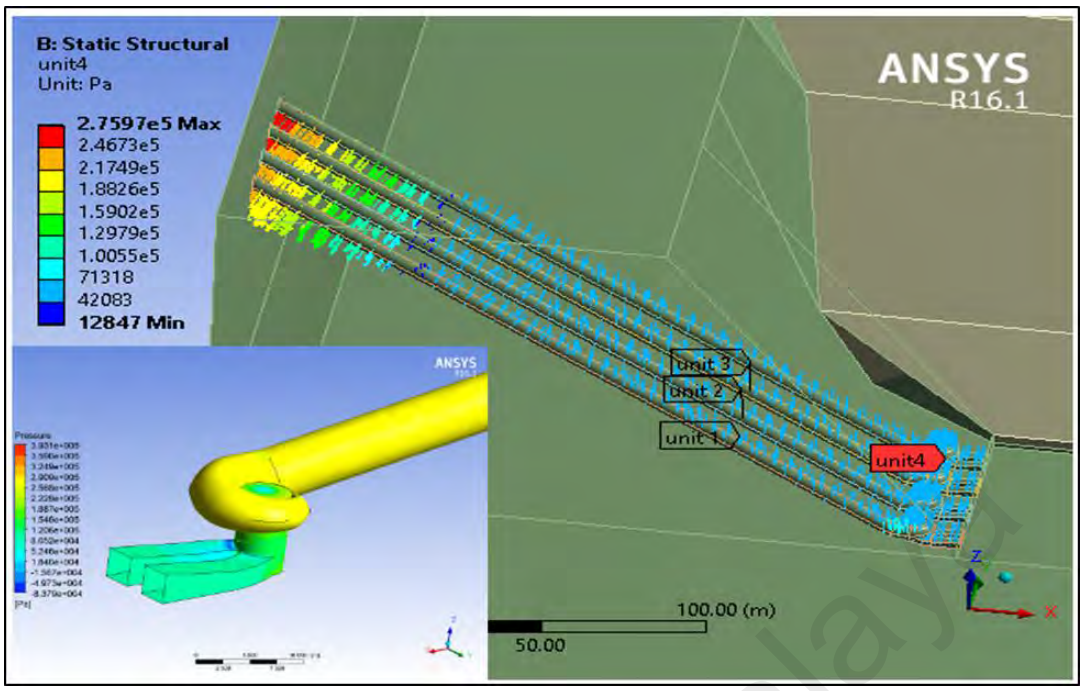

Figure 4.23: 3-D numerical Temenggor model with pressure transforming pattern for a group of 4 turbines

The results showed that the pressure decreased gradually in a random pattern according to the turbulence flow properties from the inlet to the outlet with a sudden drop in pressure when the flow around the turbine runner.

By recalling Figure 3.19 and Figure 3.20 from the previous chapter, Figure 3.20 shows the selected critical join that based on our knowledge have the major stresses influence in Haditha and Temenggor dams. The calculated stresses were in accordance with the minimum and maximum head level in the upstream of the dam that reflected on the turbines in the downstream. The framework includes Haditha dam model with importing the boundary pressures pattern from CFX-turbine model runs 130 times, 65 times with maximum water level and 65 times with minimum water level to cover all possibilities of operating the turbines. On the other hand, the framework includes Temenggor dam model with importing the boundary pressures pattern of CFX-turbine model and the framework runs 32 times, 16 times with maximum water level and 16 times with minimum water level to cover all possibilities of operating the turbines.

The numerical results showed that the maximum and minimum principal stresses located near the turbines boundary their values vary according to the changing in water level and the number and location of turbines operating. Based on Figure 4.24 (an example of six operated turbines) and appendix A visualization, the probability of operating turbines from 1 to 6 outlined in these figures. The principal stress results at the selected nodes in Haditha dam model according to the operating turbines with maximum water level =150.2 m (ASL). The principal stress results indicated that the critical values located around the cone of the turbines and the location change according to the operators of turbines to the operators of turbines. Also, the maximum principal stress occurred when all turbines are off and equal to1400.8 kPa.

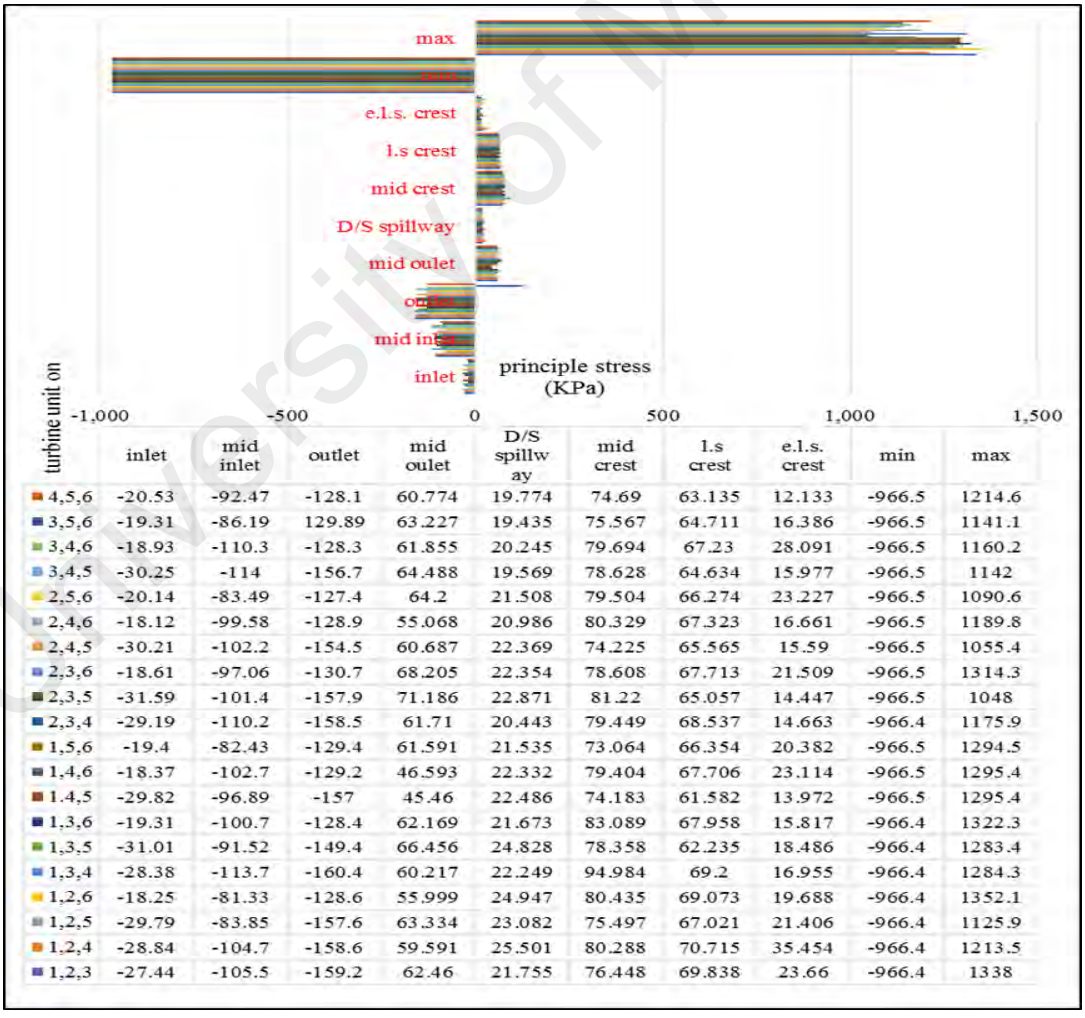

turbine unit on	inlet	mid inlet	outlet	mid oulet	D/S spillway	mid crest	l.s crest	e.l.s. crest	min	max
4,5,6	-20.53	-92.47	-128.1	60.774	19.774	74.69	63.135	12.133	-966.5	1214.6
3,5,6	-19.31	-86.19	129.89	63.227	19.435	75.567	64.711	16.386	-966.5	1141.1
3,4,6	-18.93	-110.3	-128.3	61.855	20.245	79.694	67.23	28.091	-966.5	1160.2
3,4,5	-30.25	-114	-156.7	64.488	19.569	78.628	64.634	15.977	-966.5	1142
2,5,6	-20.14	-83.49	-127.4	64.2	21.508	79.504	66.274	23.227	-966.5	1090.6
2,4,6	-18.12	-99.58	-128.9	55.068	20.986	80.329	67.323	16.661	-966.5	1189.8
2,4,5	-30.21	-102.2	-154.5	60.687	22.369	74.225	65.565	15.59	-966.5	1055.4
2,3,6	-18.61	-97.06	-130.7	68.205	22.354	78.608	67.713	21.509	-966.5	1314.3
2,3,5	-31.59	-101.4	-157.9	71.186	22.871	81.22	65.057	14.447	-966.5	1048
2,3,4	-29.19	-110.2	-158.5	61.71	20.443	79.449	68.537	14.663	-966.4	1175.9
1,5,6	-19.4	-82.43	-129.4	61.591	21.535	73.064	66.354	20.382	-966.5	1294.5
1,4,6	-18.37	-102.7	-129.2	46.593	22.332	79.404	67.706	23.114	-966.5	1295.4
1.4,5	-29.82	-96.89	-157	45.46	22.486	74.183	61.582	13.972	-966.5	1295.4
1,3,6	-19.31	-100.7	-128.4	62.169	21.673	83.089	67.958	15.817	-966.4	1322.3
1,3,5	-31.01	-91.52	-149.4	66.456	24.828	78.358	62.235	18.486	-966.4	1283.4
1,3,4	-28.38	-113.7	-160.4	60.217	22.249	94.984	69.2	16.955	-966.4	1284.3
1,2,6	-18.25	-81.33	-128.6	55.999	24.947	80.435	69.073	19.688	-966.4	1352.1
1,2,5	-29.79	-83.85	-157.6	63.334	23.082	75.497	67.021	21.406	-966.4	1125.9
1,2,4	-28.84	-104.7	-158.6	59.591	25.501	80.288	70.715	35.454	-966.4	1213.5
1,2,3	-27.44	-105.5	-159.2	62.46	21.755	76.448	69.838	23.66	-966.4	1338

Figure 4.24: Values of principal stresses for selected points at Haditha dam by operating three turbines units for maximum upstream water level

Figure 4.25 (an example of six operated turbines) and appendix B display the principal stress results at the selected nodes on Haditha dam model according to operating turbines with minimum W.L. =129 m (ASL).

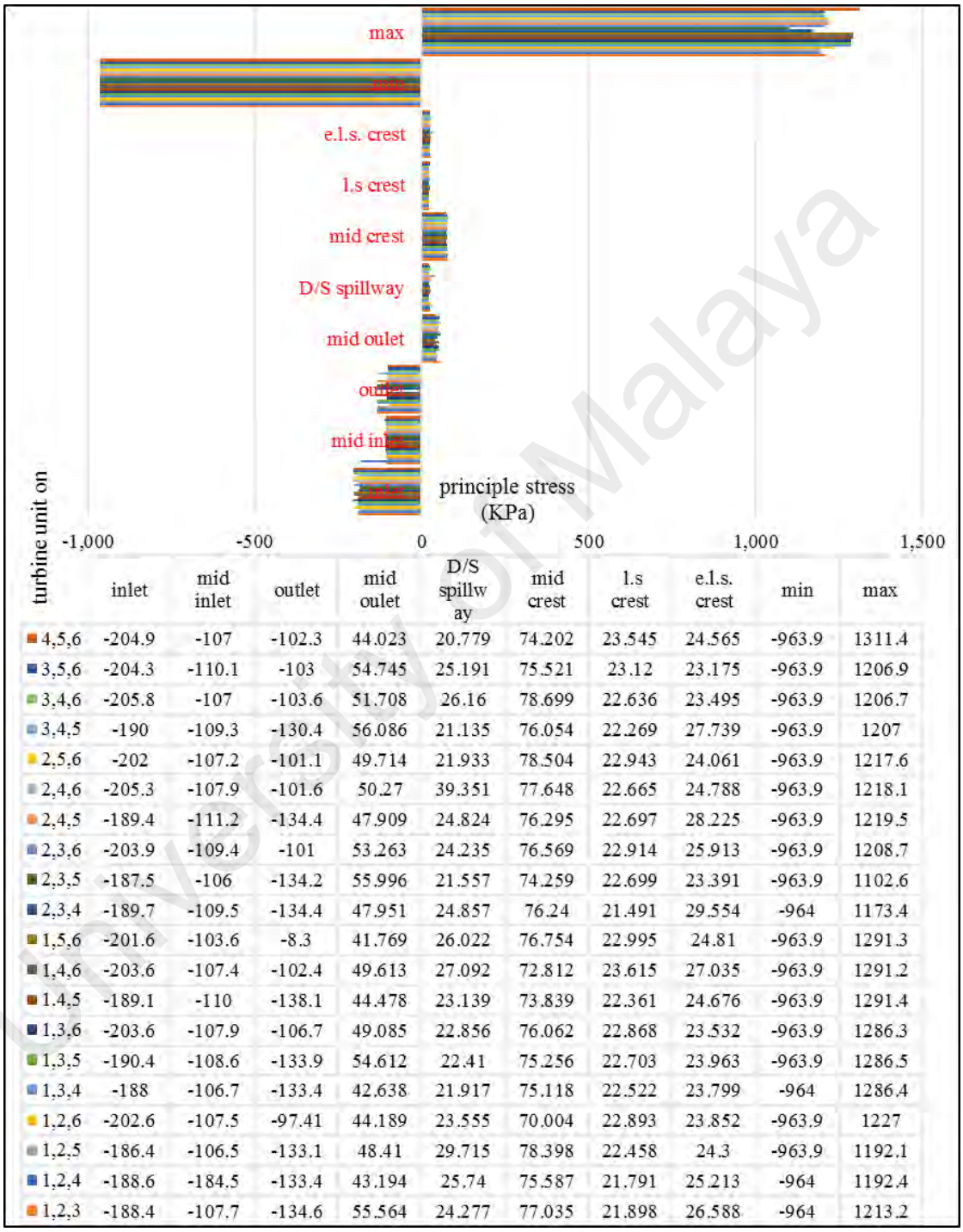

turbine unit on	inlet	mid inlet	outlet	mid oulet	D/S spillway	mid crest	l.s crest	e.l.s. crest	min	max
4,5,6	-204.9	-107	-102.3	44.023	20.779	74.202	23.545	24.565	-963.9	1311.4
3,5,6	-204.3	-110.1	-103	54.745	25.191	75.521	23.12	23.175	-963.9	1206.9
3,4,6	-205.8	-107	-103.6	51.708	26.16	78.699	22.636	23.495	-963.9	1206.7
3,4,5	-190	-109.3	-130.4	56.086	21.135	76.054	22.269	27.739	-963.9	1207
2,5,6	-202	-107.2	-101.1	49.714	21.933	78.504	22.943	24.061	-963.9	1217.6
2,4,6	-205.3	-107.9	-101.6	50.27	39.351	77.648	22.665	24.788	-963.9	1218.1
2,4,5	-189.4	-111.2	-134.4	47.909	24.824	76.295	22.697	28.225	-963.9	1219.5
2,3,6	-203.9	-109.4	-101	53.263	24.235	76.569	22.914	25.913	-963.9	1208.7
2,3,5	-187.5	-106	-134.2	55.996	21.557	74.259	22.699	23.391	-963.9	1102.6
2,3,4	-189.7	-109.5	-134.4	47.951	24.857	76.24	21.491	29.554	-964	1173.4
1,5,6	-201.6	-103.6	-8.3	41.769	26.022	76.754	22.995	24.81	-963.9	1291.3
1,4,6	-203.6	-107.4	-102.4	49.613	27.092	72.812	23.615	27.035	-963.9	1291.2
1.4,5	-189.1	-110	-138.1	44.478	23.139	73.839	22.361	24.676	-963.9	1291.4
1,3,6	-203.6	-107.9	-106.7	49.085	22.856	76.062	22.868	23.532	-963.9	1286.3
1,3,5	-190.4	-108.6	-133.9	54.612	22.41	75.256	22.703	23.963	-963.9	1286.5
1,3,4	-188	-106.7	-133.4	42.638	21.917	75.118	22.522	23.799	-964	1286.4
1,2,6	-202.6	-107.5	-97.41	44.189	23.555	70.004	22.893	23.852	-963.9	1227
1,2,5	-186.4	-106.5	-133.1	48.41	29.715	78.398	22.458	24.3	-963.9	1192.1
1,2,4	-188.6	-184.5	-133.4	43.194	25.74	75.587	21.791	25.213	-964	1192.4
1,2,3	-188.4	-107.7	-134.6	55.564	24.277	77.035	21.898	26.588	-964	1213.2

Figure 4.25: Values of principal stresses for selected points at Haditha dam by operating three turbines units for minimum upstream water level

The other case study which is Temenggor dam model, Figure 4.26 and 4.27 present the principal stress results at the selected nodes in accordance with the maximum and minimum water level values, respectively.

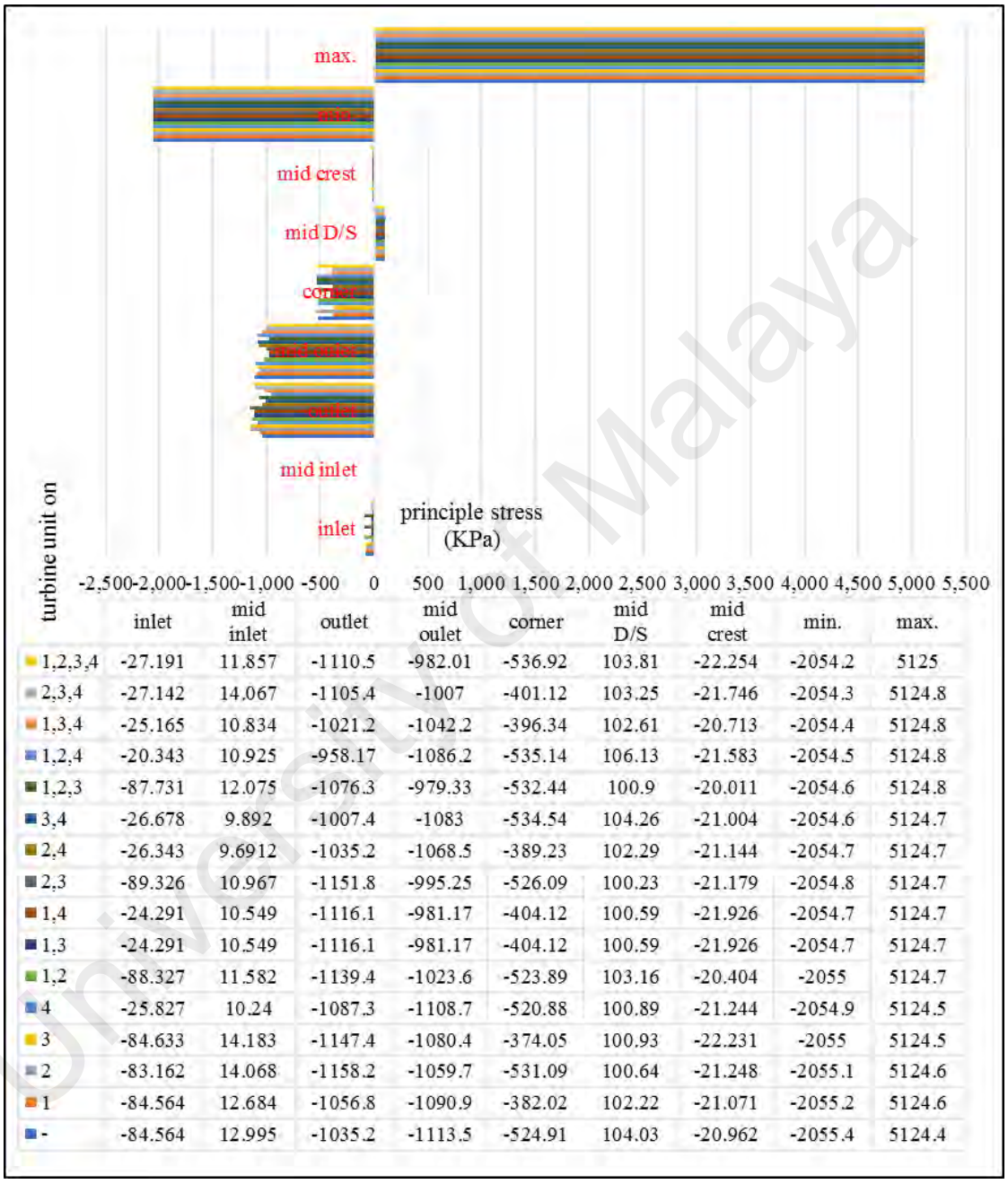

	inlet	mid inlet	outlet	mid oulet	corner	mid D/S	mid crest	min.	max.
1,2,3,4	-27.191	11.857	-1110.5	-982.01	-536.92	103.81	-22.254	-2054.2	5125
2,3,4	-27.142	14.067	-1105.4	-1007	-401.12	103.25	-21.746	-2054.3	5124.8
1,3,4	-25.165	10.834	-1021.2	-1042.2	-396.34	102.61	-20.713	-2054.4	5124.8
1,2,4	-20.343	10.925	-958.17	-1086.2	-535.14	106.13	-21.583	-2054.5	5124.8
1,2,3	-87.731	12.075	-1076.3	-979.33	-532.44	100.9	-20.011	-2054.6	5124.8
3,4	-26.678	9.892	-1007.4	-1083	-534.54	104.26	-21.004	-2054.6	5124.7
2,4	-26.343	9.6912	-1035.2	-1068.5	-389.23	102.29	-21.144	-2054.7	5124.7
2,3	-89.326	10.967	-1151.8	-995.25	-526.09	100.23	-21.179	-2054.8	5124.7
1,4	-24.291	10.549	-1116.1	-981.17	-404.12	100.59	-21.926	-2054.7	5124.7
1,3	-24.291	10.549	-1116.1	-981.17	-404.12	100.59	-21.926	-2054.7	5124.7
1,2	-88.327	11.582	-1139.4	-1023.6	-523.89	103.16	-20.404	-2055	5124.7
4	-25.827	10.24	-1087.3	-1108.7	-520.88	100.89	-21.244	-2054.9	5124.5
3	-84.633	14.183	-1147.4	-1080.4	-374.05	100.93	-22.231	-2055	5124.5
2	-83.162	14.068	-1158.2	-1059.7	-531.09	100.64	-21.248	-2055.1	5124.6
1	-84.564	12.684	-1056.8	-1090.9	-382.02	102.22	-21.071	-2055.2	5124.6
-	-84.564	12.995	-1035.2	-1113.5	-524.91	104.03	-20.962	-2055.4	5124.4

Figure 4.26: Values of principal stresses for selected points at Temenggor dam by operating the turbines units for maximum upstream water level

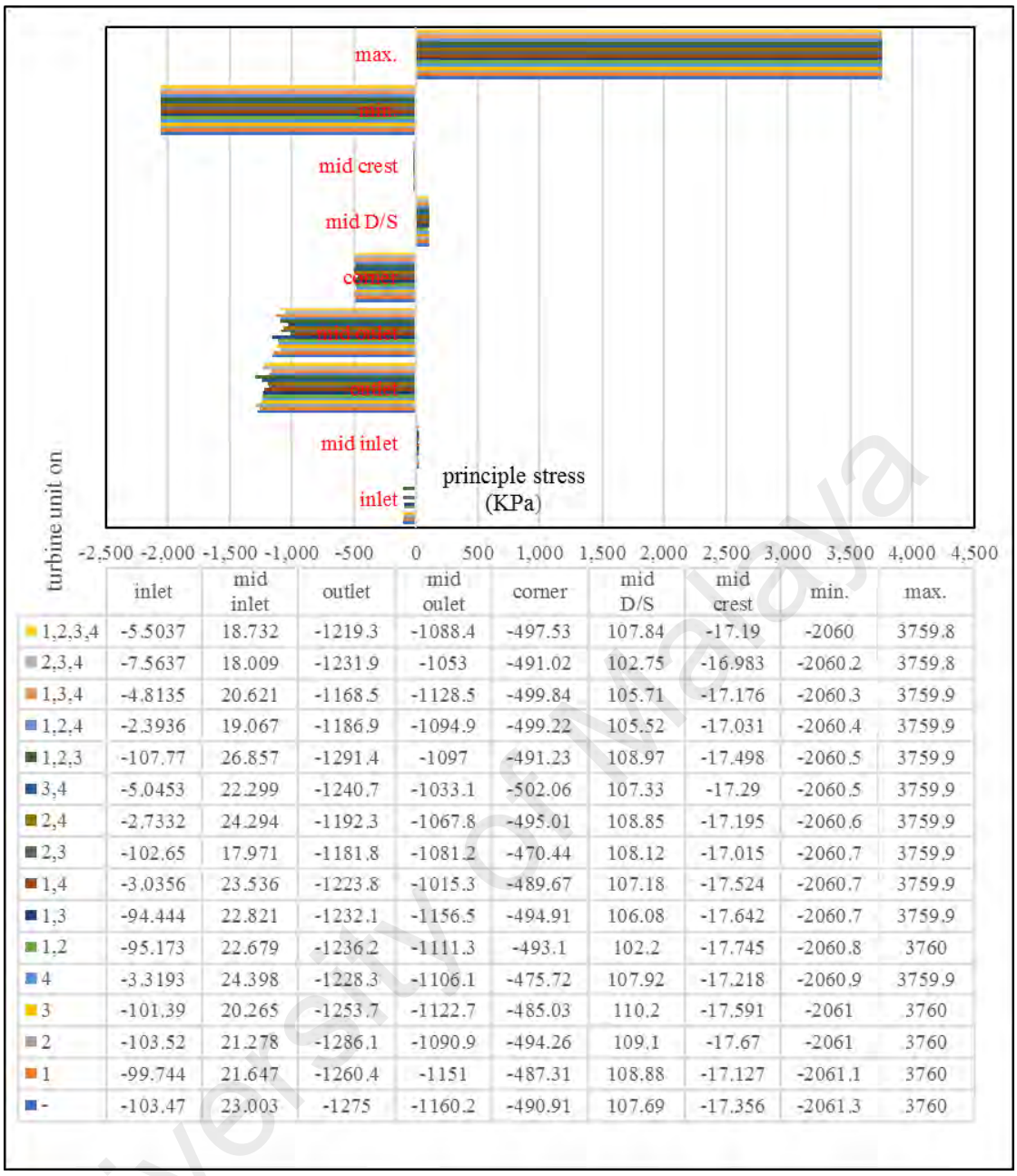

turbine unit on	inlet	mid inlet	outlet	mid oulet	corner	mid D/S	mid crest	min.	max.
1,2,3,4	-5.5037	18.732	-1219.3	-1088.4	-497.53	107.84	-17.19	-2060	3759.8
2,3,4	-7.5637	18.009	-1231.9	-1053	-491.02	102.75	-16.983	-2060.2	3759.8
1,3,4	-4.8135	20.621	-1168.5	-1128.5	-499.84	105.71	-17.176	-2060.3	3759.9
1,2,4	-2.3936	19.067	-1186.9	-1094.9	-499.22	105.52	-17.031	-2060.4	3759.9
1,2,3	-107.77	26.857	-1291.4	-1097	-491.23	108.97	-17.498	-2060.5	3759.9
3,4	-5.0453	22.299	-1240.7	-1033.1	-502.06	107.33	-17.29	-2060.5	3759.9
2,4	-2.7332	24.294	-1192.3	-1067.8	-495.01	108.85	-17.195	-2060.6	3759.9
2,3	-102.65	17.971	-1181.8	-1081.2	-470.44	108.12	-17.015	-2060.7	3759.9
1,4	-3.0356	23.536	-1223.8	-1015.3	-489.67	107.18	-17.524	-2060.7	3759.9
1,3	-94.444	22.821	-1232.1	-1156.5	-494.91	106.08	-17.642	-2060.7	3759.9
1,2	-95.173	22.679	-1236.2	-1111.3	-493.1	102.2	-17.745	-2060.8	3760
4	-3.3193	24.398	-1228.3	-1106.1	-475.72	107.92	-17.218	-2060.9	3759.9
3	-101.39	20.265	-1253.7	-1122.7	-485.03	110.2	-17.591	-2061	3760
2	-103.52	21.278	-1286.1	-1090.9	-494.26	109.1	-17.67	-2061	3760
1	-99.744	21.647	-1260.4	-1151	-487.31	108.88	-17.127	-2061.1	3760
-	-103.47	23.003	-1275	-1160.2	-490.91	107.69	-17.356	-2061.3	3760

Figure 4.27: The principal stress values in the selected points of Temenggor dam body according to operating turbine units in minimum water

After analyzing the obtained results for both inspected dams, a statistical summary of the critical values of the stresses belonging to the maximum and minimum water levels for Haditha and Temenggor dam-reservoir-foundation systems is shown in Table 4.16 to 4.19.

Table 4.16: Statistical analysis of the principal stress for Haditha dam for turbines operated with minimum upstream water level

	Inlet	Mid Inlet	Outlet	Mid Outlet	D/S Spillway	mid Crest	l.s Crest	e.l.s. Crest	Min	Max
Maximum (kPa)	-181	-103	-83	67	39	79.2	25.9	41	-963	1311
Minimum (kPa)	-215	-184	-138	41	20	70.0	20.1	21	-964	1086
Difference (kPa)	33.7	81.1	55	26	18	9.2	5.8	20	0.1	225
Percent (%)	18.5	78.5	66	38	47	11	22	49	0.01	17

Table 4.17: Statistical analysis of the principal stress for Haditha dam for turbines operated with maximum upstream water level

	Inlet	Mid Inlet	Outlet	Mid Outlet	D/S Spillway	mid Crest	l.s Crest	e.l.s. Crest	Min	Max
Maximum (kPa)	-17	-68	-121	80	29	95	77	35	-966	1400
Minimum (kPa)	-39	-125	-160	45	18	73	56	9	-966	1048
Difference (kPa)	21	56	38	34	10	21	20	26	0.3	352.8
Percent (%)	125	81	31	43	37	23	27	74	0.03	25.19

Table 4.18: Statistical analysis of the principal stress for Temenggor dam for turbines operated with minimum upstream water level

	Inlet	Mid Inlet	Outlet	Mid Outlet	D/S Spillway	mid Crest	l.s Crest	e.l.s. Crest	Min
Maximum (kPa)	-2.3	26	-1168	-1015	-470	110	-16	-2060	3760
Minimum (kPa)	-107	17	-1291	-1160	-502	102	-17	-2061	3759.8
Difference (kPa)	105	8	122	144.9	31	8	0.76	1.3	0.2
Percent (%)	97	33	10	14.27	6.72	7.26	4	0.06	0.01

Table 4.19: Statistical analysis of the principal stress for Temenggor dam for turbines operated with maximum upstream water level

	Inlet	Mid Inlet	Outlet	Mid Outlet	D/S Spillway	mid Crest	l.s Crest	e.l.s. Crest	Min
Maximum (kPa)	-20	14	-958	-979	-374	106	-20.	-2054	5125
Minimum (kPa)	-89	9.6	-1158	-1113	-536	100	-22.	-2055	5124
Difference (kPa)	68.983	4.4	200	134	162	5.9	2.243	1.2	0.6
Percent (%)	77.22	31	20	13	43	5.56	11.21	0.06	0.01

Table 4.16 and 4.17 present the operating turbines of Haditha powerhouse in which have a very slight effect on the fluctuation of the minimum principal stress values and the percentage of change of this value in maximum drawdown and floodwater levels equal to 0.01% and 0.03%, respectively. The points near the cone part of the draft tube near the outlet of powerhouse were the most affected points by the operating turbines according to the fluctuation of the principal stress values. The maximum range of principal stress change occur in flood events water level equal to 352.8 kPa, and the maximum range of principal stress change in maximum drawdown water level equal to 225 kPa. On the other hand, Table 4.18 and 4.19 show the operating turbines of Temenggor powerhouse in which have the same earlier case "slight influence of the fluctuation of the maximum and minimum principal stress values and the percentage of change of these values equal 0.01% and 0.06%, respectively". The points in the downstream near the outlet of the powerhouse (outlet and min outlet) are the most affected by operating turbines according to fluctuation the principal stress values. The maximum range of principal stress change in the outlet occurs in maximum water level equal to 200 kPa, and the maximum range of principal stress change in the mid outlet happen in minimum water level equal to 144.9 kPa.

As a final statistical analysis and based on the attained results of the principal stresses, Table 4.20 and 4.21 describe the classification of the stresses from minimum to maximum of Haditha and Temenggor dam models, respectively. According to this classification, the third objective of this thesis has been satisfied. The optimal operation of both dams has been generated in Figure 4.28 and 4.29.

Various types of soils that are used in the embankment dams fill can take different stresses. The main focus of the present study is to determine how much the stresses will increase due to the vibrational effects from the operation of powerhouse

Table 4.20: Haditha principal stress classification

Principal stress range (kPa)	Ranking	Indicator
$1000 \leq \sigma_{max} < 1100$	Excellent	
$1100 \leq \sigma_{max} < 1200$	good	
$1200 \leq \sigma_{max} < 1300$	Acceptable	
$1300 \leq \sigma_{max} < 1400$	Not acceptable	

Table 4.21: Temenggor principal stress classification

Principal stress range (kPa)	Ranking	Indicator
$900 \leq \sigma_{max} < 1000$	Excellent	
$1000 \leq \sigma_{max} < 1100$	good	
$1100 \leq \sigma_{max} < 1200$	Acceptable	
$1200 \leq \sigma_{max} < 1300$	Not acceptable	

A categorization program developed to run the turbine units in Haditha and Temenggor powerhouse depending the principal stress results with all possibilities of operating turbine models (six units in Haditha model and four units in Temenggor models). The online control program used for the operating turbines depending on the decreasing the

maximum principal stress values according to the classification tabulated in Table 4.20 and 4.21.

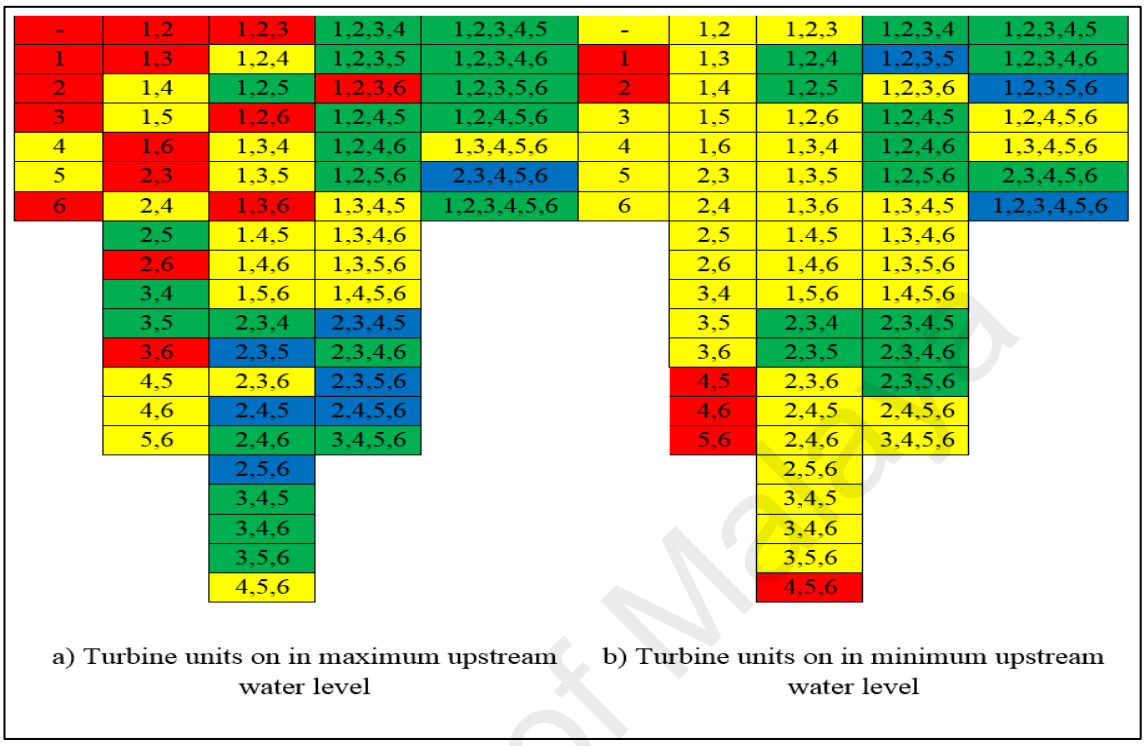

Figure 4.28: Control program for the operating turbines in Haditha powerhouse based on minimizing the principal stress

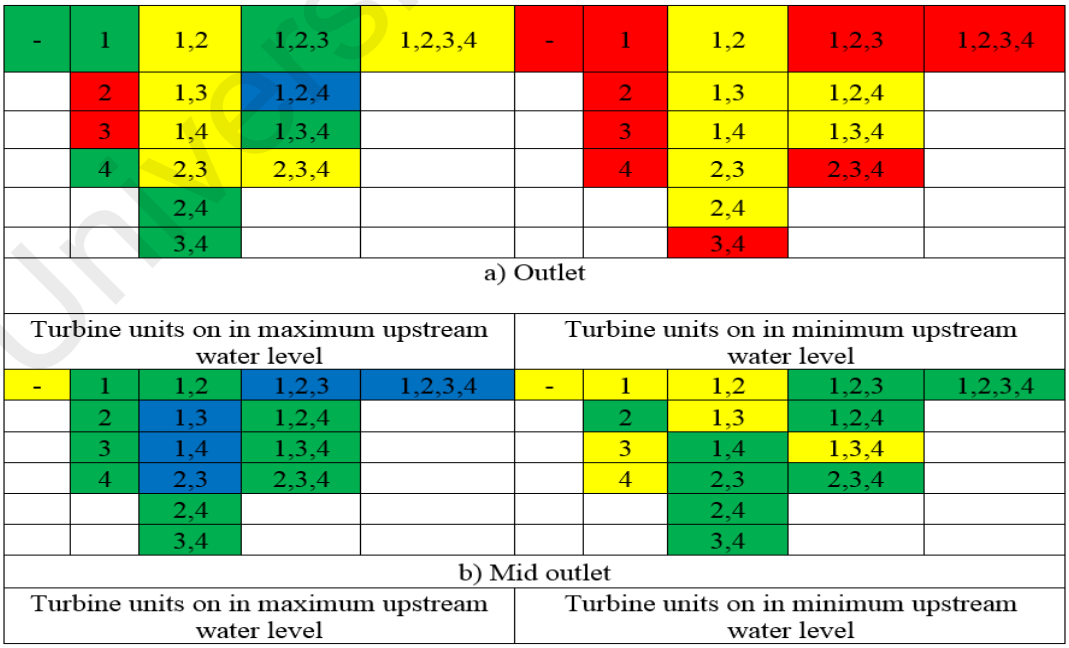

Figure 4.29: Control program for the operating turbines in Temenggor powerhouse based on minimizing the principal stress

Figure 4.28 outlines a control program for the running Haditha turbines depending on the decrease in principle stress values in the selected points according to the classification listed in Table 4.20. There were 130 total operation scenarios, with 65 operation scenarios based on maximum reservoir water level, and the other 65 operation scenarios were based on minimum reservoir water level. While, Figure 4.29 outlines a control program for the running Temenggor turbines depending on the decrease in principle stress values in the selected points according to the classification listed in Table 4.21. There were 32 total operation scenarios, with 16 operation scenarios based on maximum reservoir water level, and the other 16 operation scenarios were based on minimum reservoir water level.

The results from this study would help improve our current understanding of the consequences of the operation strategies imposed on the energy market, which tend to increase load variations, which in turn affects the lifespan of hydropower plant equipment. Therefore, the topic debated in this study is more relevant and beneficial for the research of hydraulic and water resources in the engineering community.

CHAPTER 5: CONCLUSSION AND RECOMMENDATIONS

5.1 Research Findings

The operation of the powerhouse at dam site is one of the important factors that should be considered in the analysis of dam safety. Also, the consideration of the seismic effect on dam body is another important case that should be integrated with powerhouse effect. Most of the studies were focused either on reducing the impact of cavitation and pressure fluctuations in the turbine draft tube or focused on the analysis of seismic effect only on the dam bodies. However, the present study focuses on integrating the vibrational effect due to the operation of reaction turbines with and without seismic effects. 3-D numerical turbine models are proposed to reduce pressure fluctuation at the turbine draft tubes and to simulate the pressure pattern at the common area between the dam and powerhouse. Also, 3-D numerical dam models are proposed to study the dynamic behavior of a dam bodies due to seismic effect. The turbine and the dam model were integrated taking two case studies namely Haditha earth-fill dam and Temenggor rockfill dam. After the models calibration and validation, the following conclusions can be drawn:

i. 3-D numerical turbine models were generated by using ANSYS-CFX to simulate the hydraulic performance of two types of reaction turbines namely Kaplan and Francis turbines. The hydraulic performance includes the simulation of velocity, pressure and shear walls distributions in the turbine units with and without the proposed submerged weir in the outlet of turbine draft tube. Varies weir heights were tested (0.167, 0.333 and 0.5 from the turbine outlet height) for the selected turbines types used in the powerhouses of the case studies (Haditha and Temenggor dams). The best-submerged weir height used in the outlet of the Kaplan turbine was found to be 1.33 m while that used in the Francis turbine was found to be 1.0 m. The pressure fluctuations were minimized with their heights. As a result, the vibrational effects on dam bodies were reduced too.

ii. 3-D numerical dam models were generated by using ANSYS to simulate the dynamic behavior of two embankment dams namely Haditha earth-fill dam and Temenggor rock fill dam due to seismic effect. The simulation took into consideration different foundation and depths and water levels at upstream. When the water level at upstream increased to the maximum allowable level and the foundation depth equal to the dams' height, the mass of dam reservoir foundation system increased which lead to a decrease in the natural frequencies of the system. The percentage decrease in the natural frequency for Haditha and Temenggor dams were found to be 41.6% to 68.9% respectively (for empty reservoir case). As an example, when the time between 0.5 to 10 seconds, results showed that stress was increased by 92.5% to 99.98% for Haditha and Temenggor dams respectively. A real data of a strong EQ of magnitude 7.8 M which was occurred at the island of Sumatra in Indonesia is used to determine the response of the embankment dams.

iii. Optimum operation of the turbine system is achieved by computing the principal stresses generated in the dam body and powerhouse by considering minimum and maximum water levels at upstream. The framework for Haditha dam model includes importing the boundary pressures pattern from CFX-turbine model where a total of 130 operation trials were conducted. 65 operation trials were conducted with maximum water level and another 65 operation trials were conducted with minimum water level. These trials covered all the possible operating condition of the powerhouse at the Haditha dam. On the other hand, the framework for Temenggor dam model includes importing the boundary pressures pattern from CFX-turbine model where a total of 32 operation trials were conducted. From the 32 trials, 16 operation trials were conducted with maximum water level and another 16 operation trials were conducted with minimum water level. These trials covered all the possible operating condition of the powerhouse at Temenggor dam. For Haditha dam, the principal stresses at critical locations can be reduced by 352.8 kPa when the powerhouse is operated under maximum water level, while the reduction is

225 kPa when the powerhouse operated under minimum water level. For Temenggor dam, the principal stresses at critical locations can be reduced by 200 kPa when the powerhouse is operated under maximum water level, while the reduction is 144.9 kPa when the power house operated under minimum water level. The possible optimum operations for Haditha and Temenggor powerhouses are shown in Figures 4.22 and 4.23 respectively.

The uncertainties were considered in the numerical results. The maximum water level in the reservoir which represent maximum possible flood and a real earthquake with 6.4 on Richter scale were simulated.

5.2 Further Research

This study investigates using numerical turbine and dam models the impact of vibrational effect due to powerhouse operation on dam body taking into consideration dam type, powerhouse type and turbine type. Also, the study integrates the impact of both seismic and vibration from powerhouse operation with various reservoir levels on dams' bodies. After conducting the study, future research which considers the following cases are recommended:

i. The optimization of powerhouse operation should include the shape and location of the submerged weir in order to attain a steady water flow from turbine draft tube.
ii. In this research, a fully open gate was examined. It is recommended to include the optimum operation of the powerhouse with a partially open gate.
iii. In this study, one of the major limitations of the proposed turbine models is operating the dam powerhouse using one turbine only. The vibrational effect on the dam body due to full operation of the reaction turbines in the powerhouse is required.

REFERENCES

Ahmed, Suhaili, R., & Behaya, S. (2014). A Genetic Algorithm Optimization Model for the Gravity Dam Section under Seismic Excitation with Reservoir-Dam-Foundation Interactions.

Ahn, S.-H., Xiao, Y., Wang, Z., Zhou, X., & Luo, Y. (2017). Numerical prediction on the effect of free surface vortex on intake flow characteristics for tidal power station. *Renewable Energy, 101*, 617-628.

Akbari, J., Ahmadi, M. T., & Moharrami, H. (2011). Advances in concrete arch dams shape optimization. *Applied mathematical modelling, 35*(7), 3316-3333.

Akkermann, J., Runte, T., & Krebs, D. (2009). Ship lift at Three Gorges Dam, China–design of steel structures. *Steel Construction, 2*(2), 61-71.

Al-Saadi, S. I. K., Eubaid, K., & Mohammed Salih, L. (2011). Predicting the breach hydrograph resulting due to hypothetical failure of Haditha dam. *Jordan Journal of Civil Engineering, 5*(3), 392-400.

Albano, M., Modoni, G., Croce, P., & Russo, G. (2015). Assessment of the seismic performance of a bituminous faced rockfill dam. *Soil Dynamics and Earthquake Engineering, 75*, 183-198.

Ali, M. H., Alam, M. R., Haque, M. N., & Alam, M. J. (2012). Comparison of Design and Analysis of Concrete Gravity Dam. *Natural Resources, 3*(01), 18.

Altunişik, A. C., Günaydin, M., Sevim, B., Bayraktar, A., & Adanur, S. (2015). CFRP composite retrofitting effect on the dynamic characteristics of arch dams. *Soil Dynamics and Earthquake Engineering, 74*, 1-9.

Anagnostopoulos, J. S., & Papantonis, D. E. (2007). Optimal sizing of a run-of-river small hydropower plant. *Energy Conversion and Management, 48*(10), 2663-2670.

Anastasiadis, A., Klimis, N., Makra, K., & Margaris, B. (2004). *On seismic behaviour of a 130 m high rockfill dam: an integrated approach.* Paper presented at the 13th Conference on Earthquake engineering, Vancouver, Canada, 2933p.

Anup, K., Thapa, B., & Lee, Y.-H. (2014). Transient numerical analysis of rotor–stator interaction in a Francis turbine. *Renewable Energy, 65*, 227-235.

Attarnejad, R., & Kalateh, F. (2012). Numerical simulation of acoustic cavitation in the reservoir and effects on dynamic response of concrete dams. *International Journal of Civil Engineering, 10*(1).

Avakyan, T. (2017). *Distribution systems with renewable sources*. Czech technical university in Prague.

Birk, C., & Ruge, P. (2007). Representation of radiation damping in a dam–reservoir interaction analysis based on a rational stiffness approximation. *Computers & Structures, 85*(11), 1152-1163.

Bosioc, A. I., Tanasa, C., Muntean, S., & Susan-Resiga, R. (2010). Pressure recovery improvement in a conical diffuser with swirling flow using water jet injection. *Proceedings of the Romanian Academy, Series A: Mathematics, Physics, Technical Sciences, Information Science, ISSN*, 1454-9069.

Bouaanani, Paultre, P., & Proulx, J. (2003). A closed-form formulation for earthquake-induced hydrodynamic pressure on gravity dams. *Journal of Sound and Vibration, 261*(3), 573-582.

Bouaanani, N., & Lu, F. Y. (2009). Assessment of potential-based fluid finite elements for seismic analysis of dam–reservoir systems. *Computers & Structures, 87*(3), 206-224.

Bouaanani, N., & Paultre, P. (2005). A new boundary condition for energy radiation in covered reservoirs using BEM. *Engineering analysis with boundary elements, 29*(9), 903-911.

Burman, A., Nayak, P., Agrawal, P., & Maity, D. (2012). Coupled gravity dam–foundation analysis using a simplified direct method of soil–structure interaction. *Soil Dynamics and Earthquake Engineering, 34*(1), 62-68.

Caishui, H. (2012). Three-dimensional Numerical Analysis of Flow Pattern in Pressure Forebay of Hydropower Station. *Procedia Engineering, 28*, 128-135.

Casanova García, F., & Mantilla Viveros, C. A. (2010). Experimental analysis of the vibration on the draft tube of a Francis hydraulic turbine during operation at different power levels. *Revista Facultad de Ingeniería Universidad de Antioquia*(55), 90-98.

Castelli, F., Lentini, V., & Trifarò, C. A. (2016). 1D seismic analysis of earth dams: the example of the Lentini site. *Procedia Engineering, 158*, 356-361.

Cetin, M., & Mengi, Y. (2003). Transmitting boundary conditions suitable for analysis of dam-reservoir interaction and wave load problems. *Applied mathematical modelling, 27*(6), 451-470.

Chen, Y., Fan, E., & Yuen, M. (2017). Explicitly self-similar solutions for the Euler/Navier–Stokes–Korteweg equations in RN. *Applied Mathematics Letters, 67*, 46-52.

Cobb, B. R., & Sharp, K. V. (2013). Impulse (Turgo and Pelton) turbine performance characteristics and their impact on pico-hydro installations. *Renewable Energy, 50*, 959-964.

Dakoulas, P. (2012). Longitudinal vibrations of tall concrete faced rockfill dams in narrow canyons. *Soil Dynamics and Earthquake Engineering, 41*, 44-58.

Demirel, E. (2015). Numerical simulation of earthquake excited dam-reservoirs with irregular geometries using an immersed boundary method. *Soil Dynamics and Earthquake Engineering, 73*, 80-90.

Dixon, S. L., & Hall, C. (2013). *Fluid mechanics and thermodynamics of turbomachinery*: Butterworth-Heinemann.

Doyle, M. W., Harbor, J. M., & Stanley, E. H. (2003). Toward policies and decision-making for dam removal. *Environmental Management, 31*(4), 0453-0465.

Drtina, P., & Sallaberger, M. (1999). Hydraulic turbines—basic principles and state-of-the-art computational fluid dynamics applications. *Proceedings of the Institution of Mechanical Engineers, Part C: Journal of Mechanical Engineering Science, 213*(1), 85-102.

Ebrahimian, B. (2012). *Non-Linear Numerical Analysis of Earthquake-Induced Deformation of Earth-Fill Dams*: Intech Open Access Publisher.

Favrel, A., Müller, A., Landry, C., Yamamoto, K., & Avellan, F. (2015). Study of the vortex-induced pressure excitation source in a Francis turbine draft tube by particle image velocimetry. *Experiments in Fluids, 56*(12), 215.

Fenves, G., & Chopra, A. K. (1985). Simplified earthquake analysis of concrete gravity dams: Separate hydrodynamic and foundation interaction effects. *Journal of engineering mechanics, 111*(6), 715-735.

Ferziger, J. H., & Peric, M. (2012). *Computational methods for fluid dynamics*: Springer Science & Business Media.

Foster, M., Fell, R., & Spannagle, M. (2000). The statistics of embankment dam failures and accidents. *Canadian Geotechnical Journal, 37*(5), 1000-1024.

Fu, T., Deng, Z. D., Duncan, J. P., Zhou, D., Carlson, T. J., Johnson, G. E., & Hou, H. (2016). Assessing hydraulic conditions through Francis turbines using an autonomous sensor device. *Renewable Energy, 99*, 1244-1252.

Gazetas, G., & Dakoulas, P. (1992). Seismic analysis and design of rockfill dams: state-of-the-art. *Soil Dynamics and Earthquake Engineering, 11*(1), 27-61.

Gazetas, G., Debchaudhury, A., & Gasparini, D. (1981). Random vibration analysis for the seismic response of earth dams. *Geotechnique, 31*(2), 261-277.

Gebreslassie, M. G., Tabor, G. R., & Belmont, M. R. (2013). Numerical simulation of a new type of cross flow tidal turbine using OpenFOAM–Part I: Calibration of energy extraction. *Renewable Energy, 50*, 994-1004.

Ghaemmaghami, A., & Ghaemian, M. (2008). Experimental seismic investigation of Sefid-rud concrete buttress dam model on shaking table. *Earthquake engineering & structural dynamics, 37*(5), 809-823.

Gielen, D. (2012). Renewable energy technologies: cost analysis series. *Sol Photovolt, 1*, 52.

Glatzel, T., Litterst, C., Cupelli, C., Lindemann, T., Moosmann, C., & Niekrawietz, R. (2008). Computational fluid dynamics (CFD) software tools for microfluidic applications–A case study. *Computers & Fluids, 37*(3), 218-235.

Grassmann, H., & Ganis, M. (2005). On partially static Kaplan turbines. *Renewable Energy, 30*(2), 179-186.

Gui, M.-W., & Chiu, H.-T. (2009). Seismic response of Renyitan earth-fill dam. *Journal of GeoEngineering, 4*(2), 41-50.

Hariri-Ardebili, M., & Mirzabozorg, H. (2011). Reservoir fluctuation effects on seismic response of high concrete arch dams considering material nonlinearity. *Journal of Civil Engineering Research, 1*(1), 9-20.

Hariri-Ardebili, M., & Seyed-Kolbadi, S. (2015). Seismic cracking and instability of concrete dams: Smeared crack approach. *Engineering Failure Analysis, 52*, 45-60.

Iliescu, M. S., Ciocan, G. D., & Avellan, F. (2008). Analysis of the cavitating draft tube vortex in a Francis turbine using particle image velocimetry measurements in two-phase flow. *Journal of Fluids Engineering, 130*(2), 021105.

Jafari, M. K., & Davoodi, M. (2004). Dynamic characteristics evaluation of Masjed-soleiman embankment dam using forced vibration test. *13th World Conference on Earthquake Engineering*.

Jain, S. V., Swarnkar, A., Motwani, K. H., & Patel, R. N. (2015). Effects of impeller diameter and rotational speed on performance of pump running in turbine mode. *Energy Conversion and Management, 89*, 808-824.

James, L. A. (2005). Sediment from hydraulic mining detained by Englebright and small dams in the Yuba basin. *Geomorphology, 71*(1), 202-226.

Javadi, A., & Nilsson, H. (2014). *Unsteady numerical simulation of the flow in the U9 Kaplan turbine model.* Paper presented at the IOP Conference Series: Earth and Environmental Science.

Javadi, A., & Nilsson, H. (2017). Detailed numerical investigation of a Kaplan turbine with rotor-stator interaction using turbulence-resolving simulations. *International Journal of Heat and Fluid Flow, 63*, 1-13.

Jošt, D., & Lipej, A. (2011). Numerical prediction of non-cavitating and cavitating vortex rope in a Francis turbine draft tube. *Strojniški vestnik-Journal of Mechanical Engineering, 57*(6), 445-456.

Khazaee, A., & Lotfi, V. (2014). Application of perfectly matched layers in the transient analysis of dam–reservoir systems. *Soil Dynamics and Earthquake Engineering, 60*, 51-68.

Khosravi, S., & Heydari, M. (2013). Modelling of Concrete Gravity Dam Including Dam-Water-Foundation Rock Interaction. *World Applied Sciences Journal, 22*(4), 538-546.

Ko, P., & Kurosawa, S. (2014). *Numerical simulation of turbulence flow in a Kaplan turbine-Evaluation on turbine performance prediction accuracy*. Paper presented at the IOP Conference Series: Earth and Environmental Science.

Kumar, P., & Saini, R. (2010). Study of cavitation in hydro turbines—A review. *Renewable and Sustainable Energy Reviews, 14*(1), 374-383.

Lai, X., Liao, G., Zhu, Y., Zhang, X., Gou, Q., & Zhang, W. (2012). *Lateral vibration of hydro turbine-generator rotor with varying stiffness of guide bearings*. Paper presented at the IOP Conference Series: Earth and Environmental Science.

Lavrov, A., Rodrigues, J., Gadelho, J., & Soares, C. G. (2017). Calculation of hydrodynamic coefficients of ship sections in roll motion using Navier-Stokes equations. *Ocean Engineering, 133*, 36-46.

LI, S.-m., Liang, H., & LI, A.-m. (2008). A semi-analytical solution for characteristics of a dam-reservoir system with absorptive reservoir bottom. *Journal of Hydrodynamics, Ser. B, 20*(6), 727-734.

Lipej, A., Jošt, D., Meznar, P., & Djelic, V. (2009). Numerical prediction of pressure pulsation amplitude for different operating regimes of Francis turbine draft tubes. *International Journal of Fluid Machinery and Systems, 2*(4), 375-382.

Liu, J., Feng, X.-T., Ding, X.-L., Zhang, J., & Yue, D.-M. (2003). Stability assessment of the Three-Gorges Dam foundation, China, using physical and numerical modeling—Part I: physical model tests. *International Journal of Rock Mechanics and Mining Sciences, 40*(5), 609-631.

Lomax, H., Pulliam, T. H., & Zingg, D. W. (1999). Fundamentals of computational fluid dynamics. *Applied Mechanics Reviews, vol, 55*, B61.

Lotfi, V. (2003). Seismic analysis of concrete gravity dams by decoupled modal approach in time domain. *Electronic Journal of Structural Engineering, 3*, 102-116.

Lotfi, V., & Zenz, G. (2016). Transient analysis of concrete gravity dam-reservoir systems by Wavenumber-TD approach. *Soil Dynamics and Earthquake Engineering, 90*, 313-326.

Luna-Ramírez, A., Campos-Amezcua, A., Dorantes-Gómez, O., Mazur-Czerwiec, Z., & Muñoz-Quezada, R. (2016). Failure analysis of runner blades in a Francis hydraulic turbine—Case study. *Engineering Failure Analysis, 59*, 314-325.

Luo, Li, C., Min, X., & Xiaolei, T. (2012). Review of dam-break research of earth-rock dam combining with dam safety management. *Procedia Engineering, 28*, 382-388.

Maity, D. (2005). A novel far-boundary condition for the finite element analysis of infinite reservoir. *Applied Mathematics and Computation, 170*(2), 1314-1328.

Mehdipour, B. (2013). Effect of Foundation on Seismic Behavior of Concrete Dam Considering the Interaction of Dam-Reservoir. *Journal of Basic and Applied Scientific Research*.

Minakov, A., Platonov, D., Dekterev, A., Sentyabov, A., & Zakharov, A. (2015). The numerical simulation of low frequency pressure pulsations in the high-head Francis turbine. *Computers & Fluids, 111*, 197-205.

Miquel, B., & Bouaanani, N. (2013). Accounting for earthquake-induced dam-reservoir interaction using modified accelerograms. *Journal of Structural Engineering*.

Mircevska, V. J., Bickovski, V., & Garevski, M. (2007). A 3D nonlinear dynamic analysis of a rock-fill dam based on IZIIS software. *Acta geotechnical Slovenica, 4*(2), 16-32.

Mirzabozorg, H., Kordzadeh, A., & Hariri-Ardebili, M. (2012). Seismic response of concrete arch dams including dam-reservoir-foundation interaction using infinite elements. *Electronic Journal of Structural Engineering, 12*(1).

Mo, Z., Xiao, J., & Wang, G. (2016). Numerical research on flow characteristics around a hydraulic turbine runner at small opening of cylindrical valve. *Mathematical Problems in Engineering, 2016*.

Moradi, S., Yeganeh, A., & Salimi, M. (2013). CFD-modeling of effects of draft tubes on operating condition in spouted beds. *Applied mathematical modelling, 37*(4), 1851-1859.

Muis, A., Sutikno, P., Soewono, A., & Hartono, F. (2015). Design optimization of axial hydraulic turbine for very low head application. *Energy Procedia, 68*, 263-273.

Narita, K. (2000). Design and construction of embankment dams. *Dept. of Civil Eng., Aichi Institute of Technology*.

Negru, R., Muntean, S., Marsavina, L., Susan-Resiga, R., & Pasca, N. (2012). Computation of stress distribution in a Francis turbine runner induced by fluid flow. *Computational Materials Science, 64*, 253-259.

Nicolet, C. (2007). Hydroacoustic modelling and numerical simulation of unsteady operation of hydroelectric systems. *LMH, LME*.

Olson, L. G., & Bathe, K.-J. (1983). A study of displacement-based fluid finite elements for calculating frequencies of fluid and fluid-structure systems. *Nuclear Engineering and Design, 76*(2), 137-151.

Paish, O. (2002). Small hydro power: technology and current status. *Renewable and Sustainable Energy Reviews, 6*(6), 537-556.

Pennacchi, P., Borghesani, P., & Chatterton, S. (2015). A cyclostationary multi-domain analysis of fluid instability in Kaplan turbines. *Mechanical Systems and Signal Processing, 60*, 375-390.

Punmia, B., Lal, P. B. B., Jain, A. K., & Jain, A. K. (2009). *Irrigation and water power engineering*: Laxmi Publications, Ltd.

Qian, Z.-d., Yang, J.-d., & Huai, W.-x. (2007). Numerical simulation and analysis of pressure pulsation in Francis hydraulic turbine with air admission. *Journal of Hydrodynamics, Ser. B, 19*(4), 467-472.

Rahman, S. (2003). Green power: What is it and where can we find it? *IEEE Power and Energy Magazine, 99*(1), 30-37.

Ravens, T. M. (2007). Comparison of two techniques to measure sediment erodibility in the Fox River, Wisconsin. *Journal of hydraulic engineering, 133*(1), 111-115.

Ribeiro, A., Guedes, M., Smirnov, G., & Vilela, S. (2012). On the optimal control of a cascade of hydro-electric power stations. *Electric Power Systems Research, 88*, 121-129.

Rikui, Z., Mao, F., Wu, J.-Z., Chen, S.-Y., Wu, Y.-L., & Liu, S.-H. (2009). Characteristics and control of the draft-tube flow in part-load Francis turbine. *Journal of Fluids Engineering, 131*(2), 021101.

Samii, A., & Lotfi, V. (2012). Application of H–W boundary condition in dam–reservoir interaction problem. *Finite elements in analysis and design, 50*, 86-97.

Samora, I., Hasmatuchi, V., Münch-Alligné, C., Franca, M. J., Schleiss, A. J., & Ramos, H. M. (2016). Experimental characterization of a five blade tubular propeller turbine for pipe inline installation. *Renewable Energy, 95*, 356-366.

Sarkar, R., Paul, D., & Stempniewski, L. (2007). Influence of reservoir and foundation on the nonlinear dynamic response of concrete gravity dams. *ISET Journal of Earthquake technology, 44*(2), 377-389.

Shariatmadar, H. (2009). Modal Response of Dam-Reservoir-Foundation Interaction. *Journal of Mathematics*.

Sinagra, M., Sammartano, V., Aricò, C., Collura, A., & Tucciarelli, T. (2014). Cross-Flow turbine design for variable operating conditions. *Procedia Engineering, 70*, 1539-1548.

Singh, P. (2017). The choice between turbine expanders and variable speed pumps as replacement for throttling devices in non-thermal process applications. *Energy, 123*, 198-217.

Stein, P., Sick, M., Dörfler, P., White, P., & Braune, A. (2006). *Numerical simulation of the cavitating draft tube vortex in a Francis turbine.* Paper presented at the Proceedings of the 23rd IAHR Symposium on Hydraulic Machinery and Systems, Yokohama, Japan.

Stone, R. (2011). Hydropower. The legacy of the Three Gorges Dam. *Science (New York, NY), 333*(6044), 817.

Suul, J. A., Uhlen, K., & Undeland, T. (2008). *Variable speed pumped storage hydropower for integration of wind energy in isolated grids: case description and control strategies.* Paper presented at the Nordic Workshop on Power and Industrial Electronics (NORPIE/2008), June 9-11, 2008, Espoo, Finland.

Temiz, A. (2013). Decision making on turbine types and capacities for run-of-river hydroelectric power plants a case study on eglence-1 hepp.

Thapa, B. S., Thapa, B., & Dahlhaug, O. G. (2012). Empirical modelling of sediment erosion in Francis turbines. *Energy, 41*(1), 386-391.

Trivedi, C., Cervantes, M. J., Gandhi, B., & Dahlhaug, O. G. (2013). Experimental and numerical studies for a high head Francis turbine at several operating points. *Journal of Fluids Engineering, 135*(11), 111102.

Urquiza, G., Garcia, J., Gonzalez, J., Castro, L., Rodriguez, J., Basurto-Pensado, M., & Mendoza, O. (2014). Failure analysis of a hydraulic Kaplan turbine shaft. *Engineering Failure Analysis, 41*, 108-117.

Versteeg, H. K., & and Malaskekera, W. (2007). *An Introduction to Computational Fluid Dynamic*.

Wang. (2014). High-order computational fluid dynamics tools for aircraft design. *Phil. Trans. R. Soc. A, 372*(2022), 20130318.

Wang, Jin, F., Prempramote, S., & Song, C. (2011). Time-domain analysis of gravity dam–reservoir interaction using high-order doubly asymptotic open boundary. *Computers & Structures, 89*(7), 668-680.

Watanabe, Kikuchi, K., & Cao, Z. (1996). Vibration Modes of a Rockfill Dam Based on the Observations of Microtremors and an Earthquake. *Thammasat International Journal of Science and Technology, 1*(1).

Watanabe , a. K. (1995). Characteristics of elementary dynamic behavior for three dimensional seismic response of a fill dam. *Soils & foundations, 35*(1), 45-54.

Wel, & Zhang. (2010). Vibration analysis of hydropower house based on fluid-structure coupling numerical method. *Water Science and Engineering, 3*(1), 75-84.

Wieland, M. (2010). Features of seismic hazard in large dam projects and strong motion monitoring of large dams. *Frontiers of Architecture and Civil Engineering in China, 4*(1), 56-64.

Xavier, L. V. (2012). Campos Novos Hydropower Plant on Canoas River.

Yah, N. F., Oumer, A. N., & Idris, M. S. (2017). Small scale hydro-power as a source of renewable energy in Malaysia: A review. *Renewable and Sustainable Energy Reviews, 72*, 228-239.

Yamaguchi, Y., Hall, R., Sasaki, T., Matheu, E., Kanenawa, K.-i., Chudgar, A., & Yule, D. (2004). *Seismic performance evaluation of concrete gravity dams.* Paper presented at the Proceedings of the 13th World Conference on Earthquake Engineering.

Yilmazturk, S. M., Arici, Y., & Binici, B. (2015). Seismic assessment of a monolithic RCC gravity dam including three dimensional dam–foundation–reservoir interaction. *Engineering Structures, 100*, 137-148.

Zeidan, B. A. (2015). Effect of foundation flexibility on dam-reservoir-foundation interaction. *Eighteenth International Water Technology Conference*.

Zhang, Mao, F., Wu, J.-Z., Chen, S.-Y., Wu, Y.-L., & Liu, S.-H. (2009). Characteristics and control of the draft-tube flow in part-load Francis turbine. *Journal of Fluids Engineering, 131*(2), 021101.

Zhang, & Zhang, L. (2012). Numerical simulation of cavitating turbulent flow in a high head Francis turbine at part load operation with OpenFOAM. *Procedia Engineering, 31*, 156-165.

LIST OF PUBLICATIONS AND PAPERS PRESENTED

Published paper:

1- Ameen Ameen, Zainah Ibrahim, Faridah Othman (2017) **Three-Dimensional Seismic Response Analysis for a Rockfill Dam**. Journal of Computational and Theoretical Nanoscience Vol. 14, 1–11.

http://www.ingentaconnect.com/content/asp/jctn/2017/00000014/00000012/art00048

2- Ameen Mohammed Salih Ameen, Zainah Ibrahim, Faridah Othman*, Nadhir Al-Ansari*, Zaher Mundher Yaseen (2018) **Minimizing the principle stresses of powerhoused rock-fill_dams_using control turbine running units: Application of finite element method**. Water 2018, 10(9), 1138; https://doi.org/10.3390/w10091138.

Accepted paper:

1- Ameen Ameen, Zainah Ibrahim, Faridah Othman, Zaher Yaseen (2018) **Water Flow Stabilization Using Submerged Weir for Draft Tube Reaction Hydraulic Turbine.** Scientia Iranica. Paper (Ref. No: SCI-1712-1476).